January 2011

The Role Of Inflammation In Pathogenesis And Treatment Of Globoid-Cell Leukodystrophy

Adarsh Reddy
Washington University in St. Louis

WASHINGTON UNIVERSITY IN SAINT LOUIS
Division of Biology and Biomedical Sciences
Program in Neuroscience

Dissertation Examination Committee:
Mark Sands, Chair
Anne Cross
Keiko Hirose
Robyn Klein
Paul Kotzbauer
John Russell

THE ROLE OF INFLAMMATION IN PATHOGENESIS AND TREATMENT OF GLOBOID-CELL LEUKODYSTROPHY

by

Adarsh Surya Reddy

A dissertation presented to the
Graduate School of Arts and Sciences
of Washington University in
in partial fulfillment of the
requirements for the Degree
of Doctor of Philosophy
August 2011
Saint Louis, Missouri

Abstract of the Dissertation

The Role of Inflammation in pathogenesis and treatment of Globoid-Cell Leukodystrophy

by

Adarsh Surya Reddy

Doctor of Philosophy in Biology and Biomedical Sciences (Neurosciences)

Washington University in St. Louis

Mark S. Sands, Chairperson

Globoid-cell leukodystrophy (GLD, Krabbe's disease) is an autosomal recessive disease caused by a deficiency of the lysosomal enzyme galactosylceramidase (GALC). It results in altered catabolism of the myelin lipid Galactosylceramide. The disease predominantly affects the white matter of the CNS and the myelin sheath of the peripheral nerves. The infantile form of the disease is characterized by early onset between 3-6 months of age with symptoms of irritability, dysphagia, spasticity, cognitive and sensory deterioration and seizures. Death usually occurs by two years of age. Currently, hematopoietic stem cell transplantation is the only available option for patients with the disease. Inflammation is a prominent component of the disease and possibly plays an important role in determining the efficacy of therapy. The goal of the thesis is to understand the role of inflammation in the pathogenesis and treatment of GLD.

In order to understand the role of inflammation, the murine model (twitcher) was used. The twitcher mouse is an authentic model of GLD. It is deficient in the same enzyme as that of the human counterpart and has similar phenotypic manifestations. Previous studies have shown that there is a synergistic

therapeutic effect when bone marrow transplantation is combined with AAV2/5 mediated gene therapy. Our current study found that the synergistic effect could be further improved upon by targeting spinal cord with gene therapy in addition to the brain. The current study also found that AAV2/5 mediated gene therapy is associated with an increase in CD4 and CD8 T-cells and activated microglia in the brains and this could possibly limit the effectiveness of the viral vectors. Interestingly, addition of BMT to AAV2/5 reduced the T-cell and activated microglia, without further increasing the enzyme levels or decreasing the levels of toxic substance called psychosine in the CNS. This strongly suggests that BMT provides synergy by modulating inflammation. Other markers of inflammation that were highly elevated in the CNS, like the cytokine KC, were also reduced in mice that received treatment. Among all the cytokines that were measured, KC was the most highly elevated one in the CNS of the twitcher mice. KC is a strong chemoattractant to macrophages and neutrophils and it is also involved in oligodendrocyte precursor proliferation and migration. Since both components are important part of Krabbe's disease. The role of this cytokine was explored in further detail.

Lack of KC or its receptor CXCR2 in the CNS or periphery or both did not alter the inflammation, oligodendrocyte proliferation or course of the disease in the twitcher mice. This could be explained by the compensatory increase in other cytokines and growth factors like MIP-2, FGF-2 and PDGF-BB. Although, KC and CXCR2 probably exert their effects in combination with other cytokines and growth factors, inflammation is clearly an important player in the pathogenesis and treatment of Krabbe's disease, but targeting the primary enzyme

deficiency appears to be more important for therapy.

Acknowledgements

Many, many people were involved in bringing this thesis work to fruition. If I have excluded some names, it is unintentional.

I thank Hunters Hope foundation and National Tay-Sachs and Allied Diseases Association for funding support.

My sincere thanks to my mentor Dr. Mark Sands, who decided to take me in to his lab with no molecular biology training whatsoever. His guidance and patience at every step of the process is highly appreciated.

I owe a special thanks to Kevin O'Dell for his excellent and diligent management of the animal colonies. This work would not have been completed without his help.

I also thank Marie Nuñez for her help in getting me started with molecular biology lab work and for being a supportive "lab mom".

I also thank my fellow graduate students Anthony Donsante, Jacqui Hawkins Salsbury, Shannon Macauley and Josh Woloszynek. They are all extraordinary students and it has been a privilege to learn science from them through helpful discussions and constructive criticism. I also thank Elizabeth Qin for an opportunity to mentor her for one summer. I probably learnt more from her than she from me!

Much of the current thesis is dependent on animal work and I thank Beth Eultgen and Jeanie, support staff at the animal facility for their help in maintaining the colonies.

I also thank my members of my thesis committee (Drs. Robyn Klein, Anne Cross, Keiko Hirose, Paul Kotzbauer and John Russell) for evaluating and cri-

tiquing my work and directing my progress. Ideas for many of the experiments arose out of helpful discussions from my thesis committee members.

The work presented in this thesis is no small undertaking. It involved the expertise of several of our collaborators. I thank Robyn Klein for her valuable guidance with regard to addressing neuroinflammation seen in the disease. I hope this fruitful collaboration will continue in the future. I also thank Steve Fowler (University of Kansas), for his direction and help in the tremor project. It was a valuable learning experience for me. I also thank David Wozniak for help with behavioral analysis and statistics. I also thank Jigisha Patel, for her help with oligodendrocyte proliferation studies. Special thanks to Joong Kim and Victor Song for helping with the diffusion tensor imaging. We also received a lot of help with histology from Carole Vogler (St. Louis University School of Medicine), Nuri Farber and Haihui Wang (histology core). I also thank Xianlin Han for help with mass spectrometry. A special thanks to Elisabeth Tracy (Duke University) for training me in performing the intrathecal injections.

I also received a lot of support from people in the neighboring labs. A special thanks to Mike Rettig, Bill Eades, Michelle Becker-Hapak, Sheng Cai and Adam Greenbaum. A big thanks to Sally Vogt, Gretchen Carnoskeand Shirley McTigue for their help with administrative work.

I can't finish this section without profusely thanking my family and friends. My father was very influential in my decision to pursue my dreams. Unfortunately, he passed away after prolonged sickness. I think he would have been very proud of me if he was here today. My mother was very always very supportive of my pursuits and I owe her much. My brother has done much back

home to keep me away from all the family responsibilities. I am proud to see him become successful in his own pursuits. I also thank my relatives especially my uncles S.V. Gopal Reddy and Muni Reddy and also my cousin Ramachandra for all the support.

My friends in St. Louis have made my life infinitely more fun. Alaji Bah was my every weekend buddy until he graduated. I will fondly remember the biking days and having some great dinner conversations. The Yttris (Eric, Jen and Pam, Emily and Allen) have made acculturation process much easier and I have spent some really memorable moments with them. Giri, Vikram and Ankit have been extraordinary friends and have spent many a good times in St. Louis with them. I also thank Ghada Kunter for her friendship and support.

Last but not the least I also like to thank the families affected by Krabbe's disease and other lysosomal storage diseases for all the encouragement and research support. They certainly make this effort worthwhile.

Dedication

To my father, whose high ideals I strive for...

to my mother, for her unstinting dedication and support...

to my brother, for shouldering family responsibilities that help me complete this thesis...

and to my mentor Mark Sands, for all the training that I received.

Contents

List of Figures

Abbreviations

AAV	adeno-associated virus
CNS	central nervous system
CO2	carbon dioxide
GALC	galactosylceramidase
GFAP	glial fibrillary acidic protein
GFP	Green fluorescent protein
GLD	Globoid-cell Leukodystrophy
H_2O_2	hydrogen peroxide
IFN-γ	interferon gamma
IL	interleukin
KC	Keratinocyte Chemoattractant
LSD	lysosomal storage disease
MCP-1	monocyte chemotactic protein-1
MIP-1	macrophage inflammatory protein-1
NGS	normal goat serum
PAS	Periodic acid-Schiff stain
PBS	phosphate buffered saline
PFA	paraformaldehyde
PNS	peripheral nervous system
RANTES	regulated upon activation, normal T-cell expressed and secreted
SC	spinal cord
TBS	tris-buffered saline
TNF-α	Tumor Necrosis Factor
WT	wildtype

Chapter 1

Background and Significance

1.1 Lysosomal Storage Diseases

Lysosomal storage diseases are a group of diseases caused by the deficiency or dysfunction of lysosomal enzymes or associated proteins. There are currently about 45 inherited diseases that fall in to this category. Individually, they are rare, but taken together as a group, they have an incidence of about 1 in 5000 (Meikle et al., 1999). The various storage diseases share common pathophysiologic manifestations and certain common therapeutic principles are involved in treating most of the diseases. Hence they are often considered as a class. The lysosome is the organelle which is the "garbage disposal" of the cell. Several catabolic pathways for the major cellular constituents are localized in this organelle. The mileu of the lysosome is maintained at an acidic pH and is essential for functioning of most lysosomal enzymes. Based on the pathways that are affected, there are various subsets of lysosomal storage diseases like glycogen storage diseases (e.g., Pompe's disease), sphingolipidoses

(e.g., Krabbe's disease), mucopolysaccharidosis e.g., MPS VII (Sly disease), disorders of glycoprotein degradation (e.g., α-mannosidosis) etc. Although, the clinical manifestations of the individual diseases vary, the reticulo-endothelial system and the CNS are often involved. The diseases are usually chronic and usually present in early to late childhood with a progressive course. The treatment principles are also similar for the group of diseases with subsets of diseases having the same treatment.

1.2 Krabbe's disease

Globoid-cell leukodystrophy (GLD, Krabbe's disease, OMIM $\#$ 245200) is a autosomal recessive disease caused by a deficiency of the lysosomal enzyme galactosylceramidase (GALC) (Suzuki et al., 2000). The incidence of the disease is estimated to be about 1:100,000 live births (Suzuki et al., 2000). It results in altered catabolism of the myelin lipid galactosylceramide. The disease predominantly affects the white matter of the CNS and the myelin sheath of the peripheral nerves. The infantile form of the disease is characterized by early onset between 3-6 months of age with symptoms of irritability, dysphagia, spasticity, cognitive and sensory deterioration and seizures. Death usually occurs by two years of age. Currently, hematopoietic stem cell transplantation is the only available option for patients with the disease.

1.3 History and milestones in Krabbe's disease

The disease was first described as a separate pathological entity by Knud Krabbe, a Danish neurologist and neuropathologist in 1916 in his study titled "A new familial, infantile form of diffuse brain sclerosis" (Krabbe., 1916). Krabbe also described the characteristic globoid-cells and associated them with the disease. Until recently, much of the clinical management for the disease was supportive. The study of the disease was greatly aided by the twitcher mouse. The mouse was discovered as a spontaneous mutant at The Jackson Laboratories, Bar Harbor, Maine (Duchen et al., 1980). The mouse was named for its prominent tremor or twitching phenotype. The twitcher mouse has been an invaluable tool in understanding the pathogenesis and designing new therapies for Krabbe's disease. When the lipid profile was analyzed in the twitcher mouse brains, a catabolite galactosylsphingosine was highly elevated (Iguzu and Suzuki., 1984). Its toxic effects on cells lead to the "psychosine hypothesis", as a mechanism for rapidly progressive CNS pathology seen in this disease. In another study bone marrow transplantation significantly prolonged the median lifespan of the twitcher mouse (Yeager et al., 1984). When a similar study was performed in humans (Krivit et al., 1997), there was only a minimal improvement in the disease. When umbilical cord blood transplants were performed in pre-symptomatic infants, there was a much better improvement in symptoms and the disease course was favourably altered (Escolar et al., 2005). Subsequent to the study, Krabbes disease is beginning to be included in the neonatal screening programs (Duffner et al., 2009). Although progress has been made, much research still needs to be done in terms of effective therapies and in terms

of understanding of the pathogenesis of the disease.

1.4 Twitcher mouse

As mentioned above, the murine model of GLD (twitcher mouse) was discovered as a spontaneous mutant. The mutation was later identified as a point mutation in the exon of the GALC gene leading to a premature termination codon with very low transcriptional activity(Sakai et al., 1996). The twitcher mouse recapitulates most of the features of its human counterpart. The mean lifespan of the untreated twitcher mouse is about 38 days. Recently, a mouse model for the adult onset disease has been described (Luzi et al., 2008). Large animal models of Krabbe's disease include rhesus monkey, dog and sheep (Wenger et al., 2001) and could be important tools in translational research in Krabbe's therapies.

1.5 Pathology and Pathogenesis

The neuropathology of the twitcher mouse is characterized by the infiltration of periodic acid-Schiff (PAS)-positive cells (globoid cells) in the CNS and PNS, progressive demyelination, apoptotic death of oligodendrocytes and the activation of astrocytes and microglia (Wenger et al., 2001). Although, GALC is expressed in most cell types, the synthesis of galactosylceramide in the nervous system is almost exclusively localized to oligodendrocytes and Schwann cells where it forms an important constituent of the myelin sheath. The cell types that are affected most severely are oligodendrocytes and Schwann cells and several

lines of evidence points towards these cells being affected first in the disease. Transgenic correction of oligodendrocytes by expressing GALC under oligodendrocyte specific promoter (Myelin Basic Protein promoter) leads to rescue of the twitcher phenotype (Matsumoto et al.,1997, De Gasperi et al., 2004). Transduction of twitcher oligodendrocytes by injecting a GALC-expressing retrovirus leads to their morphological improvements of in vivo (Meng et al., 2005). Galactosylceramide accumulation also occurs in the kidney in the twitcher mouse, but such accumulation is not seen in human patients with early onset disease (Igisu et al., 1983).

Biochemically, the lack of GALC activity leads to an altered breakdown of galactosylceramide, a sphingolipid consisting of a sphingosine (which is synthesized from fatty acyl-coA and serine), a long-chain fatty acid and galactose (Figure 1.1).

Surprisingly, abnormal accumulation of galactosylceramide does not occur in the nervous system despite the genetic catabolic block. Instead, the galactosylceramide is converted to galactosylsphingosine (psychosine), which accumulates in the brains of twitcher mice and is believed to cause the death of oligodendrocytes (Suzuki 1998)(Figure 1.2). It is not known for certain if psychosine is actually responsible for the death of oligodendrocytes, however, there are several lines of evidence which support this hypothesis. Psychosine, which is undetectable in normal brains, progressively accumulates in the brains of twitcher mice (Igisu et al., 1984). The levels of psychosine in one hundred day old twitcher mice receiving treatment (BMT) are comparable to the untreated terminal twitcher mice at 40 days (Ichioka et al., 1987). Psychosine levels re-

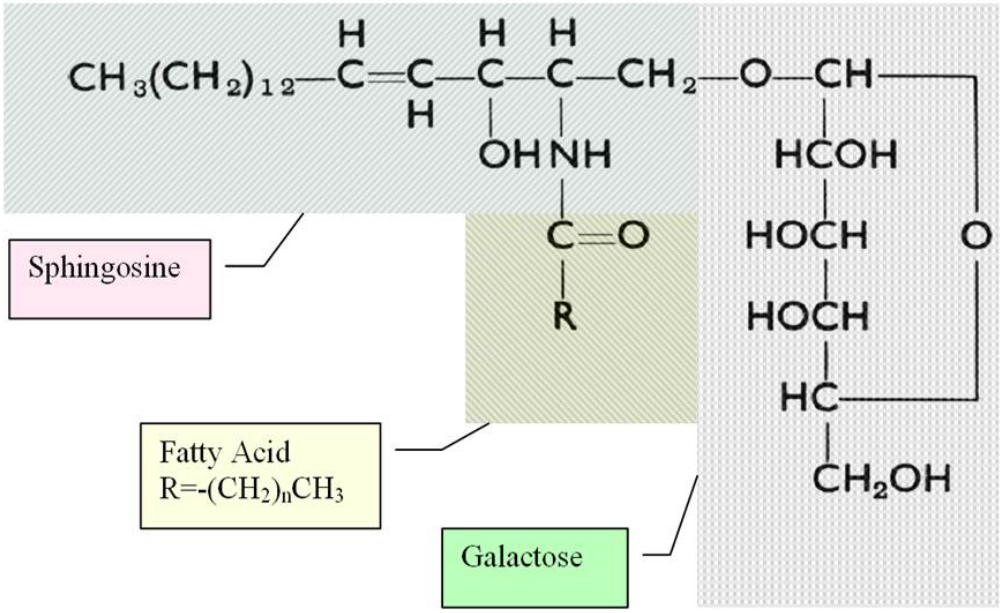

Figure 1.1: Structure of Galactosylceramide. The main components are sphingosine, fatty acid and galactose. Figure adapted from Wenger et al., 2001.

turn to undetectable levels in the adult-onset model receiving BMT which live for over one year (Luzi et al., 2005). Psychosine can induce apoptosis in cultured oligodendrocytes *in vitro* (Jatana et al., 2002), the exact molecular mechanism of which remains unknown. Two main ways in which psychosine is hypothesized to act is by: a) activation of Phospholipase C (Hannun and Bell, 1997) and b) by non-specific effect of disruption of lipid rafts (White et al., 2011). Activation of reactive oxygen species is also known to occur (Khan et al., 2005), although the exact mechanism by which this occurs is not known.

The death of oligodendrocytes likely elicits an inflammatory reaction which leads to infiltration of immune cells into the CNS and the peripheral nervous

system. Infiltration of inflammatory cells probably leads to further death and destruction of the glia and neurons which in turn accelerates the progression of disease. In summary, the progression of the disease can be broken down in to two interdependent pathways: primary enzyme deficiency leading to multiple secondary pathologic events like accumulation of psychosine, cellular apoptosis/death, immune cell activation, formation of reactive oxygen species, etc. (see Figure. 1.3).

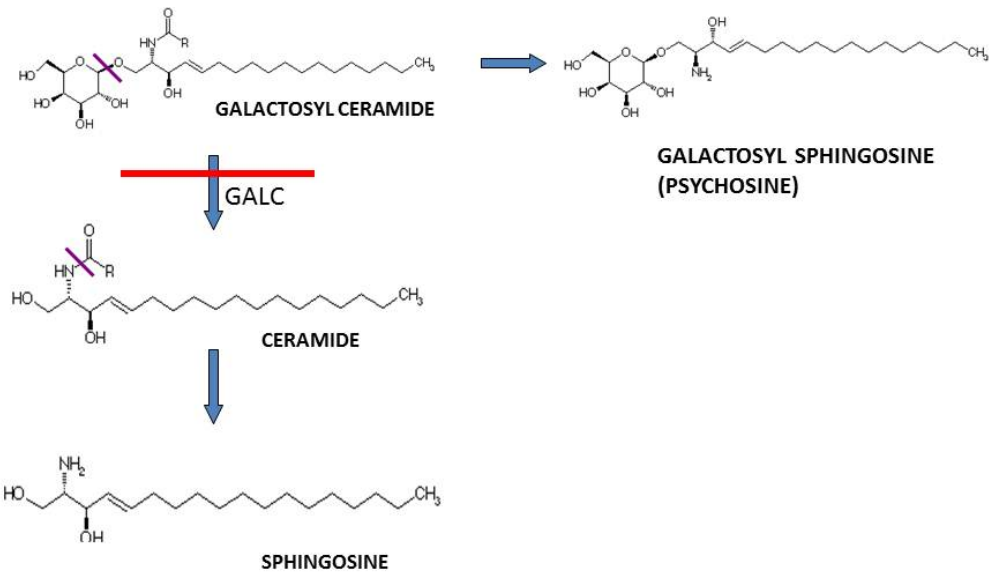

Figure 1.2: Catabolism of Galactosylceramide. The enzyme GALC degrades Galactosylceramide in to galactose and ceramide which is spontaneously degraded to sphingosine. In the absence of GALC, Galactosylceramide is catabolized to Galactosylsphingosine (psychosine) which is hypothesized to be toxic to cells.

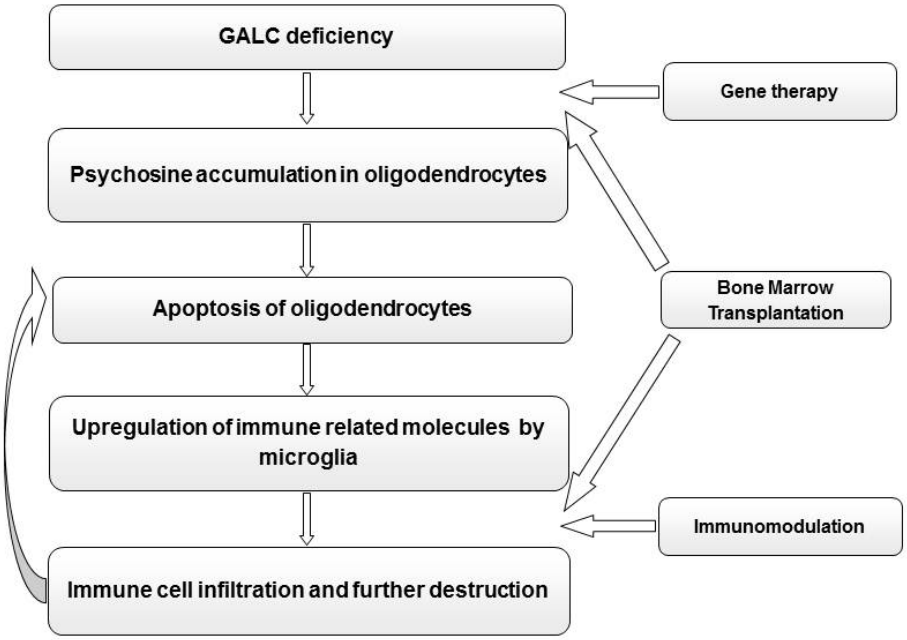

Figure 1.3: Presumed pathological sequence of events in Krabbe's disease and the possible sites of therapeutic effects.

1.6 Role of Inflammation in Krabbe's disease

It appears that inflammation plays a prominent role in the disease. Globoid cells are a characteristic feature of the disease and they are modified macrophages. Elevation of numerous cytokines in the CNS of the twitcher mice have been previously described (Wu et al., 2001). Additionally, inflammation also seems to play an important role in the efficacy of therapy. Current strategies used to treat the disease in pre-clinical studies include bone marrow transplantation (Yeager et al., 1984), gene therapy (for e.g., Shen et al., 2001; Rafi et al.,2005; Lin et al., 2005; Lin et al., 2007; Gentner et al., 2011). and substrate reduction

therapies (Biswas and Levine, 2001). The goal of both BMT and gene therapy is to supply the normal enzyme whereas substrate reduction therapies reduce the accumulation of the metabolite by inhibition of the enzyme that is involved in its synthesis. Previous studies in our lab showed that there is a dramatic synergy when BMT and intracranial gene therapy with Adeno-associated Virus 2/5 (AAV/BMT) are combined, when compared with either therapy alone (Lin et al., 2007). Wu et al., 2001, have shown that there is a decrease in immune-related molecules and infiltrating immune cells after BMT. Combining the above two observations, we hypothesized that the dramatic synergy observed in our previous study (Lin et al., 2007) could be the result of the combined effects of decreased inflammatory response by BMT and enzyme supplied by AAV2/5. Since inflammation appeared to play an important role in the pathogenesis and treatment of the disease, its role was further explored and these formed the objectives of the current thesis. The goals of our research are to understand the role of the immune system in the treatment and the pathogenesis of the disease.

Chapter 2

Role of Inflammation in Therapy of Globoid-cell Leukodystrophy

2.1 Therapeutic Principle (Cross-Correction)

The treatment of the lysosomal storage disease is based on the observation that the lysosomal enzymes are secreted from the cells that produce them and that these enzymes can be taken up by neighboring cells (Fratantoni et al., 1968). This uptake is mediated by recognition of the phosphorylated or non-phosphorylated mannose moieties present on the enzyme by the Mannose-6-Phosphate or Mannose receptors, respectively (Achord et al., 1978; Kornfeld., 1992). In theory only a small percentage of cells producing or overexpressing the enzyme should be sufficient to correct the disease since only a small amount ($<$5% of normal) of enzyme is required to reverse the pathological storage seen in these disorders (Wolfe et al., 1992; Sands et al., 1993; Vite et al., 2005).

2.2 Therapeutic strategies for Krabbe's disease

The only available treatment for Krabbe's disease is hematopoietic stem cell transplantation, using either umbilical cord blood (Escolar et al., 2005) or using bone marrow cells (Krivit et al., 1997). Although, the treatment improves the symptoms when pre-symptomatic newborns are treated, it is not curative. Also, neonatal transplantation is associated with high mortality of approximately 50%. Current strategies used to treat the disease in pre-clinical studies include gene therapy, bone marrow transplantation, enzyme replacement therapy, substrate reduction therapy and a combination of two or more therapies. Some of these strategies are discussed in detail below.

2.2.1 Gene Therapy

Gene therapy for lysosomal storage diseases that affect the brain, including GLD, aims to exploit the therapeutic principle of cross correction. As discussed previously, oligodendrocytes appear to be the primary cells that are affected by the disease. Adenovirus, lentivirus and Adeno-associated Virus (AAV) gene transfer vectors have been used successfully in various intracranial gene therapy protocols in a number of CNS diseases (Mandel et al., 2006).

A previous study from our lab has shown that an AAV2/5 vector (AAV2 genome packaged with AAV5 capsid proteins) gives much greater level expression of GALC in brains of twitcher mice compared to an AAV2 vector (Lin et al., 2005). Although about 25-fold higher than normal levels of enzyme can be obtained with AAV2/5, there was only a modest improvement in lifespan to about

55 days compared to untreated twitcher mice whose mean lifespan is about 38 days. This finding was surprising since comparable levels of enzyme are sufficient to correct the CNS disease in other lysosomal storage diseases like α-mannosidosis (Vite et al., 2005), Mucopolysaccharidosis VII (Frisella et al., 2001) and Metachromatic Leukodystrophy (Consiglio et al., 2001). It is possible that the virus and enzyme levels are insufficient to reach oligodendrocytes in distant sites. Alternatively, the progress of the disease is too rapid compared to the rate of correction.

2.2.2 Bone Marrow Transplantation (BMT) and Stem Cell Transplantation

BMT performed in young animals (8-9 days of age) using myeloablative conditioning (900 rads) prolongs the median lifespan of twitcher mice from about 40 days to about 80 days (Yeager et al., 1984). Although it was originally believed that donor derived cells in the CNS supplied sufficient GALC activity to correct the disease, the exact mechanism of the therapeutic effect of BMT in GLD probably involves multiple mechanisms.

Bone marrow (BM)-derived cells differentiate into a wide variety of cell types. BM contains a heterogeneous population of stem and progenitor cells including hematopoietic stem cells, marrow stromal cells, and perhaps other progenitor cells (Hess et al., 2004). When a clonal population of Lin-, CD34-, c-kit+, and Sca-1+, EGFP+ transgenic marrow precursor cells was allowed to proliferate in vitro and then transplanted along with short-term repopulating cells into the wild type mice, all the GFP labeled cells in the CNS were parenchymal microglial

cells and perivascular cells (Hess et al., 2004). Although normal or near normal levels of enzyme are reported in the brains of twitcher mice receiving BMT in some studies, (for e.g. see Ichioka et al., 1987) most studies report a variable intermediate level of enzyme in the brain (for e.g. See Hoogerbrooge et al., 1989). The enzyme level is undetectable in twitcher mice undergoing myeloreductive ablation, where about 25-35% of donor chimerism is obtained in a previous study (Lin et al., 2007). A study on α-galactosidase and β-glucosidase uptake in various cell cultures show that these enzymes are not taken up by the oligodendrocytes and most of the enzyme is taken up by astrocytes (Hill et al., 1985). Further, immunostaining showed that there are no M-6-P receptors on the oligodendrocytes. A somewhat contradictory study (Luddi et al., 2001) shows that oligodendrocytes co-cultured with GALC expressing fibroblasts (GALC activity- 270 nmol/hr/g) can take up some activity from the media (3.6 nmol/hr/g). It is not clear if the enzyme transfer can occur in vivo from the few microglia expressing normal levels of GALC. Based on these data, it is unlikely that the bone marrow cells are supplying the oligodendrocytes with high levels of GALC activity.

Interestingly, BMT has been shown to reduce the inflammatory infiltrate in the CNS as well as in the sciatic nerve (Yeager et al., 1984; Suzuki et al., 1988) . BMT also reduces the number of globoid cells (Yeager et al., 1984). As discussed above, immune related molecules are down regulated in twitcher mice after BMT (Wu et al., 2001).

Based on the above evidence, it is reasonable to hypothesize the following sequence of events. The death of oligodendrocytes elicits an immune response

which activates the microglia. The microglia secrete chemokines and cytokines which recruits more immune cells which could be responsible for further damage in the CNS. When the twitcher mouse is treated with BMT, an immune response recruits normal donor-derived microglia which can digest the galactosylceramide and the immune response is reduced compared to animals not receiving BMT. Since the enzyme deficiency is not completely corrected, the oligodendrocytes continue to die, albeit at a slower rate, and ultimately lead to the florid CNS pathology.

Recently umbilical cord blood transplantation has been attempted in a clinical setting (Escolar et al., 2005). This leads to significant clinical improvements if performed early in life ($<$6 months of age). However, long term follow-up studies are needed to completely assess the efficacy of this form of therapy. Also, inherent variation in the disease expression even among siblings, makes the results difficult to interpret. Transplantation of bone marrow cells transduced with a lentiviral vector was also shown to be effective in treating the disease, especially when the GALC overexpression is suppressed in the stem cells using micro-RNA (Gentner et al., 2010).

When neural stem/ progenitor cells transduced with a GALC expressing retroviral vector were injected into the brains of the neonatal twitcher mouse, donor oligodendrocytes preferentially migrated to areas of demyelination, however the improvement in the lifespan was only about 16 days (Pellegatta et al., 2006).

2.2.3 Combination Therapy

Among all the lysosomal storage diseases, there are only isolated instances where a single approach corrects most of the biochemical, histological and clinical features of the disease. This is likely owing to the complex nature of these diseases, as well as the inaccessibility of certain tissues, primarily the CNS. In addition, most of the promising results have been observed under carefully controlled laboratory conditions. Although the primary insult in LSDs is a single-gene defect, multiple secondary mechanisms play a role in the pathogenesis (Vitner et al., 2010). These include accumulation of secondary metabolites, inflammation, oxidative stress, and possibly other mechanisms like altered calcium homeostasis, abnormal lipid trafficking, increased autophagy, ER stress, unfolded protein response and autoimmunity. Each of these secondary effects is a potential therapeutic target. It is likely that one or more of these pathogenic mechanisms are at play by the time therapy is initiated, limiting the efficacy of the primary approach. Therefore, several groups have begun combining therapies in order to target either different aspects of disease or different tissues. Additionally, the timing of various therapies can, and has been optimized in order to take advantage of the strengths of each approach. Interestingly, both additive and synergistic effects have been documented when two or more treatments are combined (reviewed by Hawkins-Salsbury et al., 2011).

2.3 The role of immunomodulation in treating the neuropathology seen in twitcher mouse

Both gene therapy and BMT lead to significant improvements in the clinical course of disease in the twitcher mouse. However, the improvements are modest. When forebrain directed AAV2/5 is combined with BMT, it results in a dramatic synergy in the lifespan, behavioral and neuropathological improvements (Lin et al., 2007). This synergy cannot be explained by the difference in the enzyme levels or engraftment between the combination group and the AAV2/5 or BMT groups. Although this synergy is striking, the mechanistic basis of it is not understood. It is possible that there is a greater reduction of cytokine levels when compared to animals treated with BMT alone observed in the previous study (Wu et al., 2001). Also, the disease remains largely uncorrected in the spinal cord and cerebellum. Therefore, myeloreductive BMT was combined with AAV2/5 gene delivery to forebrain, cerebellum and spinal cord. Additional targeting of the cerebellum and spinal cord, resulted in significant improvement in most outcome measures. The only exception was the tremor phenotype, which was not improved in animals receiving BMT. In order to understand the mechanism of synergy, several inflammatory markers were qualitatively and quantitatively assessed. Despite providing essentially no enzyme activity and no decrease in psychosine, addition of BMT virtually eliminated the inflammation and greatly enhanced the effects of AAV2/5. The data strongly suggest that BMT when combined with AAV2/5, decreases inflammation which provides the dramatic therapeutic synergy.

2.4 Materials and Methods

2.4.1 Animals

Heterozygous twitcher (GALC+/-) mice on a congenic C57BL/6 background were obtained from The Jackson Laboratory (Bar Harbor, ME). Mice were maintained under the supervision of M.S.S. at Washington University School of Medicine. The mice were housed under standard conditions with ad libitum access to food and water. Homozygous twitcher mice (GALC-/-) were obtained by heterozygous by heterozygous matings. The genotype was determined by twitcher-specific PCR (Sakai et al., 1996). Only the mice surviving till weaning were used for the study. All animal experiments were approved by the Institutional Animal Care and Use Committee at Washington University School of Medicine.

2.4.2 Recombinant AAV2/5 vector

The AAV2/5 vector used in this study has been previously described (Lin et al., 2005; 2007). The expression of murine GALC is under the control of chicken β-actin promoter and CMV enhancer. The 3' end of the GALC cDNA has the 3' untranslated region from the rabbit β-globin gene and SV40 polyA sequences. Adeno-associated Virus 2 pseudotyped with the AAV 5 capsid (AAV2/5) was made at University of Florida viral vector core using previously published methods (Zolotukhin et al., 1999). The AAV2/5 titer was determined by dot blot hybridization of DNase-resistant viral DNA and compared to known quantities of vector plasmid. The virus was diluted to a final titer of 1.3 X 10^{12} particles/ml

and stored at -70 °C till use.

2.4.3 Therapeutic regimen

The study consisted of the following groups: untreated wildtype (untreated wt), untreated twitcher (untreated mut), BMT-only wildtype (BMT-WT), BMT-only twitcher (BMT-mut), AAV2/5-only twitcher (AAV-mut) and combination-treated twitcher (AAV+BMT- mut). The regimen for the AAV+BMT-mut group consisted of AAV2/5 injections on day 2 or 3 of life and BMT on the following day. Prior to injections, the newborn mice were anesthetized by inducing hypothermia on ice packs for 10-15 minutes. CNS-directed gene therapy consisted of an intrathecal injection (Elliger et al., 1999) and 6 intracranial injections. Injections were done into the neonatal spine in the midline at the upper lumbar vertebral column. A total of 20 μl of virus [15 μl of AAV2/5 and 5 μl of filter-sterilized 6% green food coloring (Durkee products, Ankeny, Iowa) in Ringer's lactate] was injected using a 50 μl Hamilton syringe (Hamilton Company, Reno, NV). The procedure was considered successful only if the green dye reached the posterior fontanelle. For intracranial delivery, 2 μl of AAV2/5 was injected at each of six sites (3 sites/ hemisphere) into the brain. Injections were performed using a Hamilton Syringe fitted with a 32-guage needle based on the sutural landmarks visible in a day 2 neonatal mouse. The depth of injection was controlled by using a guard on the needle. The injection sites were: a) forebrain- 2mm lateral and 1mm caudal to bregma and 1.5mm deep, b) thalamus- 2mm lateral and 2.5mm caudal to bregma and 2.5mm deep; and c) cerebellum- 1mm lateral and 3mm posterior to lambda and 2.5mm deep.

For BMT, the bone marrow donors were sex-matched syngeneic WT (GALC +/+) mice expressing GFP under the control of CAGGS promoter (Okabe et al., 1997). Newborn mice received 400 rads of total body γ radiation from ^{137}Cs source for conditioning followed by injection of 10^6 GFP(+) sex-matched unfractionated nucleated bone marrow cells in 100 μl volume into the superficial temporal vein (Sands and Barker, 1999).

2.4.4 Flow cytometry

In order to quantify the hematopoietic-derived cells in the CNS (Sedgwick et al., 1991; Campanella et al., 2002; Cardona et al., 2006; McCandless et al., 2006), perfused mice brains were treated with collagenase/ DNase buffer after homogenization and passed through a 70 μm filter. The hematopoietic-derived cells were isolated by separation on a percoll gradient. Cells were then counted using a hemocytometer and stained with fluorophore-conjugated antibodies after Fc receptor block. The following cells were identified and quantified by flow cytometry: Resting microglia (CD11b+, CD45^{lo}), activated microglia/ macrophages (CD11b+ CD45^{hi}), CD8 T-cells, CD4 T-cells and neutrophils (Gr1^{hi}, F4/80-). Spleen and bone marrow from wildtype animals were used for positive controls. Data were acquired using Cell Quest pro software (BD biosciences, San Jose, CA) and analyzed using FloJo software (Tree Star Inc., Ashland, OR). The absolute cell numbers isolated from each brain were calculated using the hemocytometer cell counts and the percentage of cells that are stained with a respective combination of fluorophores. For quantifying donor hematopoietic engraftment, bone marrow was harvested from femurs at 36 days of age and

the percentage of GFP(+) cells were determined.

2.4.5 Quantitation of Psychosine

Psychosine levels were quantified in the brains and spinal cords at post-natal day 36, essentially as described previously (Jiang et al., 2009). Briefly, tissues were flash-frozen, pulverized and weighed. Internal standard N,N-dimethyl psychosine was added at this stage and lipids were extracted with 2:1 chlorofom:methanol containing 5% ammonium hydroxide. Extracted lipids were treated with 1.0 M lithium hydroxide in methanol, then washed with diethyl ether and hexanes, and extracted with chloroform. Lipids were then dried under nitrogen, and resuspended in 1:1 chloroform:methanol. This sample was analyzed by mass spectrometry as described previously (Jiang et al., 2009). Psychosine concentration was calculated by comparing the psychosine peak intensity to that of the internal standard.

2.4.6 Multiplex sandwich immunoassays

This assay is based on a procedure described by (Hulse et al., 2004). The Bio-Plex multiplex cytokine kit (Bio-Rad laboratories, Hercules, CA) was used for these analyses and the assays were performed essentially as per manufacturers' specifications. The following cytokines were quantified: IL-1α, IL-1β, IL-2, IL-3, IL-4, IL-5, IL-6, IL-9, IL-10, IL-12(p40), IL-12(p70), IL-13, IL-17, Eotaxin, G-CSF, GM-CSF, IFN-γ, KC, MCP-1, MIP-1α, MIP-1β, RANTES and TNF-α. PBS-perfused mice brains were homogenized in a solution consisting of 10 mM Tris, 150 mM NaCl, 1 mM Dithiotreitol, 0.2% Triton-X and 20 μl/ml

of Protease Inhibitor Cocktail (P8340, Sigma, St. Louis, MO). The supernatant from brain homogenates was diluted to obtain a protein target concentration of 0.5-1.0 mg/ml and stored at -70°C. Once thawed, the supernatant from the homogenates was incubated with the fluorescent beads from the kit, washed and then incubated with biotin-labeled antibody cocktail. The samples were then incubated with streptavidin-PE and the fluorescence values were read and analyzed by the flow cytometry based Bio-Plex 2200 system (Bio-Rad laboratories, Hercules, CA). The concentration of the cytokine in each sample was calculated by using the standard curve generated for each cytokine by the standards supplied in the kit.

2.4.7 Protein assay

Protein assays were performed in order to normalize cytokine levels, GALC activity and psychosine levels. Total protein concentration was determined using a protein assay reagent based on Coomasie dye-binding assay (Bio-Rad, Hercules, CA). A standard curve was generated using known concentrations of bovine serum albumin (BSA).

2.4.8 Immunohistochemistry

Brains and spinal cords were collected after the animals were perfused with phosphate buffered saline. The tissue was immersion fixed in 4% paraformaldehyde overnight at 4°C followed by cryoprotection in 30% sucrose at 4°C. The tissues were then frozen in tissue-tek O.C.T. compound (Sakura Finetek, Torrance, CA) and cryosectioned. For immunostaining, the tissues were fixed in

4% paraformaldehyde for 30 minutes followed by peroxidase quenching with hydrogen peroxide for 15 minutes. The sections were then stained with the appropriate dilution of primary antibodies overnight at 4°C. The primary antibody was detected using the appropriate secondary antibody (1:1000 for , streptavidin conjugated using Vectastain kit (PK-6101,Vector laboratories, Burlingame, CA) and developed using Peroxidase kit (Vector laboratories, Burlingame, CA). The sections were then mounted, dehydrated and coverslipped. The antibodies used were rabbit anti-mouse GFAP (1:200, Immunostar Inc., Hudson, WI), rat anti-mouse CD68 (1:1000, ABD serotec, Oxford, England) anti-rabbit secondary from Vectastain kit (PK-6101, Vector laboratories, Burlingame, CA) and mouse absrobed anti-rat secondary (Vector laboratories, Burlingame, CA).

2.4.9 GALC activity

Brains and spinal cords were flash frozen in liquid nitrogen after perfusion. They were then homogenized and the supernatant was frozen at -70°C until ready to use. GALC activity was determined by cleaving radioactively labeled ^{3}H-galactosylceramide (Wenger, 1991). Excess uncleaved substrate was extracted using chloroform:methanol saturated with galactose. The free ^{3}H-Galactose activity was measured in a scintillation counter as counts per minute (CPM) and the specific activity of the enzyme was calculated as nanomoles of substrate cleaved per hour per mg of total protein.

Histochemical staining for GALC activity was performed using the previously described method (Dolcetta et al., 2004). Brains and spinal cords were processed for histology as above. Sections on slides were incubated in citrate-

phosphate (CP) buffer (pH 4.5) for 15 minutes. They were then transferred to a solution containing 5 mg/ml taurodeoxycholic acid and 5 mg/ml oleic acid in CP buffer for 15 minutes. They were then incubated for 2 hours in a solution containing taurodeoxycholate, oleic acid, 5mM potassium ferrocyanide, 5mM potassium ferrocyanide and 2 mg/ml X-Gal (Gold Biotechnology, St. Louis, MO) in CP buffer. Sections were counterstained with Nuclear Fast Red (Sigma, St. Louis, MO), dehydrated and coverslipped.

2.4.10 Histology

For Luxol Fast Blue and Periodic Acid-Schiff (LFB/PAS) staining, tissues were processed as above and embedded in paraffin. Ten-micron-thick sagittal sections of the brain and transverse sections of the spinal cord were stained using standard procedures (Lin et al., 2007).

2.4.11 Tremor monitoring

Quantitative analysis of tremor was performed using an ultrasensitive force-plate actometer essentially as described (Reddy et al., submitted). The animals were acclimated for at least 30 minutes in the same room prior to tremor monitoring. Data recording was conducted between 2 pm and 6 pm. Data were collected for 6 min, but only the first minute, when movement was maximal, was used for the tremor analyses. Briefly, 12-bit integer raw data files were acquired with a LabMaster interface (Scientific Solutions, Mentor, Ohio) that was controlled by a DOS-based Free Pascal program (http://www.freepascal.org). Custom-written Free Pascal programs was used to calculate distance traveled

and the number of low mobility bouts (see below).

The following data were extracted from the raw data files (Fowler et al., 2001): (a) Fz- the net force exerted by the animal. Each time series (Fz(t)) was Fourier transformed using the fft function in MATLAB (The Mathworks, Inc., Natick, MA). A 500-point Hanning time-domain data window was used. The individual frequencies obtained after Fourier transformation were plotted as a continuous function (power spectrum) after filtering to retain frequencies between 2.5 and 30.0 Hz. (b) The frequency at peak power was taken as the frequency at which the power was at its maximum. (c) Power between 13 and 20 Hz was obtained by integrating the area under the power spectrum curve between 13 and 20 Hz. The aforementioned power spectrum variables (a-c) were computed for each individual mouse, and these variables were then subjected to standard statistical treatments (see below).

2.4.12 Lifespan and behavioral testing

The life span was measured by noting the date of death or sacrifice. Animals were humanely sacrificed if they had hindlimb paralysis or appeared moribund. Body weight was measured weekly. Behavioral testing was performed using previously established protocols (Lin et al., 2007). Accelerating rotarod and wire hang tests were performed every five days starting at 25 days of age. In the accelerating rotarod (3-9 rpm), the maximum time for the animal to fall off the rotarod was noted. In the wire hang test, the latency of the animal to fall, from holding an inverted cage lid, was noted. The maximum latency for both the tests was 60 seconds and the best value from three trials was used for analysis.

An n of 10-15 were used per group. Repeated measures analysis could not be performed due to attrition. Insteasd, ANOVA was performed across groups at two pre-determined time points (35d and 70d).

2.4.13 Diffusion Tensor Imaging (DTI)

Briefly, five 36-day-old animals from different treatment groups underwent DTI, as described previously (Hofling et al., 2009), with isoflurane/oxygen anesthesia. Diffusion weighted images were obtained using Stejskal-Tanner spin-echo diffusion weighted sequence (Stejskal and Tanner, 1965) in a Oxford Instruments 200/330 magnet (4.7 T, 40 cm clear bore) equipped with a 10-cm inner diameter, actively shielded Magnex gradient coil (maximum strength = 60 G/cm; rise time = 200 ms). The magnet, gradient coil, and gradient power supply were interfaced with a Varian Unity INOVA console (Palo Alto, CA, USA) controlled by a Sun Blade 1500 workstation (Sun Microsystems, Santa Clara, CA, USA). Multiple transverse slices covering L1 - L3 spinal cord levels were obtained with the following parameters: TR =1500 ms (determined by the respiratory rate of the mouse), TE = 37 ms, slice thickness = 1.0 mm, field of view = 1 cm x 1 cm, data matrix = 128 ’ 128 (zero-filled to 256 ’ 256). Diffusion-sensitizing gradients were applied in six orientations: (Gx,Gy,Gz) = (E,E,0), (E,0,E), (0,E,E), (-E,E,0), (0,-E,E), and (E,0,-E) where E = 0.707 with a gradient strength = 13.5 G/cm, gradient duration (d) = 7 ms, and gradient separation (D) = 18 ms resulting in b values of 0 and 1000 s/mm2. The diffusion tensor for each pixel was estimated using a weighted linear least-squares method (Koay et al., 2006). Eigenvalue decomposition was then applied to the tensor, yielding a set of eigenvalues (l1,

l2, l3) and eventually axial diffusivity (λ || = l1), and radial diffusivity (λ = (l2 + l3)/2) diffusivity for each pixel. Regions of interest (ROIs) for dorsal spinal cord white matter (DWM) and ventrolateral spinal cord white matter (VLWM) were drawn using ImageJ software. The DTI parameters for each ROI were averaged across three spinal cord levels (L1-L3), including eight 1-mm consecutive slices.

2.4.14 Statistical methods

Graphpad prism (GraphPad Software, Inc., La Jolla, CA) and R (www. R-project. org) software were used to generate graphs and perform statistical analyses. Survival curves were generated by Kaplan-Meier method and analysis was done using log-rank test. Multiple group comparisons were done using ANOVA, and was followed by Bonferroni's multiple comparison procedures. Analysis of behavioral data was done using one-way ANOVA at specific time points with post-hoc Bonferroni comparisons.

2.5 Results

2.5.1 GALC activity

To provide a sensitive test for evaluating conditions with decreased GALC activity, we conducted an ANOVA followed by pair-wise comparisons on the untreated wt, untreated mut, and BMT-mut groups. A significant ANOVA (p=0.0048) indicated that the groups differed in GALC activity. Post-hoc comparisons showed that GALC activity in the untreated mut group was significantly less than that of

the untreated wt group, and compared to the untreated mut group, there was no significant increase in GALC activity in the BMT-mut group (Figure 2.1 A). A similar ANOVA model was used to evaluate treatments that increased GALC activity and included untreated wt, AAV-mut, and AAV+BMT mut groups. In the AAV-mut and AAV+BMT-mut groups, GALC activity was significantly different ($p<0.0001$) and approximately five-fold greater than untreated wt levels. There was no significant difference between the AAV-mut and AAV+BMT-mut groups (Figure 2.1 B) The distribution of enzyme activity in the brain and the spinal cord was evaluated using a histochemical stain for GALC (Dolcetta et al., 2004; 2.1 C-N). Galactosylceramidase activity in the forebrain is concentrated in the lateral ventricles in the AAV-mut and AAV+BMT-mut groups (asterisk; Figure 2.1 E and F). There are also GALC-positive cells spread throughout the cortex and hippocampus. In the hindbrain, the enzyme activity is prominent in the ependyma of the fourth ventricle (asterisk in Figure 2.1 I and J). In the spinal cord, intense enzyme activity is seen in the meninges (Figure 2.1 M and N). There appears to be a spread of the activity along the initial part of the spinal nerve roots to the spinal grey matter (Figure 2.1 M and N, arrowheads).

2.5.2 Hematopoietic engraftment and donor-derived cells in the CNS

Hematopoietic chimerism and donor cell infiltration into the CNS were measured at 36 days of age using flow cytometry by determining the percentage of GFP(+) cells in the bone marrow and brain, respectively (Figure 2.2). All groups receiving BMT had hematopoietic chimerism between 3 and 29%. There was

no significant difference in the levels of bone marrow engraftment between the various groups receiving BMT (Figure 2.2 A). There was no significant increase in GFP (+) cells (FL1 channel) in the brains of animals receiving BMT compared to background fluorescence (Figure 2.2 B).

2.5.3 Psychosine levels

Psychosine is a toxic metabolite that is known to accumulate in the CNS of the twitcher mice (Igisu and Suzuki, 1984) and is used as a biochemical surrogate to assess efficacy of treatment (Ichioka et al., 1987). Statistical analyses similar to that performed for GALC activity were used to compare psychosine levels between different groups. Psychosine levels in the brain and the spinal cord (Figure 2.3 A and C) showed that the levels are significantly increased in the untreated mut group compared to the untreated wt group. In the brains and spinal cords of the AAV-mut and in AAV+BMT-mut groups (Figure 2.3 B and D), the levels of psychosine are significantly less than untreated twitcher mice and approach those of normal animals. Interestingly, BMT alone does not reduce psychosine levels in either brain or spinal cord compared to untreated twitcher mice (Figure 2.3 A and C).

2.5.4 Histology-LFB and PAS

Brains and spinal cord of various treatment groups were examined for myelin architecture and globoid cells using LFB/PAS staining. The corpus callosum of the brains of untreated wt mice (Figure 2.4 A) showed extensive staining with LFB and no PAS-positive cells. Three 36-day-old untreated mut brains

had numerous PAS-positive cells within the white matter (arrowheads in Figure 2.4 B). Occasional PAS-positive cells were also seen in the cortex. Two of the three mice in the AAV-mut group (Figure 2.4 C) and all three mice examined in the AAV+BMT-mut group (Figure 2.4 D) appeared to have a slight reduction in the number of PAS-positive macrophages in the white matter. Two of the three mice in the AAV+BMT-mut group also had cerebellar dysplasia with loss of the normal cerebellar architecture. The brains of the BMT-mut group animals were not examined.

There appeared to be a slight reduction in the number of PAS+ cells in the spinal cords of all three animals from both the AAV-mut and AAV+BMT-mut groups (Figure 2.4 G and H). The three mice examined from the BMT-mut group failed to show any obvious reduction in the PAS-positive cells in the spinal cord (data not shown), and the sections appeared histologically indistinguishable from those seen in the untreated mut group (Figure 2.4 F).

2.5.5 Diffusion Tensor Imaging (DTI) of the Spinal Cord

Using Diffusion tensor imaging, axial diffusivity ($\lambda||$) and radial diffusivity ($\lambda\perp$) were measured in vivo in the dorsal (DWM) and ventrolateral white matter (VLWM) from all study groups. The radial and axial diffusivity heatmaps are shown in Figure 2.5 A-H. In the DWM, axial diffusivity of the untreated mut and the AAV-mut groups show a significant reduction compared to the untreated wt group (Figure 2.5 I). Interestingly, there is a significant increase in the axial diffusivity in the AAV+BMT-mut group compared to the untreated mut group (Figure 8I). In the VLWM, a significant decrease in the axial diffusivity was observed

in the untreated mut group compared with the untreated wt group (Figure 2.5 J). In both the AAV-mut and AAV+BMT-mut groups, $\lambda||$ was comparable to that of the untreated wt group (Figure 2.5 J).

The in vivo radial diffusivity in the DWM of the untreated mut group (Figure 2.5 K) was significantly higher than that of the untreated wt group. There was no significant difference between the untreated wt group and the AAV-mut or AAV+BMT-mut groups. In the VLWM, a significant increase in radial diffusivity was seen in untreated mut mice relative to the untreated wt, AAV-mut, and AAV+BMT-mut groups (Figure 2.5 L).

2.5.6 Lifespan and Behavior

Twitcher mice have a significantly shortened median lifespan (41d) compared to normal littermates. There is a significant ($p<0.001$) increase in median lifespan to 71 days (Figure 2.5 A) in the AAV-mut group. There is a further increase in the median lifespan to 123 days (range: 92-282 days) in animals from the AAV+BMT-mut group. The increase in median lifespan of the AAV+BMT-mut group compared to the AAV-mut group was highly significant ($p<0.001$).

Untreated mut mice have significant behavioral deficits as measured by the rotarod and wire-hang tests (Figure 2.5 B and C). At 35 d, the AAV-mut and AAV+BMT-mut groups performed significantly better than untreated mut mice on the accelerating rotarod. At 70 days of age, the AAV-mut and AAV+BMT-mut groups had significantly reduced latencies on the accelerated rotarod (Figure 2.5 B) compared to the untreated wt group. Interestingly, long-lived AAV+BMT-mut animals showed a sustained higher level of performance on the rotarod

until they were terminally ill. In contrast, the untreated mut and AAV-mut groups showed a steady decline in motor function as they aged. These observations suggest that hindlimb paralysis or weakness, which is prominent in the untreated mut group, appeared much less severe in the AAV+BMT-mut group.

The results from the wire-hang test were consistent with these observations in that latencies to fall were significantly longer in the AAV+BMT-mut group compared to the untreated mut and the AAV-mut groups at the 35d time point (Figure 2.5 C). There was no significant difference in performance between the AAV-mut group and the untreated mut group. At 70 days, the latency on the wire-hang test was significantly higher in the AAV+BMT-mut group compared to the AAV-mut group, but the improvement was modest.

There is a significant increase in body weights in both the AAV-mut and AAV+BMT-mut groups at day 35 (Figure 2.5 D) compared to the untreated mut group. The animals in the AAV-mut group steadily lose lost weight beyond 40d whereas the animals in AAV+BMT-mut group maintained their weight for the duration of the study.

2.5.7 Effect of treatment on tremor

Tremor is one of the characteristic phenotypes of the twitcher mouse. The effect of various treatments on the tremor phenotype was evaluated using a specially constructed force-plate actometer (Reddy et al., submitted). The force variation created by the individual mice was analyzed after Fourier transformation of the raw data and the power spectra were generated from the output. The averaged power spectra of the untreated wt and AAV-mut groups appear similar (Figure

2.7 A). The untreated mut and AAV+BMT-mut groups appear similar to each other but different from the untreated wt and AAV-mut groups. Compared to the untreated wt group, the frequency of peak power and the power between 13 to 20 Hz were significantly increased in the AAV+BMT-mut group, but not in the AAV-mut group (Figure 2.7 B and C). There was no significant difference between the AAV-mut and AAV+BMT-mut groups with respect to the total distance traveled (Figure 2.7 D) or the number of low mobility bouts (data not shown). The similarities (i.e., non-significant differences) between untreated wt and AAV-mut shown in Figure 2.7 A-D, collectively represent the therapeutic benefit of CNS-directed AAV2/5-mediated gene therapy on the tremor phenotype. The therapeutic benefit of CNS-directed AAV2/5-mediated gene therapy on tremor phenotype seemed to be negated with the addition of BMT.

In order to directly assess the effect of myeloreductive conditioning and BMT on tremor, the phenotype of wildtype mice that received BMT (BMT-WT) was assessed. The BMT-WT group had greater power in both the frequencies around 10-12 Hz and in the higher frequencies in the 13-20 Hz range compared to the untreated wt group (Figure 2.7 A). The power between 13 and 20 Hz (Figure 2.7 C) was significantly increased in the BMT-WT group compared to the untreated wt group. The total distance traveled was significantly decreased in the BMT-WT group compared to the untreated wt group (Figure 2.7 D).

2.5.8 CNS inflammation

Central nervous system inflammation is a prominent pathologic feature of GLD. Numerous PAS-positive globoid cells (macrophages with engulfed myelin de-

bris) are found in the white matter (Figure 2.4; Suzuki et al., 2000). Using flow cytometry, the various inflammatory cells in the brain were quantified (Figure 2.8). Compared to the untreated wt group, the untreated mut group showed a trend towards an increase in CD45^{hi}CD11b+ cells (activated microglia/macrophages; Figure 11B and F). There is a significant increase in activated microglia/macrophages, CD4, and CD8 T-cells in the AAV-mut group compared to the untreated wt group (Figure 2.5 A, C and D). The presence of CD4 and CD8 T-cells was unique to the AAV-mut group. Interestingly, the increases in activated microglia, CD4 and CD8 T-cells were reversed in the AAV+BMT-mut group (Figure 2.8 A-D and F). There was no increase in neutrophil (Gr1^{hi}F4/80-) numbers in any groups compared to the untreated wt group (data not shown).

Another important component of inflammation are the cytokines and chemo kines. Several cytokines and chemokines were found to be altered in the brains of the twitcher mouse (Figure 2.9). The most highly elevated cytokines in the untreated mut group compared to the untreated wt groups were KC (Keratinocyte Chemoattractant; CXCL1) and IL-12(p40). Interestingly, KC and IL-12 (p40) are significantly decreased ($p<0.001$) in the AAV-mut and AAV+BMT-mut groups compared to the untreated mut group. There was a significant elevation in KC in the BMT-mut group compared to the untreated mut group. The cytokine MCP-1 was detected in the untreated mut and BMT-mut groups, but not in untreated wt, AAV-mut and AAV+BMT-mut groups. The cytokines TNF-α and MIP-1β were decreased in the untreated mut group compared to the untreated wt group. The levels of these cytokines in the AAV-mut and AAV+BMT-mut

groups were similar to that of the untreated wt group. Interestingly, no increase in these two cytokines was seen in the BMT-mut group.

The brains and spinal cords of the animals of various groups were immunostained for Glial Fibrillary Acidic Protein (GFAP). Regions showing increased GFAP staining represent sites of active inflammation. GFAP staining was extensive in the brain and spinal cord of the untreated mut group (Figure 2.10 B, F J and N). In the brains of the AAV-mut group (Figure 2.10 C and G), GFAP staining appeared to be similar or slightly decreased compared to that of the untreated mut group. However, in the brains of the AAV+BMT-mut group (Figure 2.10 D and H), the staining was much less than either the untreated mut or the AAV-mut groups, although it seemed to be slightly more than that of the untreated wt group. In contrast, GFAP staining in the AAV-mut spinal cord seems to be similar to the AAV+BMT-mut group and much less than the untreated mut group (Figure 2.10 J, K and L).

Similarly, when the brains and the spinal cords were immunostained for CD68 (macrosialin), increased immunoreactivity was seen in untreated mut group (Figure 2.11 B, F and J) compared to the untreated wt group (Figure 2.11 A, E and I). In the AAV-mut group, the CD68 immunostaining was decreased in the forebrain and spinal cord (Figure 2.11 C and J), but appeared to be increased in the hindbrain. This correlates well with the overall similarity in the microglial number by flow cytometry (Figure 2.11 F). In the AAV+BMT-mut group, there appeared to be an overall decrease in the CD68 immunostaining in forebrain, cerebellum and spinal cord compared to either untreated mut mice or AAV-mut mice (Figure 2.11 D, H and L).

2.6 Discussion

It is clear that, no single therapy to date can completely treat GLD. Previous studies have shown that combining BMT with substrate reduction therapy, lentiviral-mediated or AAV2/5-mediated gene therapy resulted in additive or synergistic improvements (Biswas and LeVine, 2002; Lin et al., 2007; Galbiati et al., 2009). Combining BMT with AAV2/5 gene therapy (Lin et al., 2007) resulted in synergistic benefits. In the previous study (Lin et al., 2007), the AAV2/5-mediated gene therapy component was limited to the forebrain. Perhaps not surprisingly, there were no decreases in the disease markers in the cerebellum and spinal cord. In the current study, myeloreductive BMT was combined with AAV2/5-mediated gene therapy directed to the forebrain, cerebellum and spinal cord. The increased gene delivery combined with BMT in the current study further improved motor function and increased lifespan. To our knowledge, this is the greatest clinical improvement observed in the twitcher mouse on the congenic C57BL/6 background. This improvement extended to the cerebellum and spinal cord. Improved myelination was observed in the spinal cord as evidenced by decreased radial diffusivity on MRI. Radial diffusivity represents water diffusion perpendicular to the axon. When myelin damage occurs radial diffusivity increases (Hofling et al., 2009). Decreased axonal damage is also observed in the spinal cord as an increase in axial diffusivity. Axial diffusivity represents the water diffusion parallel to the axon. A decrease in axial diffusivity implies compromised axonal integrity (Hofling et al., 2009). It has been hypothesized that the accumulation of psychosine in oligodendrocytes is the primary insult leading to the disease. It was recently shown that psychosine preferentially

accumulates in lipid rafts and it was hypothesized that lipid raft perturbation is the cellular mechanism of psychosine toxicity (White et al., 2009). Both CNS-directed AAV2/5 gene therapy alone and in combination with BMT significantly reduced psychosine levels in the brain and spinal cord. It will be of interest to determine if the distribution of psychosine is also altered following therapy.

Although nearly every clinical measure (lifespan, motor function and body-weight) was significantly improved in the animals receiving AAV+BMT compared to animals receiving AAV alone, the tremor was more severe in the combination -treated animals. This is clearly associated with the bone marrow transplant procedure and is most likely due to the conditioning radiation. We showed previously that conditioning radiation, even relatively low doses (200-400 rads), in neonatal animals causes cerebellar dysplasia (Sands et al., 1993). The CNS damage might be even worse with myeloablative conditioning regimens. These data demonstrate the benefits and drawbacks of BMT and highlight the need for less invasive treatments.

The combination therapy also dramatically decreased CNS inflammation. There is normalization of several cytokines, in particular IL-12 (p40), KC (Keratinocyte chemoattractant; CXCL1) and MCP-1 (Macrophage Chemoattractant Protein). Interestingly, the primary sources of these three cytokines in the brain are astrocytes and macrophages (Leonard and Yoshimura, 1990; Filipovic et al., 2003; Gee et al., 2009). The decrease in the above cytokines and chemokines correlates with the decreased number of macrophages and decreased astrocyte activation observed in the AAV-mut and AAV+BMT-mut groups, but not in the BMT-mut group. The cytokine KC is increased in the untreated mut group

compared to the untreated wt group. The primary role of KC is in neutrophil chemotaxis (Boisvert et al., 1998; Liu et al., 2010). Interestingly, there is no increase in neutrophil numbers in the brains of the untreated mut mice. However, KC is also known to affect oligodendrocyte proliferation and migration. Consistent with KC's actions on oligodendrocytes, KC is elevated in demyelinating disease models like the jimpy mice (Wu et al., 2000a) and in brains of patients with multiple sclerosis (Filipovic et al., 2003). It is possible that the primary role of KC in GLD is to act as a chemoattractant and mitogen during oligodendrocyte development and/or repair(Tsai et al., 2002). The decrease in KC in the treated animals is consistent with reduced myelin damage.

The chemokine MCP-1 is a macrophage chemoattractant and is increased in the untreated mut and BMT-mut groups, both of which have greater numbers of histologically demonstrable globoid cells and increases in CD45^{hi}CD11b+ cells by flow cytometry. The levels of the pro-inflammatory cytokines TNF-α and MIP-1β are decreased in the untreated mut group compared to the untreated wt group. Given the profound inflammatory response associated with GLD, one might predict that TNF-α would be increased. However, TNF-α signaling through TNF receptor 1 may not play a significant role in the progression of GLD. This is supported by the fact that the lack of TNF receptor 1 does not alter the course of the disease in the twitcher mouse (Pedchenko et al., 2000). The reason for the decrease of TNF-α in the untreated mut group could be indicative of the profound and persistent demyelination associated with GLD. TNF receptor 2 is upregulated during demyelination and remyelination (Arnett et al., 2001) and may act as a sink effectively reducing TNF-α levels.

The current study clearly shows that, CNS-directed AAV2/5-mediated gene therapy is associated with an increase in activated microglia, as well as CD4+ and CD8+ T-cells in the twitcher mouse. CD4 and CD8 T-cell responses are typically associated with viral infections (Doherty, 1985). An increase in CD4 and CD8 T-cells was also observed in normal control mice following an injection of the same vector expressing palmitoyl protein thioesterase 1, a ubiquitously expressed lysosomal enzyme (data not shown). Although AAV2/5-mediated gene therapy resulted in GALC levels several fold higher than normal, the increased inflammatory response could contribute to the limited clinical improvements observed with this therapy alone. When BMT is added to the regimen, the AAV2/5-associated inflammation is virtually eliminated. This is especially interesting considering the fact that BMT alone provides little or no GALC activity, no decrease in psychosine and seems to exacerbate certain aspects of the inflammatory response (KC, MCP-1 and IL-12). These data strongly support the hypothesis that BMT has a direct immunomodulatory effect on AAV2/5-mediated gene therapy and could explain the dramatic synergy. It also suggests that in order for BMT to exert its immunomodulatory effects, GALC activity must also be present. The GALC activity is likely necessary to reduce psychosine levels, thus decreasing the toxic insult.

Although the immunomodulation by BMT seems to be a plausible explanation, there appears to be a discrepancy between the cellular inflammation and the cytokines. The AAV-mut group shows a decrease in some of the elevated cytokines but an increase in the cellular inflammation. On the other hand, the AAV+BMT-mut group shows a decrease in cytokine levels as well as a decrease

in cellular inflammation. The cytokine elevations appear to correlate with the extent of demyelination rather than the infiltration of inflammatory cells.

In a different therapeutic paradigm, BMT using high dose (800-900 rads) myeloablative radiation in 9-10 day old mice is known to extend the lifespan in the twitcher mice (Yeager et al., 1984). Galactosylceramidase-positive bone marrow derived-cells have been shown to enter the CNS (Hoogerbrugge et al., 1988) and can result in GALC activity in the CNS as high as 15% of wild-type (Hoogerbrugge et al., 1989). However, this level of enzyme results in an increase in median lifespan to only about 80 days (Yeager et al., 1984; Hoogerbrugge et al., 1989). Interestingly, a similar BMT regimen is also associated with downregulation of several pro-inflammatory cytokines in the twitcher mice (Wu et al., 2001). Therefore, either decreasing inflammation or supplying enzyme, or both, appears to be responsible for the efficacy of BMT following high dose conditioning. Based on the data presented here, we believe that immunomodulation plays a significant role in the efficacy of BMT. It will be particularly interesting to perform BMT experiments in the twitcher mice using conditions that allow for higher levels of engraftment during the neonatal period (Bruscia et al., 2006). This will help determine the respective contributions of enzyme activity and immunomodulation. To summarize, myeloreductive BMT effectively augments the therapeutic benefit seen with CNS-directed AAV2/5-mediated gene therapy in GLD. Several reasons make the use of a myeloreductive conditioning regimen more attractive than the currently used myeloablative regimen. It is known that BMT is most effective when performed during the pre-symptomatic neonatal period and fully myeloablative neonatal BMT has a high mortality rate (Escolar et

al., 2005; Weinberg, 2005). Myeloreductive conditioning regimens are known to result in lower mortality, lower incidence of graft-versus-host disease, and stable engraftment (Jacobsohn et al., 2004; Shenoy et al., 2005). Therefore, we propose that combination therapy using an AAV vector and myeloreductive BMT during the neonatal period is a viable approach for treating GLD. Of course, this approach would be greatly facilitated by widespread implementation of newborn screening programs (Duffner et al., 2009). Future studies might further improve on this regimen by adding other therapies like substrate reduction (Young et al., 2004), increasing BM engraftment, increasing the number of donor-derived cells entering the brain (Young et al., 2004), and using transduced bone marrow expressing high levels of enzyme (Naldini, 2011). Two interesting observations from the study were pursued in greater detail. The alteration of tremor phenotype by BMT was contradictory to what was expected and the further characterization of the phenotype is described in chapter 4. The dramatic elevation of KC and its reduction with therapy was very interesting and the role of KC in the disease was further characterized as described in chapter 5.

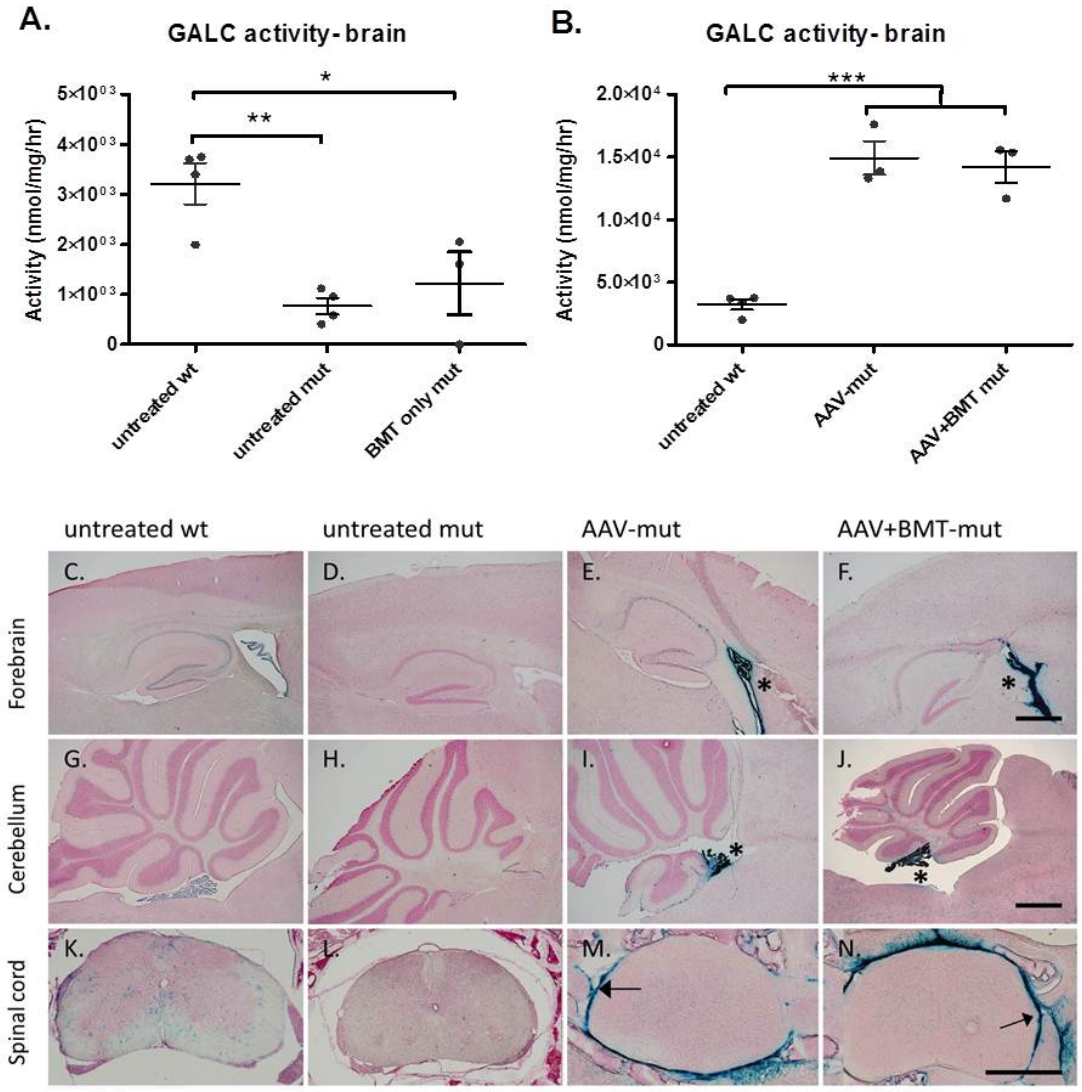

Figure 2.1: GALC activity and distribution. GALC activity was significantly higher in the untreated wt mice compared to the untreated mut and BMT-mut groups (A). There was no significant difference between the untreated mutant and BMT-mut groups (A). A separate analysis showed that the GALC activity in the brains of AAV-mut and AAV+BMT-mut groups was approximately five-fold greater and significantly different from that of the untreated wt group (B). Horizontal bars represent means and error bars represent SEM (*$p<0.05$, **$p<0.01$ and ***$p<0.001$). GALC activity can be seen histochemically in the forebrain (C), cerebellum (G) and spinal cord (K) of the untreated wt group. In contrast no GALC staining is observed in the forebrain (D), cerebellum (H) or spinal cord (L) of the untreated mut group. Intense GALC staining is observed in the ependyma of lateral and fourth ventricles of the AAV-mut and AAV+BMT-mut groups (asterisks; E, F, I and J). Intense staining was also observed in the meninges of the spinal cord and along the spinal nerve roots (arrows; M and N) of AAV-mut and AAV+BMT-mut mice. Panels C-J were imaged at the same magnification, scale bar in F and J is approximately 600 μm. Panels K-N were imaged at the same magnification, scale bar in N is approximately 600 μm.

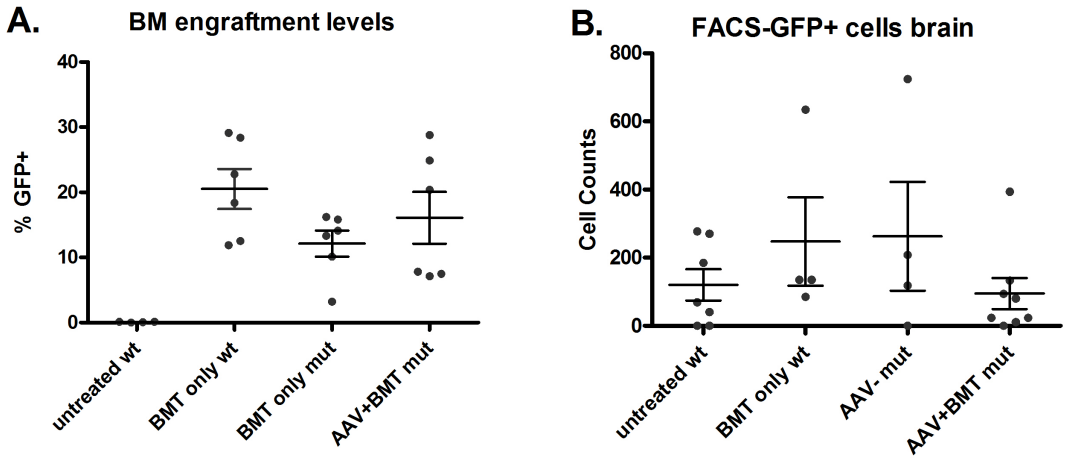

Figure 2.2: Engraftment and GFP+ cells in the brain. The number of GFP+ donor cells present in the bone marrow and brains were determined using flow cytometry. The levels of bone marrow engraftment at day 36 were between 3 and 29%. There is no significant difference in donor engraftment in various groups receiving BMT (A). The number of cells present in FL1 channel ("GFP channel") in the brain was similar in all the groups tested. There is no significant difference in the GFP+ cells in the brains between the treated and untreated groups (C).

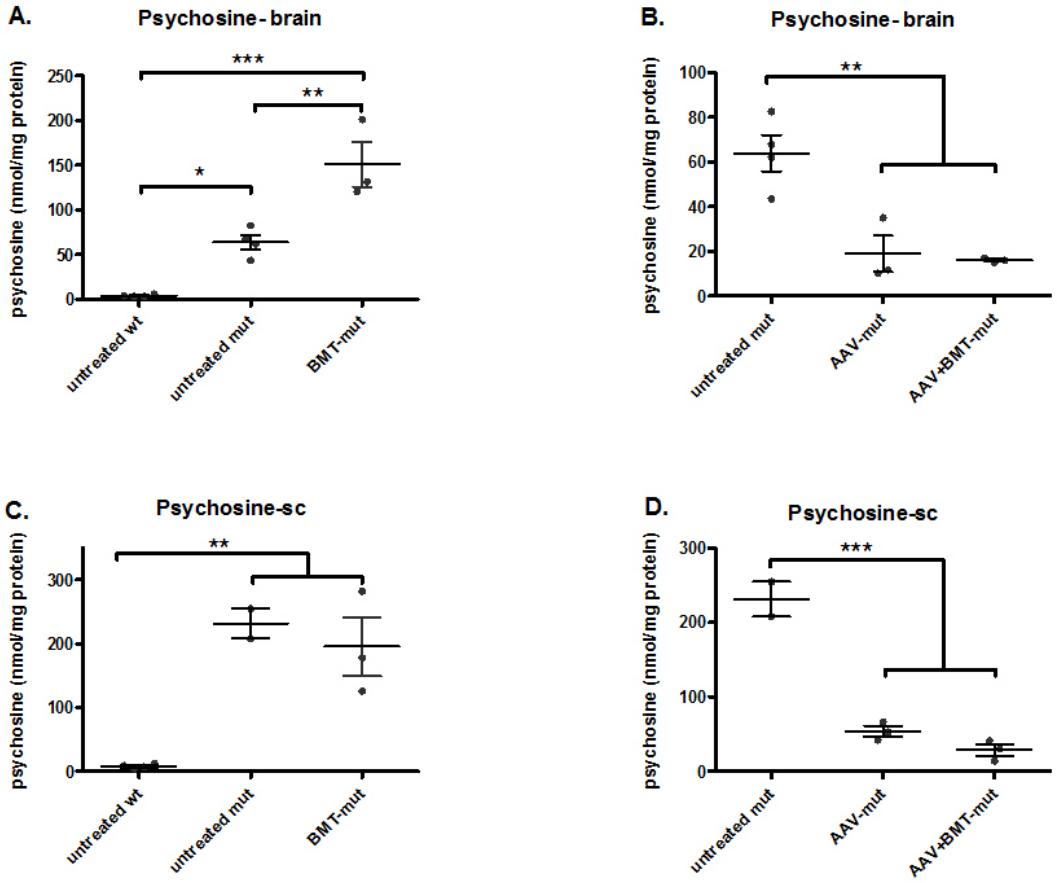

Figure 2.3: Psychosine levels in the brain (Psychosine-brain, A and B) and the spinal cord (Psychosine-sc, C and D) were measured using mass spectrometry. In the brain, the psychosine levels were highly elevated in the untreated mut compared to untreated wt group, while levels were significantly increased in the BMT-mut group relative to both the untreated wt and untreated mut groups (A). In spinal cord, both the untreated mut and BMT-mut groups had significantly increased psychosine levels compared to the untreated wt mice (C). The analyses conducted on treatments that decreased psychosine levels showed that both the AAV-mut and AAV+BMT-mut groups had significantly reduced levels of psychosine compared to the untreated mut mice in both brain (B) and spinal cord (D). There was no significant difference in psychosine levels between the AAV-mut and AAV+BMT-mut groups in either the brains or spinal cord. The horizontal bars represent the means and the error bars represent SEM. (*$p<0.05$, **$p<0.01$ and ***$p<0.001$).

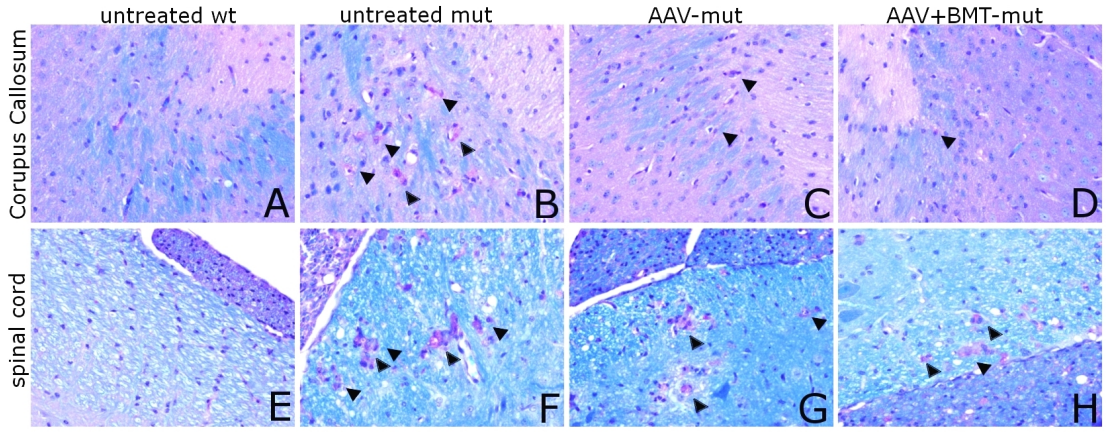

Figure 2.4: Luxol fast blue-Periodic Acid Schiff staining of the anterior commissure of the corpus callosum of representative animals is shown (A-D). The untreated wt animal (A) has essentially no PAS-positive macrophages within the white matter, the untreated mut (B) mouse shows prominent PAS-positive macrophages within the white matter (arrowheads), and both the AAV-mut (C) and AAV+BMT-mut (D) mice show a reduction in the number of PAS-positive macrophages in this region of the brain. Sections from the lateral white matter of the spinal cord from an untreated wt mouse (E) show no PAS-positive macrophages within the white matter whereas sections from the same area of an untreated 36-day-old twitcher mouse (F) show numerous PAS-positive macrophages (arrowheads). There appears to be a slight reduction of PAS-positive cells in the spinal cords of both the AAV-mut (G) and AAV+BMT-mut groups (H).

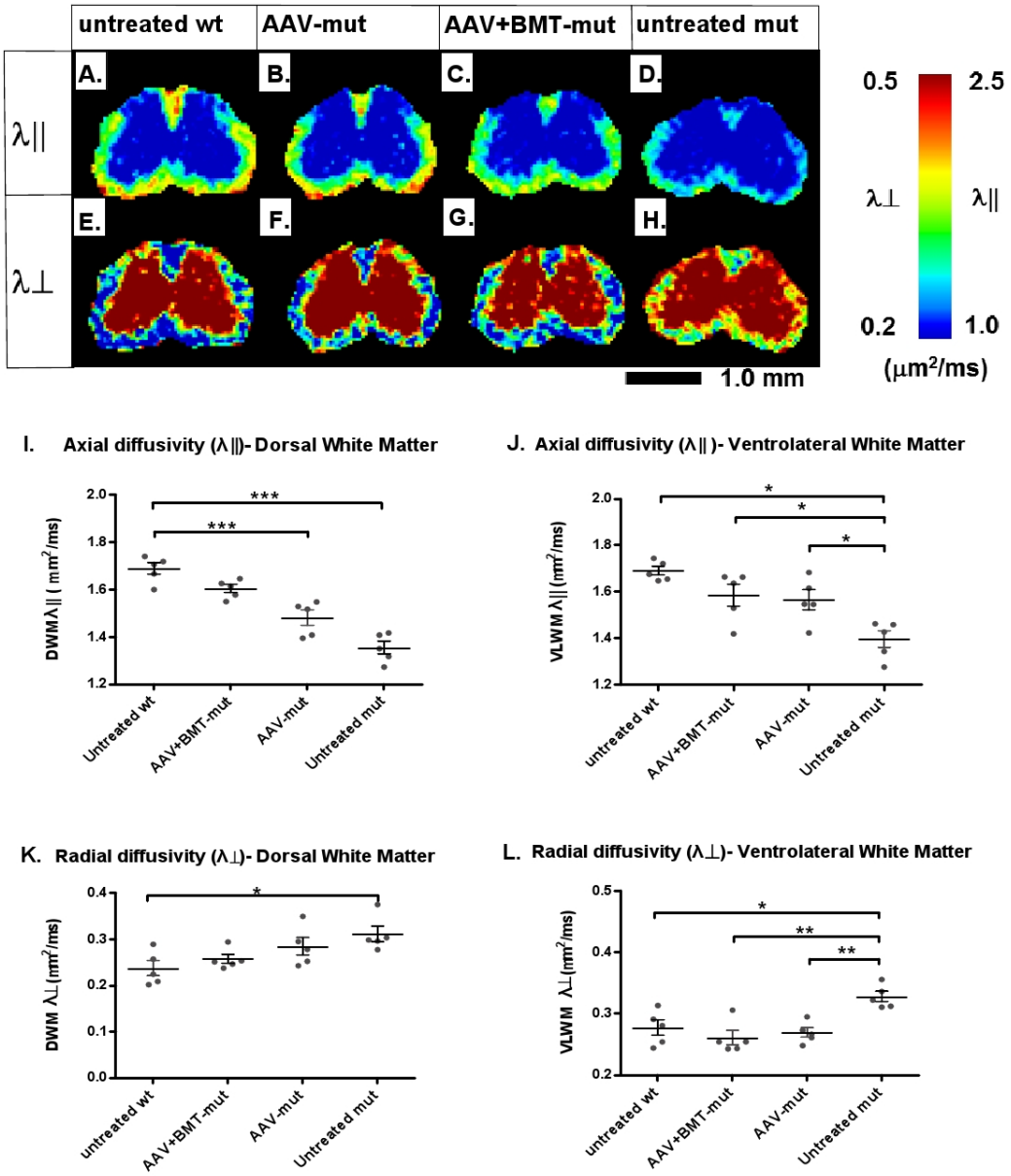

Figure 2.5: Diffusion Tensor Imaging. Heat maps of axial diffusivity ($\lambda||$, A-D) and radial diffusivity ($\lambda\perp$, E-H) in the spinal cord obtained by DTI. In the DWM (I), there is a significant decrease in the axial diffusion in the untreated mut group compared to the untreated wt group. The AAV-mut and AAV+BMT-mut groups show an increase in axial diffusion compared to the untreated mut group. In the VLWM (J), the axial diffusivity of the untreated mut is significantly decreased compared to the untreated wt and the treated groups. Radial diffusivity in the DWM (K) is significantly increased in the untreated mut compared to the untreated wt. The treated groups are intermediate between the untreated wt and untreated mut groups. In the VLWM (L), there is a significant increase in the radial diffusivity in the untreated mut compared to untreated wt. There is no significant difference between the untreated wt and the AAV-mut and AAV+BMT-mut groups. The horizontal bars represent the means and the error bars represent SEM. (*$p<0.05$, **$p<0.01$, ***$p<0.001$).

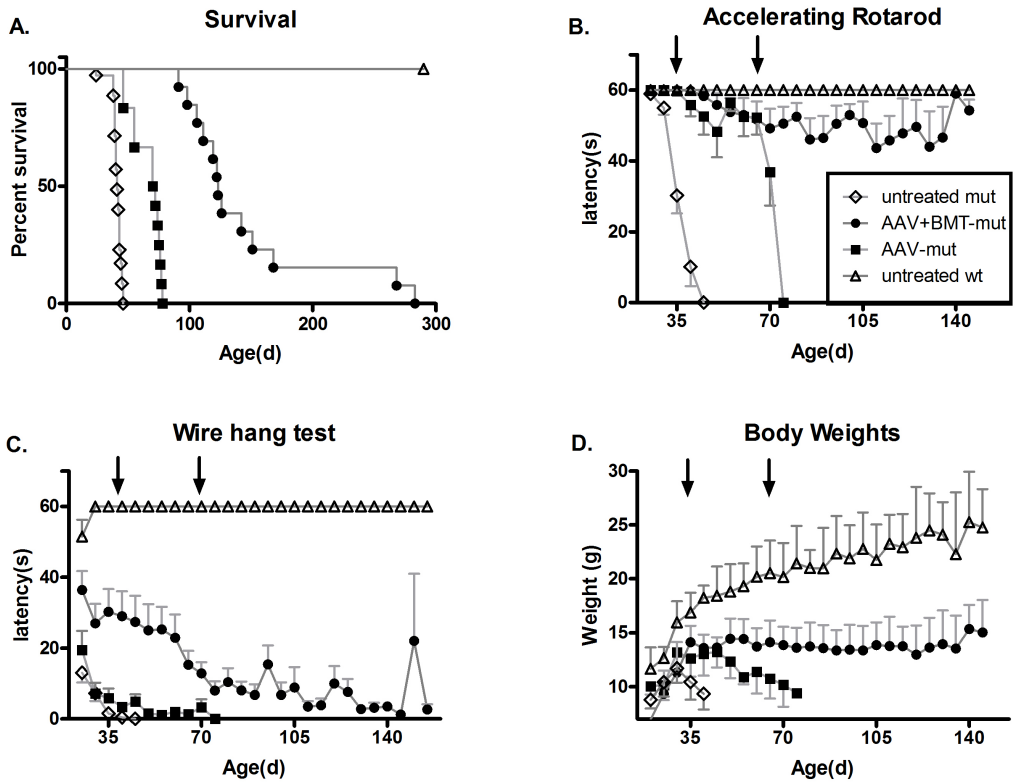

Figure 2.6: Survival and Behavior. Kaplan-Meier curves showing the survival of various treatment groups (A). The median lifespan of the AAV-mut group (71 d, range= 46-78d) was significantly greater than ($p<0.001$) that of the untreated mut group (41d, range=24-46 d). The median lifespan of the AAV+BMT-mut group (123 days, range=92-282 days) was significantly greater than that of the AAV-mut group ($p<0.001$). Behavior was evaluated using constant speed rotarod and wirehang test. Animals in the AAV-mut and AAV+BMT-mut group performed significantly better than the untreated mut group in the accelerating (B) rotarod motor function tests at 35 days and at 70 days of age (arrows). There was a statistically significant improvement in latency on wire-hang test only in the AAV+BMT-mut group (C) at day 35 of age. Body weights (D) in the AAV+BMT-mut group were significantly higher compared to the untreated mut at 35 days of age. There was no significant difference between the AAV-mut and untreated mut groups at 35 days of age. At 70 days of age, the body weights were significantly higher in the AAV+BMT-mut group compared to the AAV-mut group. The body weights were maintained in the long-lived animals from the AAV+BMT-mut group. Error bars represent SEM.

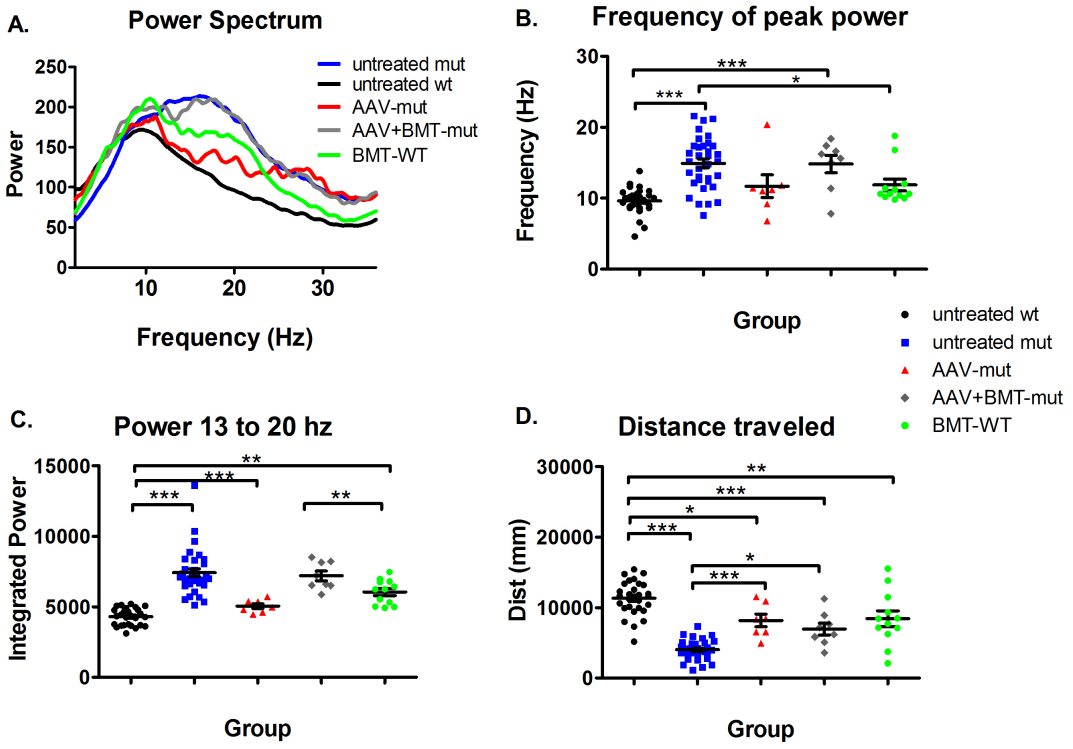

Figure 2.7: The averaged power spectrum (A) of the untreated mut group (blue line) is shifted towards higher frequencies with a broader bandwidth compared to the untreated wt group (solid black line). In the AAV-mut group (red line), the averaged power spectrum is similar to that of the untreated wildtype. In the AAV+BMT-mut group (solid gray line), the power spectrum is shifted towards higher frequencies compared to the AAV-mut group and is similar to the untreated mut group. Compared to the untreated wt group, there is a significant increase in the frequency of peak power (B) and the power between 13 and 20 Hz (C) in the AAV+BMT-mut group, but not the AAV-mut group. The distance traveled by the AAV-mut and AAV+BMT-mut groups (D) is significantly increased compared to the untreated mut group. BMT alone altered the tremor phenotype in the wildtype mouse. The averaged power spectrum (A) of the BMT-WT group (solid green line) is shifted upward and rightward compared to the untreated wt group (solid black line). The frequency of peak power (B) and the power between 13 and 20 Hz (C) were significantly increased in the BMT-WT group compared to the untreated wildtype group. The distance traveled by the BMT-WT group was significantly decreased compared to the untreated wt group (D). The horizontal bars represent the mean and the error bars represent SEM (*$p<0.05$, **$p<0.01$, ***$p<0.001$).

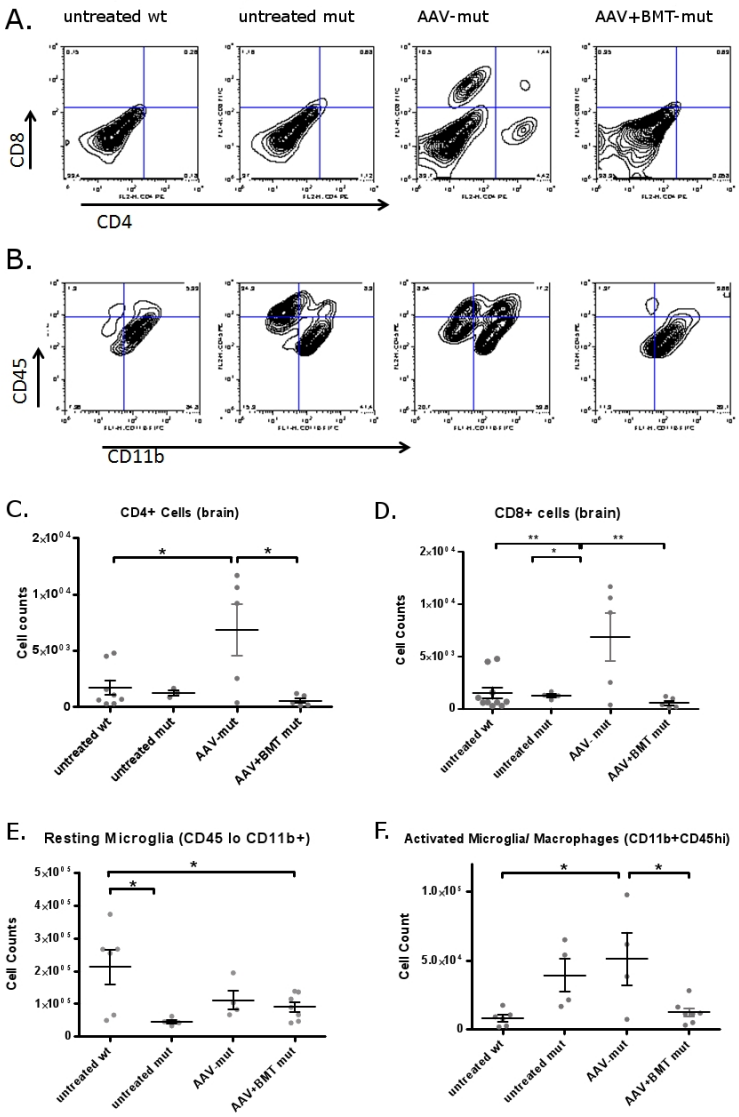

Figure 2.8: Flow Cytometry -brains. Representative bivariate plots show the relative numbers of CD4+ and CD8+ T-cells (A) and activated microglia ($CD45^{hi}$CD11b+) (B) in brains of untreated wt, untreated mut, AAV-mut and AAV+BMT-mut groups. Quantitation of T-cells shows that there is a significant increase in CD4 and CD8 T-cells (C and D) in the AAV-mut group compared to the untreated wt. There is no increase in CD4 and CD8 T-cells in the untreated mut and AAV+BMT-mut groups compared to the untreated wt group (B, C and D). There appears to be an increase in CD4, CD8 and activated microglia ($CD45^{hi}$CD11b+) in the AAV-mut group compared to other groups. Quantitation of resting microglia ($CD45^{lo}$CD11b+) (E) shows that there is a significant decrease in these cell numbers in the untreated mut and AAV+BMT-mut groups compared to the untreated wt group. Quantitation of activated microglia (F) shows that there is a significant increase in these cell numbers in the AAV-mut group compared to the untreated wt or AAV+BMT-mut group. There is no significant difference between the activated microglial numbers between untreated wt and AAV+BMT-mut groups. Horizontal bars represent means and the error bars represent SEM .(*$p<0.05$).

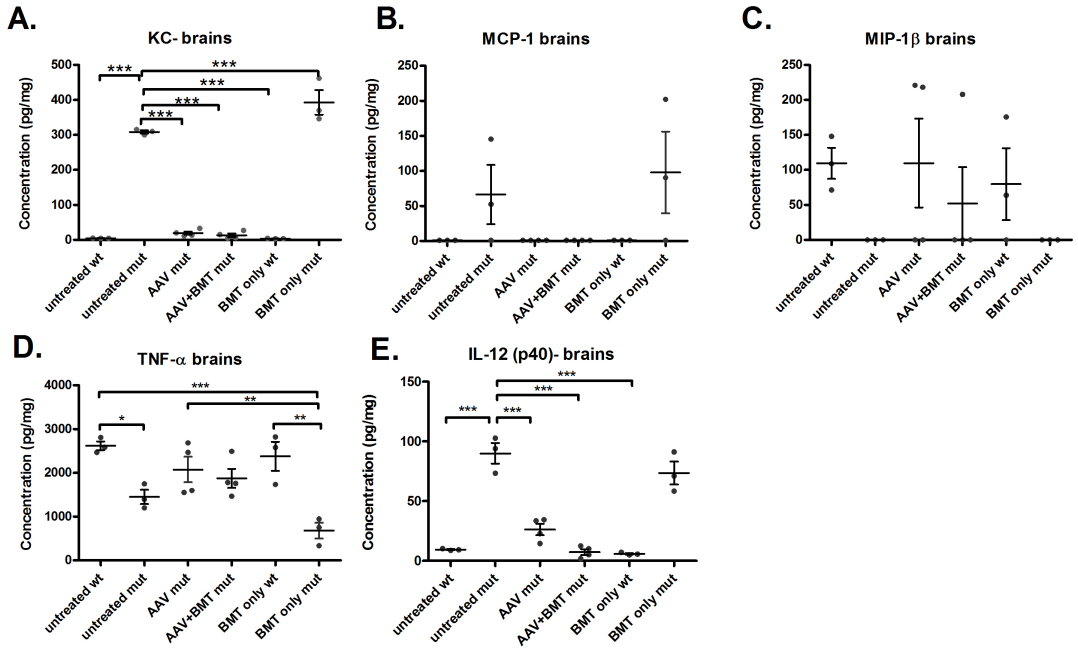

Figure 2.9: Chemokines and cytokines. There is a significant increase in KC (A) in the brains of the untreated mut animals compared to the untreated wt animals. The chemokine MCP-1 (B) is increased in the untreated mut group and is undetectable in the untreated wt group. In both the AAV-mut and AAV+BMT-mut groups, KC and MCP-1 levels are reduced similar to the untreated wt group. The BMT-mut group does not show a decrease in the above chemokines compared to the untreated mut group. The chemokine MIP-1β (C) is undetectable in the untreated mut group and is present in the AAV-mut and AAV+BMT-mut groups at levels comparable to the untreated wt group. The levels of MIP-1β in the BMT-mut group are similar to that of the untreated mut group. The cytokine TNF-α (D) is significantly decreased in the untreated mut group compared to the untreated wt group. In the AAV-mut and AAV+BMT-mut groups, the levels of TNF-α are similar to that of the untreated wt group. The levels of TNF-α in the BMT-mut group are similar to that of the untreated mut group. The cytokine IL-12(p40) (E) shows a trend similar to KC, with a significant increase in the untreated mut group compared to the untreated wt group. Levels of IL-12 (p40) in the AAV-mut and AAV+BMT-mut groups are similar to the untreated wt group. Horizontal bars represent mean and error bars represent SEM. (*p$<$0.05, **p$<$0.01, ***p$<$0.001).

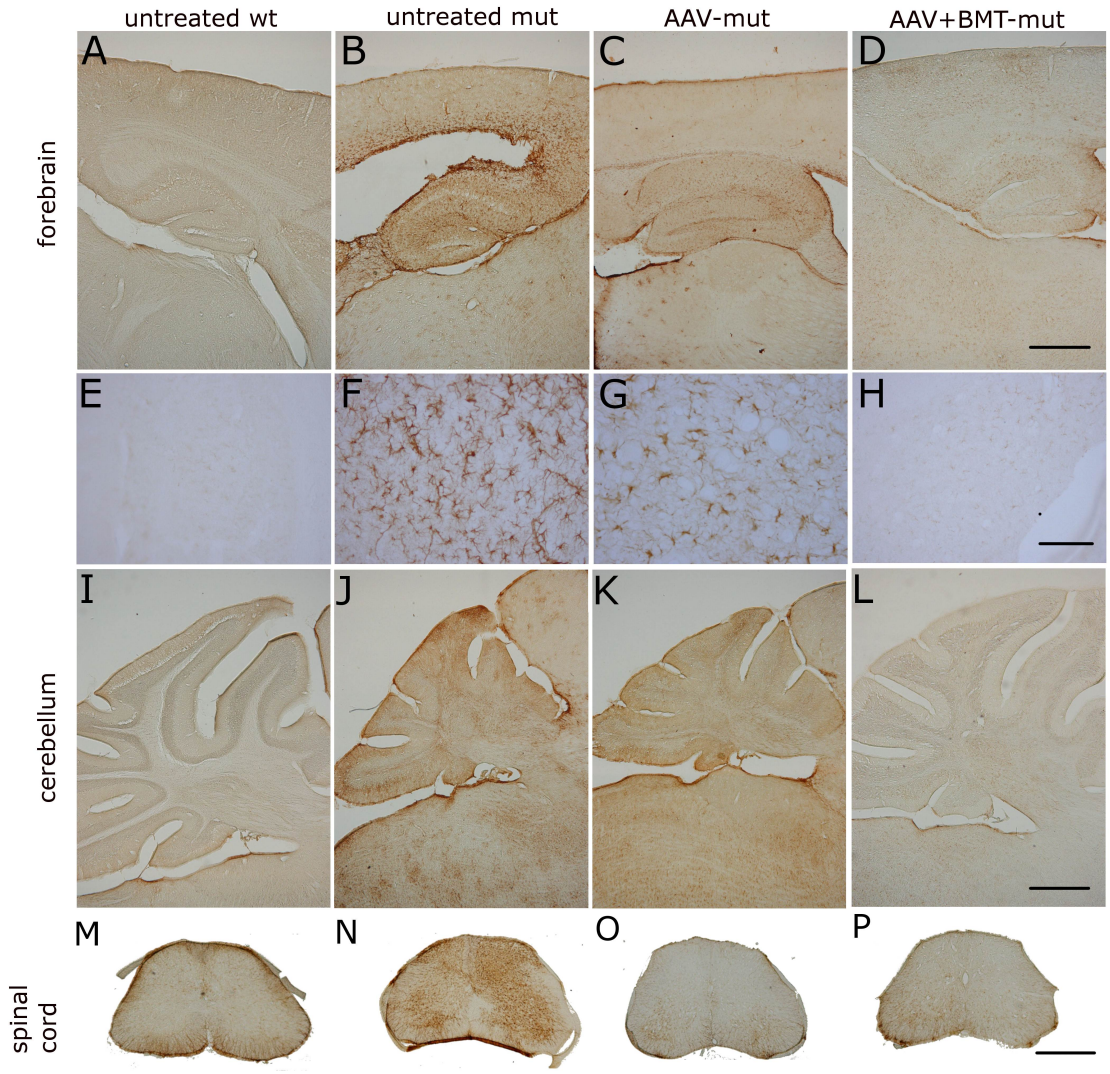

Figure 2.10: GFAP immunohistochemistry. Representative images of GFAP staining of brain and spinal cords are shown. Untreated mut animals have higher GFAP immunoreactivity in all the regions of the CNS (B,F,J and N) compared to untreated wt animals (A, E, I and M). Animals in the AAV-mut group (C, G, K and O) appear to have similar or slightly decreased GFAP staining compared to the untreated mut group. The AAV+BMT-mut group (D, H, L and P) has less intense GFAP staining compared to the untreated mut and AAV-mut groups. High magnification images (E, F, G and H) from the cortex show characteristic activated astrocyte morphology. The spinal cords of the untreated wt group have minimal GFAP staining (M) compared to the untreated mut group (N). The spinal cords of the AAV-mut (O) and AAV+BMT-mut (P) groups stain with similar intensity as that of the untreated wt group. Panels A-D and I-P were imaged at same magnification, scale bars in D, L and P are approximately 600 μm. Panels E-H were imaged at same magnification and scale bar in H is approximately 25 μm.

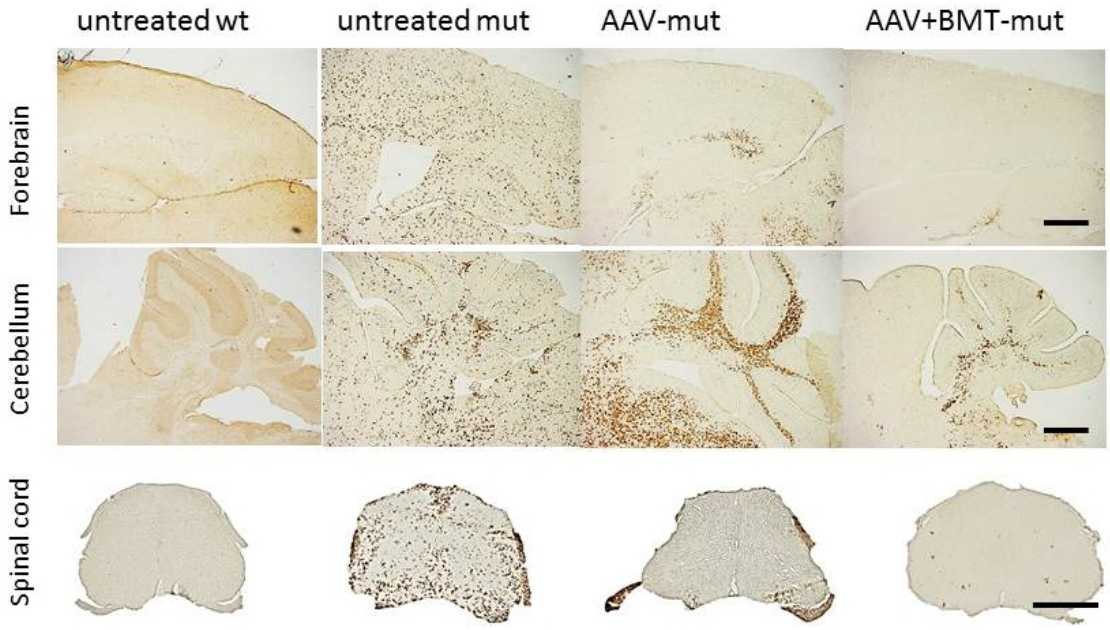

Figure 2.11: CD68 immunohistochemistry. CD68 staining of the forebrain (A-D), cerebellum (E-H) and the spinal cord (I-L) at 36 days of age show increased staining in the untreated mut group (B,F and J). In the AAV-mut cerebellum (G), the CD68 staining appears similar or increased in intensity to that of the untreated mut (F). Interestingly, there appears to be decreased staining in the spinal cord (K) and the forebrain (C). In the AAV+BMT-mut group, the CD68 staining is decreased in most regions and indistinguishable from untreated wt mice in certain regions. Panels A-H were imaged at the same magnification, scale bars in D and H are approximately 600 μm. Panels I-L were imaged at the same magnification, scale bar in L is approximately 600 μm.

Chapter 3

Phenotypic Characterization of Tremor in the Twitcher Mice and its Alteration After Therapy

3.1 Introduction

Although, tremor is a prominent phenotype in the twitcher mouse, very little is understood regarding its origin and characteristics. Also, very little is known about how the tremor is altered after various treatments, especially bone marrow transplantation (BMT) following harsh conditioning regimens. In the current study, a detailed phenotypic characterization of the tremor in the twitcher mouse was performed using a specially modified force-plate actometer (Fowler et al., 2001). The sensitive transducers of the force-plate allowed recording of the force generated by unusually small (7-13 g) mice with high temporal resolution (100 samples/s). Using Fourier analysis, the force generated by the mouse was decomposed into individual component frequencies and was plotted as a power spectrum. The power spectra and the locomotor activity of the twitcher mice were compared to the wildtype mice to reveal several important differences. The study also evaluated the efficacy of BMT in altering the tremor phenotype in the twitcher mice. The current study systematically characterizes

the tremor in the twitcher mice and establishes a quantitative tool for evaluation of the effectiveness of various therapies.

3.2 Materials and methods

3.2.1 Colony maintenance

GALC +/- and wildtype mice on the C57BL/6J background were obtained from The Jackson Laboratory (Bar Harbor, ME) and maintained under the supervision of M.S.S. at Washington University School of Medicine. The GALC-/- mice were obtained by GALC+/- X GALC+/- matings. The galc genotype was determined by twitcher-specific PCR (Sakai et al., 1996). All animals were allowed ad libitum access to food and water, except during brief (12-min or less) behavioral recording sessions. All animal experiments were approved by Institutional Animal Care and Use Committee at Washington University School of Medicine.

3.2.2 BMT and harmaline injections

Neonatal pups were genotyped on day 2 or 3 and BMT was performed on post natal day 3 or 4. The mice received 400 rads of total body irradiation from a ^{137}Cs source. The animals received an intravenous injection of 10^6 nucleated bone marrow cells from a sex-matched GALC+/+, GFP (+) donor (Okabe et al., 1997) via the superficial temporal vein (Sands and Barker, 1999).

Harmaline (1-methoxy-3, 4-dihydro-β-carboline, H1392, Sigma, St. Louis, MO) at a dose of 15 mg/kg was injected intraperitoneally 12 minutes before the start of tremor monitoring on post natal day 36.

The nomenclature for the various treatment groups and the number of animals used in the study is as follows: (a) UntWt- untreated wildtype (n=28), (b)

UntMut- untreated mutant (twitcher; n=34), (c) BmtWt- wildtype mice treated with BMT (n=12), (d) BmtMut- twitcher mice treated with BMT (n=7), (e) UntWtHarm - wildtype mice treated with harmaline (n=11), (f) UntMutHarm- twitcher mice treated with harmaline (n=8), (g) BmtWtHarm- BmtWt mice treated with harmaline (n=11), and (h) BmtMutHarm- BmtMut mice treated with harmaline (n=7).

3.2.3 Force plate actometer

The design of the original force plate actometer and the principles used in the design were described previously (Fowler et al., 2001). For the current study a force-plate actometer was custom made to accommodate the relatively low body weight and impaired force production capabilities of the untreated twitcher mice. The mean weight of the twitcher mice at 36 days was 10.4$\pm$1.6 grams compared to 16.9$\pm$1.8 grams for wildtype mice at this age. The custom-made actometer used a carbon fiber/nomex composite material for the load plate, which weighed 57 g, was 3.2 mm thick and measured 24 cm X 24 cm. The sensing area was 20 cm X 20 cm, and the cage that confined the mouse to the load plate was constructed of 6.4 mm-thick clear polycarbonate with inside dimensions of 20 cm long by 20 cm wide by 15 cm high. A removable clear polycarbonate top was perforated with ventilation holes. The load plate was supported by four Model 31a miniature strain gauge load cells purchased from Honeywell/Sensotec (Columbus, Ohio). The load cells were calibrated to yield a force resolution of 0.2 gram-force.

3.2.4 Actometer data acquisition and analysis

The animals were acclimated for at least 30 minutes in the same room prior to tremor monitoring. Data recording was conducted between 2 pm and 6 pm. For mice given harmaline, the drug or saline was injected 12 minutes prior to recording. Data were collected for 6 min, but only the first minute, when movement was maximal, was used for the tremor analyses. The recordings from the transducers were collected at 100 samples/s. The 12-bit integer raw data files were acquired with a LabMaster interface (Scientific Solutions, Mentor, Ohio) that was controlled by a DOS-based Free Pascal program (http://www.freepascal.org). The data from the raw integer files were converted to text files and formatted by Free Pascal programs for further processing by commercially available software (see Statistics section below). Custom written Free Pascal programs were used to calculate distance traveled and the number of low mobility bouts (see below). The following data were extracted from the raw data files (Fowler et al., 2001): (a) Fz- the net force exerted by the animal at a particular 0.01-s “instant” was calculated as the sum forces on each of the four transducers that supported the load plate. The digitized Fz data obtained at 100 samples/s for the first minute of the recording session were formatted into 12 consecutive 5.00-s time series. Importantly, for the tremor analyses the Fz time series data were expressed as a percent of each mouse’s body weight. This normalization made it possible to compare the power spectra across genetic and treatment conditions without potential confounding by the body weight differences. Each time series (Fz(t)) was Fourier transformed using the fft function in MATLAB (The Mathworks, Inc., Natick, MA). A 500-point

Hanning time-domain data window was used. The resulting 12 power spectra were averaged together to yield a single power spectrum for each mouse. The individual frequencies obtained after Fourier transformation were plotted as a continuous function (**power spectrum**; see Figure 3.1 C) after filtering to retain frequencies between 2.5 and 30.0 Hz. (b) The **bandwidth** was defined as the difference between the upper and lower limit of the frequencies where the power was half that of the maximum. (c) The **center frequency** was calculated as the frequency co-ordinate of the vertical line bisecting the bandwidth. (d) The **frequency at peak power** was taken as the frequency at which the power was at its maximum. (e) **Power between 13 and 20 Hz** was obtained by integrating the area under the power spectrum curve between 13 and 20 Hz. The aforementioned power spectrum variables (a-e) were computed for each individual mouse, and these variables were then subjected to standard statistical treatments (see below). Although the tremor analyses were performed for the first minute of force-plate recordings, the variables for tracking and quantifying the mouse's horizontal movements in the actometer were based on the entire 6-min session. (f) The **X-Y position** of the mouse on the force plate and (g) the **distance traveled** by the animal was calculated using the principle of moments and by calculating distance (in mm) between centers of force locations at successive time points, respectively (Fowler et al., 2001). The X-Y locations of the animal at various time points were plotted as a function of time to obtain the (h) **trajectory** of animal movement. (i) X-Y coordinates of the center of force as a function of time were additionally used to identify a **low mobility bout**, which was defined in terms of a virtual circle with a radius of 15.0 mm that was

centered on the mouse as it moved across the load plate. When 5.00 s elapsed without movement beyond the perimeter of the circle, a low mobility bout was tallied, and the 5.00-s time interval was reset in order to ”look for” the next bout. This measure gives an indication of a mouse’s proclivity to ”stay in one place” regardless of the location of that place on the load plate.

3.2.5 Statistical analyses

Systat (Systat Software Inc., Chicago, IL, USA) and Graphpad prism (Graphpad Software, Inc., La Jolla, CA) were used for generating graphs and performing statistical analyses. ANOVA or Kruskal-Wallis tests were used to compare different groups, and post-hoc multiple comparisons were done using Bonferroni tests.

3.3 Results

3.3.1 Tremor and locomotion in twitcher mice

The qualitative differences in the Fz time series between the UntWt and UntMut mice are shown in Figure 3.1 A and B. A Fourier transform was applied to the Fz time series to obtain a power spectrum (Figure 3.1 C). The power spectra of different animals were further analyzed to obtain the peak power, frequency of peak power, center frequency, and bandwidth (Figure 3.1 C). Comparison of the averaged power spectra of these two groups revealed a shift in the spectrum with a predominance of higher frequencies (Figure 3.1 D) in the UntMut group compared to the UntWt group. The center frequency and the bandwidth in the UntMut group were significantly higher than these variables for the UntWt group (Figure 3.1 E and F). The peak power (Figure 3.1 G), frequency of peak power

(Figure 3.1 H) and the integrated power between 13 and 20 Hz (Figure 3.1 I) were significantly increased in the UntMut group compared to the UntWt group ($p<0.001$ for all three comparisons; t-test). The data for the UntWt group are indicative of normal movements without any visible tremor, whereas the UntMut (twitcher) mice exhibited the obvious tremor for which they are named. This analysis shows that the tremor of the twitcher mice manifests itself as relatively broad band, high-frequency force oscillations while on the force-plate.

The UntMut group had decreased locomotion compared to that of the UntWt group. Representative trajectories of these two groups are shown in Figure 3.2A and B. The total distance traveled was significantly lower in the UntMut group compared to the UntWt group ($p<0.001$, t-test; Figure 3.2 C). One way to gain insight into the nature of the tremor phenotype of the UntMut group is to compare these mutant mice with UntWt mice that are subjected to a relatively well accepted pharmacological tremor model [harmaline treatment] (e.g., Wang and Fowler, 2001). Therefore, the tremor in the UntMut was compared to the tremor in the wildtype mice injected with harmaline (UntWtHarm). Harmaline induces a characteristic narrow-band, near 12-Hz tremor (see figure 3.6 for time series plots). When the UntMut and the UntWtHarm animals were compared (Figure 3.3), there was a robust difference in the averaged power spectra (Figure 3.3 A). When quantified, the mean of the center frequencies from the UntMut mice (15.8 Hz) was significantly higher than the UntWtHarm group ($p<0.001$; Bonferroni test, Figure 3.3 B). The UntWtHarm group had a narrow peak at approximately 12.2 Hz, and the bandwidth was significantly less than that of the UntMut group ($p<0.001$; Bonferroni test, Figure 3.3 C).

There was no statistically significant difference between the distance traveled and the number of low mobility bouts between the UntWtHarm and the UntMut groups, probably because tremor-inducing doses of harmaline in intact animals suppresses locomotion (Wang and Fowler, 2001) (data not shown).

Interestingly, when twitcher mice were injected with harmaline (UntMutHarm), there was a blunted response with no statistically significant change in center frequency or bandwidth compared to the UntMut group (Figure 3.3 B and C). In the UntWtHarm group, the peak power was significantly higher ($p<0.001$; Bonferroni test; Figure 3.3 D) while frequency of peak power was significantly lower ($p<0.05$; Bonferroni test; Figure 3.3 E) compared to the UntMut group. There was no significant difference between the UntMutHarm and UntWtHarm groups with respect to the distance traveled or the number of low mobility bouts (data not shown). Representative trajectories of animals from these groups are shown in figure 3.7.

3.3.2 Effect of treatment on tremor

In order to directly assess the effect of myeloreductive conditioning and BMT on the power spectra, tremor monitoring was performed on both wildtype and twitcher mice that received BMT (i.e., comparison of BmtWt versus BmtMut). The Fz time series recordings are shown in figure 3.6 A, B, E and F. The BmtWt group had greater power in both the frequencies around 10-12 Hz and in the higher frequencies in the 13-20 Hz range compared to the UntWt group (Figure 3.4 A). The BmtMut group had greater power in the near 10 Hz lower frequency range compared to the UntMut group. The center frequency of the BmtWt group was significantly increased compared to the UntWt group ($p<0.05$; Bonferroni

test; Figure 3.4 B). There was no significant difference in the bandwidth in the groups compared (data not shown). The peak power (Figure 3.4 C) and the power between 13 and 20 Hz (Figure 3.4 E) was significantly increased in the BmtWt group compared to the UntWt group but not in the BmtMut group compared to the UntMut group. The frequency of peak power was significantly increased in the BmtWt group compared to the UntWt group (Figure 3.4 D). There is no significant difference in the frequency of peak power between the BmtMut group and the UntMut group (Figure 3.4 D). The total distance traveled was significantly decreased (decrement in normal function) in the BmtWt group compared to the UntWt group (Figure 3.4 F). The trajectories of the various groups are shown in figure 3.7 .

3.3.3 Harmaline response in BMT animals

Since the BMT-treated animals had additional higher frequencies in the averaged power spectra, possible alteration of their olivocerebellar circuit properties were tested by comparing their spectra to those of the mice receiving harmaline after BMT (BmtWtHarm and BmtMutHarm). The Fz time series are shown in figure 3.6 E-H. Interestingly, the mice in the BmtWtHarm group were more resistant to the expression of harmaline-induced tremor than the UntWtHarm group (Figure 3.5 A). The response to harmaline in the BmtMutHarm group was similar to the UntMutHarm group (Figure 3.5 A). The center frequency and the bandwidth were significantly higher in the BmtWtHarm group compared to the UntWtHarm group (Figure 3.5 B and C). The peak power was significantly lower in the BmtWtHarm group compared to the UntWtHarm group (Figure 3.5 D). Interestingly, there was no significant difference in the center frequency,

bandwidth and peak power between the UntMutHarm and BmtMutHarm groups (Figure 3.5 B, C and D). There was no significant difference in the distance traveled or in the number of low mobility bouts in the groups compared (data not shown). The movement trajectories for the animals in the current comparison are shown in figure 3.7 .

3.4 Discussion

In the current study, a detailed quantitative characterization of the tremor phenotype (movement-related force oscillations) in the twitcher mice was performed using an ultra-sensitive force-plate actometer. Unlike the results generated from other tremor monitoring devices, the data in the current study were obtained in unconstrained animals. This allowed for the simultaneous acquisition of tremor data and locomotor activity data. One possible confounding issue with this design is the effect of group differences in ambulation on the tremor recording. However, differences in ambulation do not appear to alter the relevant power spectra that are used to evaluate the presence of tremor and the effects of treatment on tremor. For example, similar differences are observed in the relevant power spectra between twitcher mice and WT controls whether measurements are compared for the whole session or during low mobility bouts (analyses not shown).

The tremor in the twitcher mouse was seen as a relatively higher frequency with a broader bandwidth than the movement-related force oscillations exhibited by the wildtype mice moving normally on the force plate. The twitcher tremor also differed substantially from the characteristic harmaline-induced tremor dis-

played by wildtype mice. Harmaline, at the doses used in the study (15 mg/kg), is believed to disrupt olivocerebellar pathways (McMahon et al., 2004). The current data suggest that the tremor in the twitcher mouse is of complex origin and not limited to the olivocerebellar circuits. However, the olivocerebellar pathways in the twitcher mouse appear to be disrupted. This is indicated by the blunted response of the twitcher mice to harmaline compared to the wildtype mice. This behavioral result is consistent with histological findings of widespread inflammation and demyelination throughout the neuraxis, including the entire cerebellum and brainstem in twitcher mice. Although it is likely that the effects of the twitcher mutation in the CNS are complex, the current study implies the involvement of olivocerebellar circuits in the generation of the tremor phenotype. Interestingly, disruption of the olivocerebellar circuit function similar to that seen in mice lacking Kv3.3 potassium channel (McMahon et al., 2004), leads to ataxia and tremor similar to the twitcher mice. Kv3.3 is expressed mainly in the olivocerebellar circuit (McMahon et al., 2004). The olivocerebellar circuit consists of inferior olivary nucleus, Purkinje cells and the deep cerebellar nuclei (Jacobson et al., 2008). The proper functioning of the circuit is necessary for learning and timing of movements among other functions. Similar to twitcher mice, the mice lacking Kv3.3, showed no coherent rhythmic response to harmaline (McMahon et al., 2004). Harmaline, at low doses acts predominantly on the olivocerebellar pathways (Miwa, 2007). Thus, the decreased response to harmaline in the twitcher mice and the mice lacking Kv3.3 can be attributed to the existing olivocerebellar circuit dysfunction in these genetically altered mice.

The validity of tremor monitoring in evaluating the effects of various therapies

was also determined. Hematopoietic cell transplantation (either using umbilical cord blood or bone marrow) is the only available therapy for the human disease (Krivit et al., 1998; Escolar et al., 2005). Bone marrow transplantation also prolongs the lifespan in the twitcher mouse (Yeager et al., 1984; Hoogerbrugge et al., 1989; Lin et al., 2007). However, the effect of conditioning and bone marrow transplantation on the prominent tremor phenotype exhibited by the twitcher mouse had not heretofore been determined. Twitcher mice receiving BMT had power spectra that had greater power in higher frequencies, implying a worsening of tremor. This is contradictory to what is observed in terms of other measures like lifespan seen in the previous studies (Lin et al., 2007; Reddy et al., submitted). The wildtype animals receiving only BMT had altered power spectra and were resistant to the effects of harmaline compared to the wildtype animals that did not receive BMT. These data suggest that BMT and the associated conditioning could possibly disrupt the olivocerebellar circuit function during the neonatal period in the wildtype animals, and reduce the beneficial effect on tremor phenotype that could otherwise be expected. Interestingly, BMT (with radiation conditioning) is known to cause cerebellar dysplasia in neonatal mice (Sands et al., 1993). Conditioning and BMT could adversely affect some as yet unknown regions in the brain or periphery to give the same abnormal response. The current study thus highlights a possible harmful effect of conditioning in treating the disease. These effects could be explained by the presence of rapidly proliferating cells in the cerebellum during the time of conditioning and BMT (Noguchi et al., 2008). Although, the current study uses myeloreductive conditioning (400 rads) at post natal day 3 or 4, similar and perhaps more se-

vere function-compromising effects could be expected in studies that use fully myeloablative regimens (Yeager et al., 1984; Hoogerbrugge et al., 1989). Conditioning and BMT performed in newborn children (Escolar et al., 2005) may superimpose additional abnormal phenotypes on this already complex disease presentation. This could further complicate the interpretation of the therapeutic benefits of BMT for GLD.

Since detailed histological evaluation of the olivary and cerebellar circuits was not carried out in this study, the exact origin of the tremor in the above mentioned groups cannot be made. However, there is clearly pathology in the cerebellum of the mice which likely encompasses the olivocerebellar circuitry and contributes to the tremor phenotype. It would be interesting to test whether the basal ganglia are similarly functionally affected with the disease and treatments using cholinesterase inhibitors like physostigmine (Wang and Fowler, 2001).

In addition to acquiring data regarding the various frequencies of the force variation during movements, the force-plate actometer can be concurrently used to measure locomotor activity. The total distance traveled during the recording session was significantly decreased in the untreated twitcher mice compared to the untreated wildtype mice. This study establishes the use of an ultrasensitive force-plate actometer in evaluating the effects of various therapies for the twitcher mice. It also emphasizes the need to evaluate the impact of various therapeutic approaches on a wide variety of functions before drawing conclusions on their safety and efficacy.

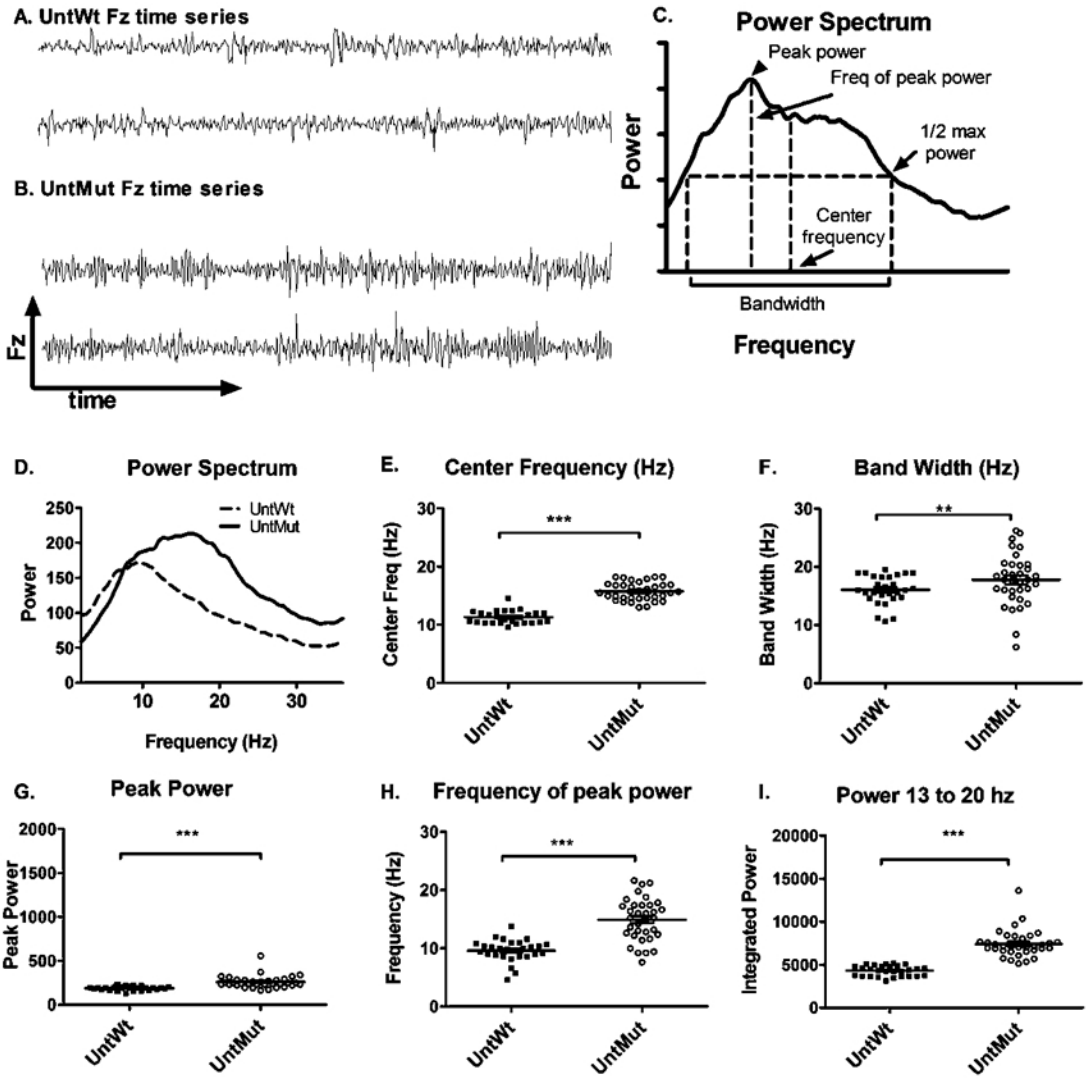

Figure 3.1: Characterization of tremor in the UntMut mice. Representative Fz time series recording from an UntWt mouse (A) and an UntMut mouse (B) over 12 seconds (each series is 6 s). The X-axis represents time and the Y-axis represents force the vertical force variation (Fz) recorded by the force plate actometer. A Fourier transformation performed on the Fz time series data yields a power spectrum that shows how much power (variance) the Fz variation contains at each frequency of oscillation. The power spectrum can then be further analyzed to yield peak power, frequency at peak power, center frequency, and bandwidth. These data are represented diagrammatically on a hypothetical power spectrum plot (C). The averaged power spectrum (D) of the UntMut mice (solid black line) was shifted towards higher frequencies compared to the UntWt mice (dashed gray line). The center frequency (E) was significantly increased in the UntMut (open circles) compared to the UntWt mice (filled squares). There was a significant increase in the band width (F) in the UntMut compared to the UntWt group. The peak power (G), frequency at peak power (H) and the power between 13 and 20 Hz (I) were significantly increased in the UntMut group compared to the UntWt group. The horizontal bars represent the mean and the error bars represent the SEM (**$p<0.01$, ***$p<0.001$).

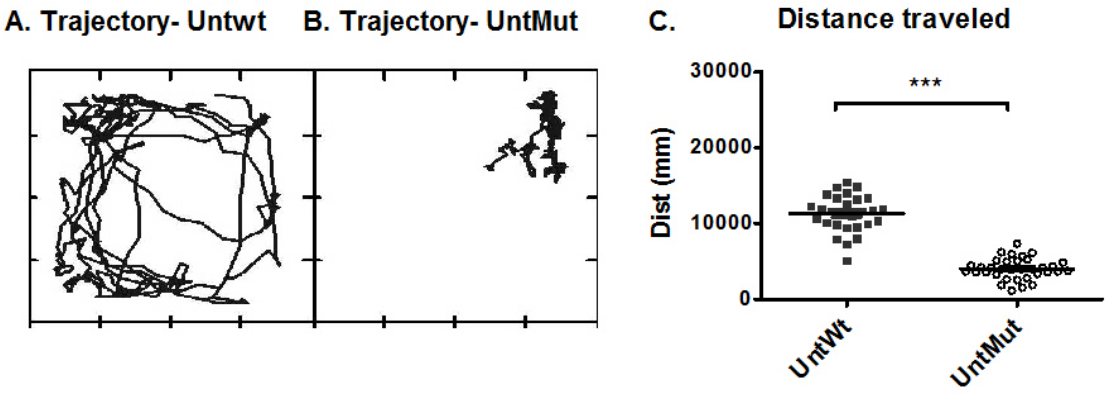

Figure 3.2: Characterization of locomotor activity in the twitcher mouse. The movement trajectory of representative UntWt and UntMut mice are shown in (A) and (B), respectively. Each panel represents the movement of the mouse for duration of 1 minute. The box in which each movement trajectory is plotted represents the inside wall of the 20 cm X 20 cm cage that confined the mouse to the load plate. Each point in the panel represents the XY location of the mouse at a certain point of time. The total distance traveled during 6 minutes is shown in (C).The total distance traveled by the UntWt mice (filled squares) is significantly higher than that of the UntMut mice (open circles). The horizontal bars represent the mean and the error bars represent the SEM (***$p<0.001$).

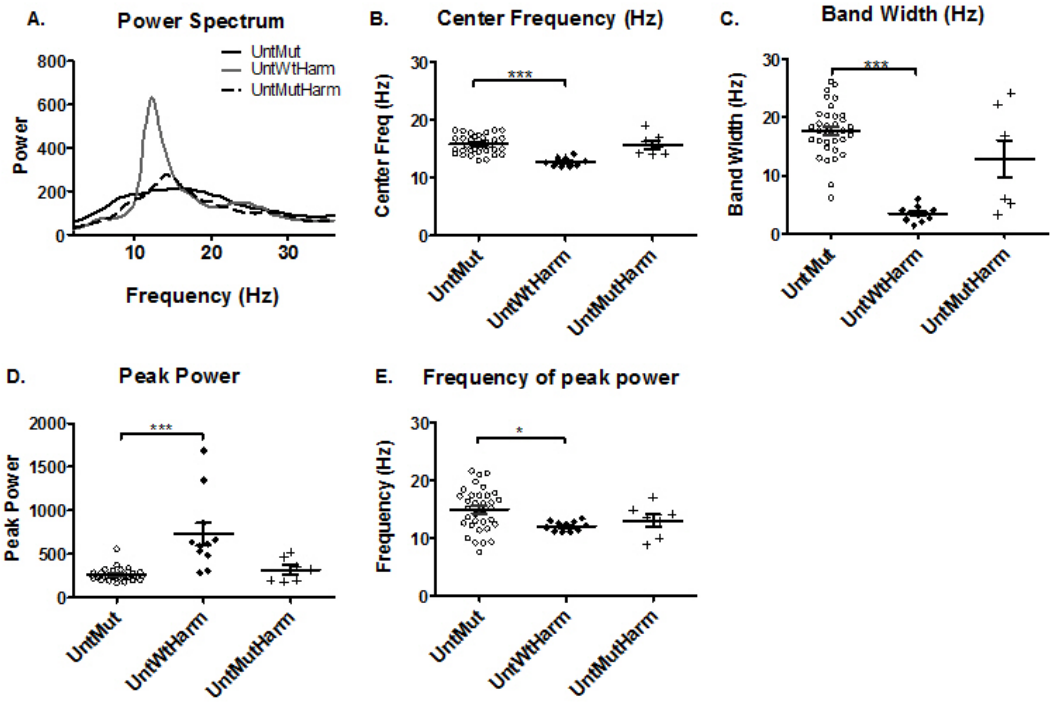

Figure 3.3: Comparison of the tremor of the UntMut mice with that of the tremor induced by harmaline. The average power spectrum (A) of the UntMut mice (solid black line) reflected a broadband tremor and that of the UntWtHarm mice (solid gray line) showed a characteristic narrow band 12 Hz tremor. The response to harmaline was blunted in the UntMutHarm mice (dashed black line). The center frequency (B) and bandwidth (C) were significantly increased in the UntMut group (open circles) compared to the UntWtHarm group (filled diamonds), which exhibited the expected characteristic narrow band tremor typically induced by harmaline in mice. The peak power (D) was significantly increased in the UntWtHarm group compared to the UntMut group. The frequency at peak power was significantly decreased in the UntWtHarm group compared to the UntMut group. There was no significant difference in the center frequency, bandwidth, peak power and the frequency of peak power between the UntMut and UntMutHarm groups (plus symbols). Horizontal bars represent the mean and the error bars represent the SEM (***$p<0.001$, **$p<0.01$ and *$p<0.05$).

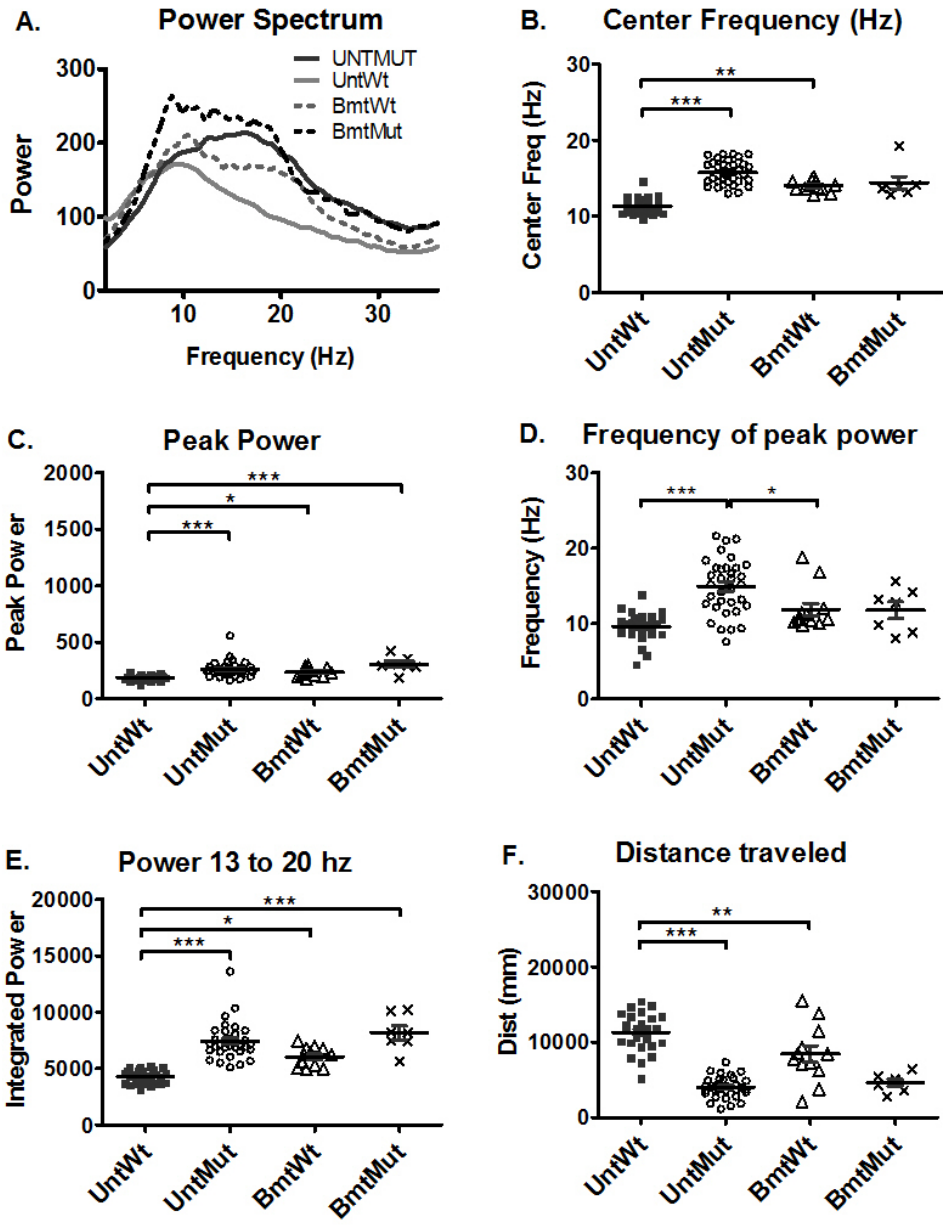

Figure 3.4: Effect of BMT on power spectra. The averaged power spectrum (A) of the BmtWt group (dashed gray line) is shifted upward and rightward compared to the UntWt group (solid gray line). Similarly, the averaged power spectrum in the BmtMut group (dashed black line) is shifted upward across a broad frequency band compared to the UntMut group (solid black line). The center frequency (B) was significantly increased in the BmtWt group (open triangles) compared to the UntWt group (filled squares). There was no significant difference between the untreated mut (open circles) and BmtMut groups (cross marks) in the center frequency. The peak power (C), frequency of peak power (D) and the power between 13 and 20 Hz (E) was significantly increased in the BmtWt group compared to the UntWt group. Compared to the UntMut group, the BmtMut group showed no significant difference in the center frequency (B), peak power (C), frequency of peak power (D) and power between 13 and 20 Hz (E). The distance traveled by the BmtWt group was significantly decreased compared to the UntWt group (F). The horizontal bars represent the mean and the error bars represent SEM (*$p<0.05$, **$p<0.01$, ***$p<0.001$).

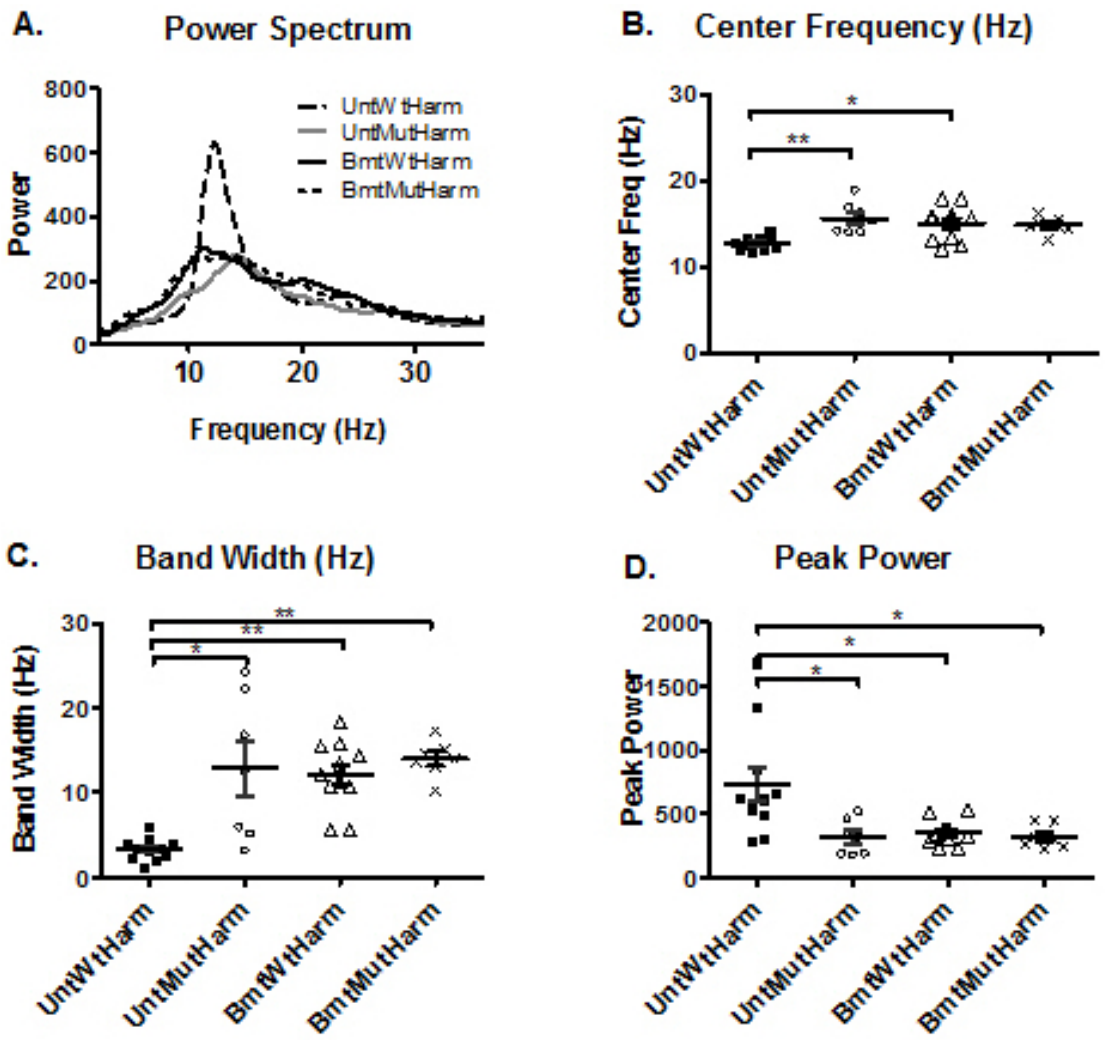

Figure 3.5: Harmaline tremor response in the BMT-treated animals. Averaged power spectra of various groups treated with harmaline (A). The averaged power spectrum of UntWtHarm group (solid gray line) appears different compared to the averaged power spectrum of the other groups in (A). The averaged power spectra of the BmtWtHarm (solid black line), UntMutHarm (dashed black line), and BmtMutHarm (solid gray line) appear very similar to each other. The center frequency (B) and the bandwidth (C) were significantly increased in the BmtWtHarm group (open triangles) compared to the UntWtHarm group (filled squares). The peak power (D) was significantly decreased in the BmtWtHarm group compared to the UntWtHarm group. There was no significant difference in center frequency, bandwidth or peak power between the UntMutHarm (open circles) and BmtMutHarm groups (cross marks). Horizontal bars represent the mean and the error bars represent the SEM . (***$p<0.001$, **$p<0.01$ and *$p<0.05$).

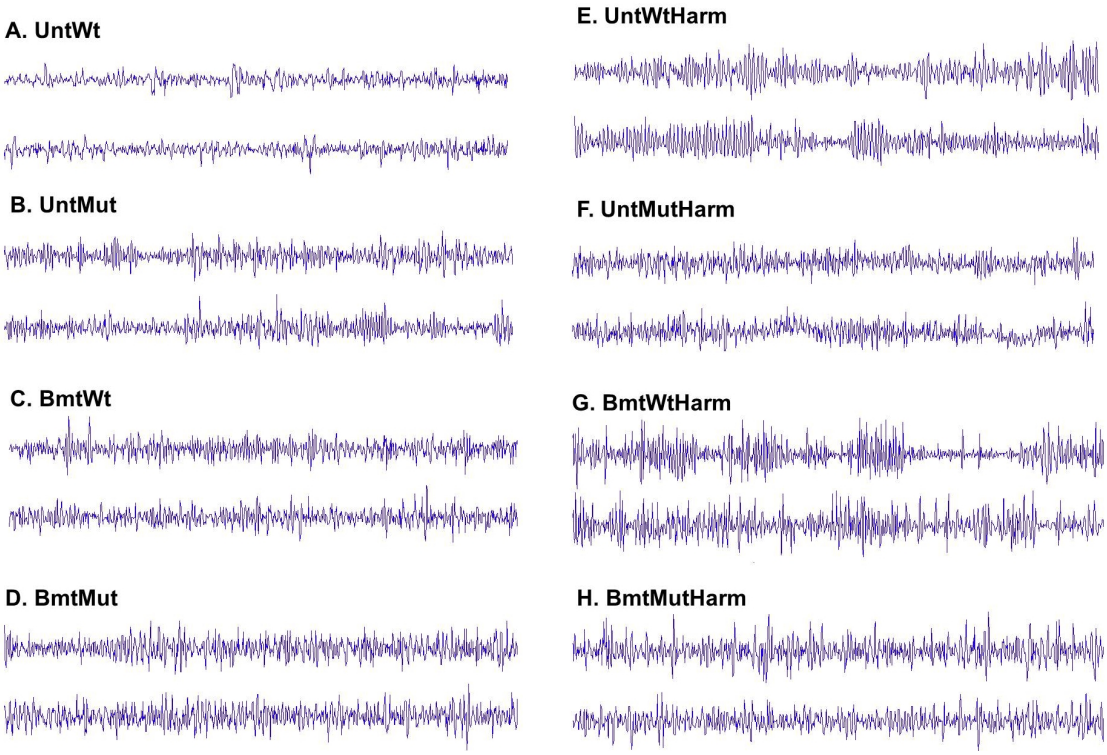

Figure 3.6: Comparison of the Fz time series in the various treatment groups. The y-axis represents the Fz and the x-axis represents time. Each row represents 6s of recording.

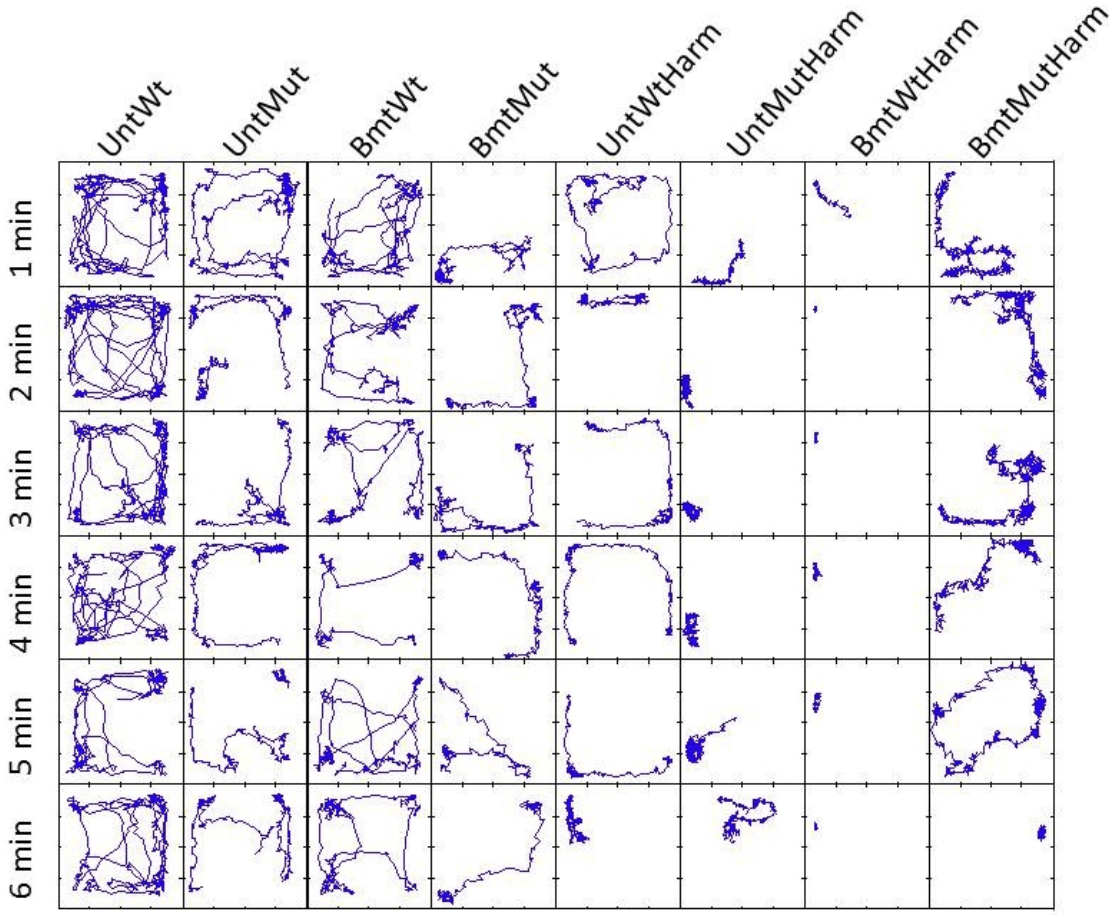

Figure 3.7: Comparison of the trajectories of representative animals from different groups. Each column represents a single animal from a group. Each box represents the movement trajectory of successive locations of center of force (position of the mouse at any moment) across a one-minute block of time.

Chapter 4

The Role of KC and CXCR2 in the Pathogenesis of Globoid-Cell Leukodystrophy

4.1 Introduction

Inflammation is a prominent histopathologic feature of GLD and is characterized by the presence of globoid cells (macrophages with engulfed myelin debris)and astrocytosis (Suzuki et al., 2000, Lin et al., 2007, Reddy et al., submitted) in the CNS. There is also an increase in some of the pro-inflammatory molecules (LeVine and Brown, 1997; Wu et al., 2001; Luzi et al., 2009). Our previous study (Reddy et al., submitted) has shown that the levels of KC (GRO-α; mouse ortholog of CXCL1) was highly elevated in the CNS of the twitcher mice and that the levels were restored after treatment.

KC belongs to the CXC family of chemokines (chemoattractant cytokines) and is a potent macrophage (Boisvert et al., 1998; 2006) and neutrophil chemoattractant (Tani et al., 1996). KC signaling through its receptor, CXCR2 synergizes with another oligodendrocyte mitogen, Platelet Derived Growth Factor (PDGF) to cause OPC proliferation, but can act independently to cause migration arrest (Tsai et al., 2002). Since the CNS of twitcher mice have demyelination and in-

flammation, we investigated the role of various cytokines in the two inter-related aspects of the disease. Our results highlight the severity of primary oligodendrocyte damage resulting from the deficiency of the enzyme and the minimal benefit of targeting the secondary processes in the disease.

4.2 Materials and Methods

4.2.1 Animal Procedures

Heterozygous (GALC +/-) mice on a congenic C57Bl/6J background were obtained from The Jackson Laboratories (Bar Harbor, ME) and maintained under the supervision of M.S.S. at the animal facility at Washington University School of Medicine. The mice were housed under standard conditions in pathogen-free facility with ad libitum access to food and water. The mutant twitcher mice were obtained by heterozygous sibling matings. CXCR2+/- mice on C57Bl/6J background were a kind gift from Dr. Ann Richmond (Vanderbilt University, Nashville, TN). KC+/- mice on the C57Bl/6J background were a kind gift from Dr. Sergio Lira (Mount Sinai School of Medicine, New York City, NY). These mice were bred to GALC+/- mice to obtain the KC-/- GALC-/- and CXCR2-/-GALC-/- mice. The CXCR2 mice were maintained on antibiotic water (Trimethoprim / Sulpha methoxazole).

4.2.2 Bone Marrow Transplantation

Animals were genotyped by PCR on postnatal day 9 or day 10. Nine day old mice received 900 rads of total body γ-radiation from a ^{137}Cs-source for conditioning followed by injection of approximately 3-4 X 10^7 GFP+ sex-matched unfractionated bone marrow cells in 300 μl volume i.p. approximately 24 hours af-

ter irradiation. Post-transplantation antibiotics included trimethoprim/ sulfamethoxazole added to the water. The bone marrow donors were sex-matched syngenic GALC +/+, GALC-/-, CXCR2+/+ or CXCR2-/- mice expressing GFP under the CAGGS promoter maintained as separate colonies.

4.2.3 Flow cytometry

Flow cytometry was used to quantify the hematopoietic-derived cells in the CNS and to measure bone-marrow chimerism with donor-derived GFP+ cells after transplantation. For quantifying the hematopoietic-derived cells in the CNS (Sedgwick et al., 1991, McCandless et al., 2006), perfused mice brains were treated with collagenase/DNase buffer after homogenization. The hematopoietic-derived cells were isolated by separation on a percoll gradient. Cells were then counted using a hemocytometer and stained with fluorophore conjugated antibodies after Fc receptor block (BD biosciences, San Jose, CA). The following cells were identified and quantified by flow cytometry: Activated microglia/macrophages (CD11b+ CD45^{hi}), resting microglia (CD11b+, CD45^{lo}), CD8+ T-cells, CD4+ T-cells and Neutrophils (Gr1^{hi} F4/80^{lo}). The data was acquired on a FACSCalibur flow cytometer (BD biosciences, San Jose, CA) using Cell Quest software (BD biosciences, San Jose, CA) and analyzed using FloJo software (Tree Star, Inc., Ashland, OR). The individual cell counts were obtained by multiplying the percentages of the various cell populations obtained by flow cytometry with the cell counts obtained by using the hemocytometer. Spleen and bone marrow cells were used for positive controls. For quantifying donor engraftment, bone marrow was harvested from the femur and the percentage of GFP+ cells was determined.

4.2.4 Cytokine sandwich immunoassays

The methods used in the study are as described previously (Hulse et al., 2004; Reddy et al., submitted). Animals were perfused with ice cold PBS after deep anesthesia. The brains and spinal cords were collected and homogenized in 10 mM Tris, 150 mM NaCl, 1 mM Dithiotreitol, 0.2% Triton-X and 20 μl/ml of Protease Inhibitor Cocktail (P8340, Sigma, St. Louis, MO). The supernatant was diluted to 0.5-2 mg protein/ml and the samples were stored at -70°C till use. The concentration of various cytokines and chemokines was determined using Bio-plex kit (Bio-Rad laboratories, Hercules, CA), a flow cytometry-based multiplex assay. The 23-plex sample kit includes the standards and antibodies for the following cytokines: IL1 α, IL-1β, IL-2, IL-3, IL-4, IL-5, IL-6, IL-9, IL-10, IL-12(p40), IL-12(p70), IL-13, IL-17, Eotaxin, G-CSF, GM-CSF, IFN-γ, KC, MCP-1, MIP-1α, MIP-1β, RANTES and TNF-α. A 3-plex kit for analyzing MIP-2, FGF-2 and PDGF-BB was also used. The supernatant from brain and spinal cord homogenates were incubated with the fluorescent beads, washed and then incubated with biotin-labeled antibody cocktail. The samples were then incubated with streptavidin-PE and the fluorescence values were read in the Bio-Plex 2200 system (Bio-Rad laboratories, Hercules, CA). Standard curves were generated for each cytokine using the standards supplied with the kit and the individual cytokine concentration in each sample was estimated. Protein concentration of the samples was determined using the Bio-Rad protein assay reagent (Bio-Rad, Hercules, CA), which is based on Coomasie dye-binding assay.

4.2.5 Histology and Immunofluorescence

For oligodendrocyte proliferation studies, the animals were injected with 5 mg/kg BrdU (B9285, Sigma, St. Louis, MO) every 8 hours for four days starting on day 32 of age. The lumbar spinal cords were collected after perfusion of the animals with PBS and 4% paraformaldehyde. The tissue was fixed in Enhanced Decalcification Formulation (SL85-32, Statlab, Lewisville, TX) for 2 days and cryoprotected in 30% sucrose. The tissues were then frozen in O.C.T. compound (Sakura Finetek, Torrance, CA) and cryosectioned. For immunostaining, the sections were stained with 1:50 dilution of NG2 antibodies (ab5320, Millipore, Billerica, MA) and 1:100 dilution of mouse anti-BrdU (B2531, Sigma, St. Louis, MO) overnight at 4°C. The secondary antibody was detected using anti-rabbit Alexafluor 555 (A-21428, Invitrogen, Carlsbad, CA) and goat anti-mouse Alexa 488 (A-11001, Invitrogen, Carlsbad, CA). The images were acquired using Ziess laser confocal microscope (Carl Ziess Microimaging, LLC, Thornwood, NY). Ten sections from each group with n=4 animals per group were used for analysis. The cell counts were done manually using LSM/Axioskop software (Carl Ziess Microimaging, LLC, Thornwood, NY). For LFB and PAS staining, the tissues were fixed overnight in 4% paraformaldehyde after perfusion with ice cold PBS and then transferred to 30% sucrose. The tissues were embedded in paraffin and the LFB and PAS staining was done using standard methods.

4.2.6 Statistical methods

GraphPad prism (GraphPad Software, Inc., La Jolla, CA) was used for statistical analyses and for generating graphs. Two-way unmatched ANOVA followed by post-hoc Bonferroni comparisons were used for analyzing figures 4.1 C, 4.1 D, 4.4 C, 4.4 D, 4.4 G, 4.4 H, 4.11 A, 4.11 B, figures 4.2 , 4.3 and 4.6. One-way ANOVA followed by post-hoc Bonferroni comparisons were used for comparing various groups in figures 4.10 A, and 4.5. Log-rank test was used to compare the Kaplan-Meier survival curves in figures 4.10 B, 4.8 A and 4.8 B. For statistical analysis of body weights, repeated measures ANOVA could not be used because of attrition, therefore one-way ANOVA at pre-determined time points was used instead in figures 4.10 C, 4.8 B and 4.8 D.

4.2.7 Genotyping

PCR for GALC was done using the protocol described previously (Sakai et al). The following primers were used for genotyping KC (Tani et al., 1996): 5'-GAA GAC AGA CTG CTC TGA TGG CAC-3' and 5'-CCC TTC TAC TAG CAC AGT GGT TGA-3'. The following primers were used for genotyping CXCR2 (Boisvert et al., 1998): 5'-CCT CGT ACT GCG TAT CCT GCC TCA G-3' and 5'-TAG CCA TGA TCT TGA GAA GTC CAT G . The lack of KC or CXCR2 was confirmed by the presence of Neo cassette in the same PCR reaction. The primers used were: 5'-GGA TTG CAC GCA GGT TCT-3' and 5'-GGA CAG GTC GGT CTT GAC AAA-3'. GFP phenotype was determined using an ultraviolet lamp held on the ventral surface of the newborn mice to detect greenish skin glow.

4.3 Results

4.3.1 Altered cytokine profiles

Since inflammation is a prominent feature of the disease, and previous studies (Wu et al., 2001; Biswas and Levine, 2001; Reddy et al., submitted) have shown alterations in cytokines, a more comprehensive survey of several cytokines and chemokines in the brains and spinal cords were measured at different time points. Several cytokines/chemokines were altered in the brains and spinal cords of twitcher mice at different time points (Figure 4.1). Among the altered molecules, the chemokine KC was most strikingly elevated in the mutant compared to the wildtype (approximately 16-fold and 25-fold in the brain and spinal cord respectively) (see Figure 4.1 A and B). KC is progressively elevated in the brains and the spinal cords of twitcher mice (Figure 4.1 C and D). Other cytokines that were altered were IL-12(p40) in the brain and IL-1α, IL-6, IL-10 and IL-12 p40 in the spinal cord. Detailed alterations of the various molecules that were assayed in the brain and spinal cords are shown in Figure 4.2 and Figure 4.3.

4.3.2 Cellular inflammation in the CNS of twitcher mice

KC (CXCL1) is a chemokine known to be chemotactic to neutrophils and macrophages (Tani et al., 1997; Boisvert et al., 1998). Review of the twitcher literature showed no previous description of neutrophils in histopathological sections of the brain and spinal cord. Our previous study (Reddy et al., submitted) also did not show an elevation in the neutrophils in the CNS of the twitcher mice at 36 days of age. Therefore, we hypothesized that elevated KC is responsible

for recruitment of macrophages into the CNS. Flow cytometry of the brains of the various animals at different timepoints was performed to quantify the various hematopoietic-derived cells (Figure 4.4). Two-way ANOVA showed that there is a significant interaction effect by the genotype and the timepoint for both resting and activated microglia. Post-hoc tests showed a significant increase in activated microglia (CD45^{hi}CD11b+) in the twitcher brains at day 30. There was no significant difference in the number of neutrophils (Gr1^{hi}F4/80-) that were detected in the brains of the wildtype or twitcher mice at different timepoints (data not shown). Since IL-12(p40) was also elevated in the twitcher brains and spinal cords, CD4 and CD8 T-cells in the brains were also quantified.

4.3.3 Inflammation in KC-/-GALC-/- mice

Since elevated KC correlated with an increase in activated microglia/ macrophages (CD45^{hi}CD11b+)in the twitcher mice, we hypothesized that twitcher mice lacking KC would have decreased activated microglia in the CNS. Hence, KC-/-GALC-/- mice were generated. Surprisingly, KC-/-GALC-/- mice did not show an alteration in the various inflammatory cells in the brain and spinal cord, when compared with that of KC+/+GALC-/- mice (Figure 4.5 and 4.6). Also, histology of the brain and spinal cord did not reveal any major differences when examined using LFB/ PAS staining (Figure 4.7). There was also no alteration in the lifespan (Figure 4.8 A) or body weights (data not shown) of KC-/-GALC-/- mice when compared with the KC+/+GALC-/- mice .

4.3.4 Inflammation in CXCR2-/-GALC-/- mice

The similarity in the inflammatory profile between KC-/-GALC-/- and KC+/+GALC-/- mice could be due to redundancy amongst the various cytokines and chemo kines. In the CNS, KC acts predominantly on the CXCR2 receptor. CXCR2 is involved in oligodendrocyte migration in the CNS (Tsai et al., 2002) and is involved in the macrophage and neutrophil chemotaxis in the periphery (Boisvert et al, 2002). Interestingly, several other chemokines (CXCL1-3, 6 and 7) also act on the CXCR2 receptor (Bozic et al., 1994). It is possible that elevation of any of the other four ligands could compensate for the lack of KC. Therefore, we hypothesized that twitcher mice lacking CXCR2 would have decreased activated microglia and macrophages (globoid cells) in the CNS. CXCR2-/-GALC-/- mice were generated in order to test the above hypothesis. When the histology of the brains of CXCR2-/-GALC-/- mice were compared to CXCR2+/+GALC-/- mice, using LFB/PAS, there was no qualitative difference between the two groups (Figure 4.9). There was also no difference in lifespan (Figure 4.8 B) and body weights (data not shown) in the CXCR2-/-GALC-/- mice when compared to CXCR2+/+GALC-/- mice .

4.3.5 BM chimera experiments

Previous studies have shown that CXCR2+ cells are involved in demyelination and transplantation of CXCR2 deficient bone marrow decreases the severity of demyelination in the cuprizone model of demyelination (Liu et al., 2010). Although our study did not find any alteration in neutrophils, macrophages are prominent in the CNS of the twitcher mice. In the current study, global lack of

KC or CXCR2 in the the twitcher mice does not alter the activated microglia / macrophages or prevent demyelination. However, it is possible that the beneficial effect of KC and CXCR2 deficiency in the bone marrow and other peripheral tissues are negated by their lack in the CNS or vice-versa, where they would be important in promoting repair. We hypothesized that selective deficiency of CXCR2 in the bone marrow or selective deficiency of KC in the CNS would lead to decrease inflammation and alter the course of the disease. In the twitcher mice, bone marrow transplantation supplies enzyme to the CNS and by itself prolongs the lifespan (Yeager et al., 1984). Therefore, appropriate controls were used to control for this therapeutic effect. Twitcher hematopoietic chimeras lacking CXCR2 in the bone marrow or KC in the periphery (bone marrow) did not show any difference in lifespan after comparable levels of bone marrow engraftment (Figure 4.10 A and B). There was also no difference in the weights of the various groups of twitchers that received transplantation (figure 4.10 C)

4.3.6 Role of KC and CXCR2 in oligodendrocyte proliferation

The striking elevation of KC in the brains and spinal cords of the twitcher mice seem to have no apparent effect on the cellular inflammatory profile in the CNS. Another important function of KC and CXCR2 is the proliferation of oligodendrocytes (Tsai et al, 2002). KC and CXCR2 have been shown to be involved in oligodendrocyte precursor proliferation and migration in other mice models of demyelinating diseases like the cuprizone model, jimpy mice and Theiler's encephalitis (Robinson et al., 1997, Wu et al., 1998). In the twitcher mouse, as reported in previous studies , there is an increase in proliferating oligodendro-

cytes in the spinal cord (Taniike and Suzuki., 1995). Therefore, we hypothesize that KC elevation is important in promoting oligodendrocyte proliferation seen in the twitcher spinal cord. Since hindlimb paralysis is a prominent feature in late stage of the disease in the twitcher mice, the ventral region of the lumbar spinal cord will be evaluated for proliferating oligodendrocyte cells by Brdu/ NG2 double immunostaining.

4.3.7 Elevation of other chemokines and growth factors

Since KC and CXCR2 deficiency in either the CNS or the bone marrow had minimal effect on the disease progression, the deficiency of the chemokine and the receptor might be compensated by elevation of other cytokines or growth factors or both. Measurement of cytokines that could potentially act on CXCR2 (for e.g., CXCL2 or MIP-2), and other oligodendrocyte mitogens like FGF-2 and PDGF-BB in the spinal cord (Figure 4.11) show that there is a progressive and a significant elevation in their levels with time. This elevation could compensate for the lack of CXCL1 and CXCR2 and could bring about continued activation of microglia. Similarly, there may be no difference in the oligodendrocyte proliferation in the mice lacking KC and CXCR2 due to elevation of other growth factors like FGF-2 and PDGF-BB.

4.4 Discussion

A previous study (Reddy et al., submitted) has shown that KC is highly elevated in the CNS of the twitcher mouse and the levels of KC correlate well with the effectiveness of therapy. In the current study, the significance of the key finding of elevated KC in the twitcher brains and spinal cords was explored in

further detail. The elevation of KC was similar to that seen in other mouse models of demyelinating diseases like jimpy mice (Wu et al., 2000), Theiler's encephalitis and EAE mice (Carlson et al., 2008). There was also a significant increase in activated microglia in the terminal stages of the disease. This correlates well with the histological observation of increased globoid cells in the brain and spinal cord. Since KC and its receptor were known to be involved in macrophage recruitement (Boisvert et al., 2004), we hypothesized that increase in KC was detrimental to the progression of the disease by recruitment and activation of microglia/macrophages. Contradictory to our prediction, there was neither a decrease in the number of activated microglia nor was there a alteration in the overall course of the disease in KC-/-GALC-/- mice.

Since there is considerable redundancy among the cytokines and chemokines, we hypothesized that the compensatory effects of ligands could be overcome by receptor knockout. Again, there was no alteration in the globoid-cells or the overall course of the disease in the CXCR2-/-GALC-/- mice compared to the CXCR2+/+GALC-/- mice. This observation could be explained again by the redundancy in the chemokine system. KC could act on its alternative receptor CXCR1 (Horuk et al., 1997) and bring about the same effects in the absence of CXCR2.

As mentioned before, it is also possible that the beneficial effect of lack of KC and CXCR2 in the bone marrow and other peripheral tissues are negated by their lack in the CNS, where they would be important in promoting repair. So, bone marrow chimeras in which the GALC-/- mice lacked either KC in the CNS or CXCR2 in the bone marrow were created. Again, these chimeric mice

showed no alteration in the course of the disease compared to GALC-/- mice that received GALC+/+ marrow. From the above experiments, the role of KC and CXCR2 in disease progression is not clear. It is possible that the primary role of KC and CXCR2 is in oligodendrocyte proliferation and migration that is a response to myelin destruction that is seen in the disease. Studies are currently underway to determine if KC or CXCR2 have any role in oligodendrocyte proliferation seen in the twitcher spinal cords. It is possible that the role of KC and CXCR2 is highly redundant even in oligodendrocyte proliferation and migration in response to injury. This could be possible because of the highly elevated levels of FGF-2 and PDGF-BB in the spinal cords of the twitcher mice that was found in the current study.

Although preliminary evidence of elevated growth factors was found in the current study, the chemokine profiles that were altered in the twitcher mice lacking KC or CXCR2 either in the entire body or in CNS and bone marrow compartment was not characterized. This would help in delineating the exact molecular pathways that could be important in creating the redundancy.

It was also surprising that elevation of KC had minimal effect on neutrophil recruitment. Transgenic over-expression of KC in the CNS leads to a massive infiltration of neutrophils (Tani et al., 1997). It is however possible that expression of KC in the endothelial cells played a prominent role in the neutrophil recruitment. Among several studies discussing the neuropathology in the twitcher mice, none of them have documented the presence of neutrophils.

Contrary to our expectation, there were activated microglia/ macrophages in the CNS of the twitcher mice lacking KC and CXCR2. This implies that neither

of the molecules are important for the recruitment /activation of the microglia and macrophages or there are other redundant pathways. In a recent study (Liu et al., 2010), it was shown that bone marrow chimeras with CXCR2-/- bone marrow show reduced demyelination in response to cuprizone. It appears that the lack of CXCR2 decreases the number of neutrophils (and possibly macrophages) and reduces demyelination. When similar chimeras were made in the GALC-/- mice, no such effect was seen, implying that the myelin damage in the twitcher mouse is very profound with minimal to no effect of the immune system on the disease progression. Alternatively, the incomplete bone marrow chimerism obtained by irradiating 9-10 day old mice could leave enough CXCR2+/+ cells in the bone marrow to cause demyelination. Since the disease is rapidly progressive, generating complete bone marrow chimeras would be challenging. All the above experiments strongly suggest that KC and CXCR2 have minimal to no effect on the inflammation in GLD. The other aspect that is affected by KC and CXCR2 is the oligodendrocyte migration and proliferation. These pathways could be activated in response to injury as seen in other models of demyelination (Robinson et al., 2008; Wu et al., 1998). Therefore, in vivo oligodendrocyte proliferation was measured by quantitating the BrdU labelling in the lumbar spinal cords of twitcher mice lacking KC or CXCR2. Although, the oligodendrocyte proliferation in the twitcher spinal cords is higher than the wildtype (Taniike and Suzuki., 1995), there could be no difference in oligodendrocyte proliferation in twitcher mice lacking KC or CXCR2. It is possible that the proliferative response is also compensated by other growth factors like FGF-2 and PDGF-BB which are found to be elevated in the spinal cords of the twitcher

mice.

To summarize, although KC is highly elevated in the CNS of the twitcher mice, its deficiency has no apparent effect on the inflammation, oligodendrocyte proliferation or on the overall progression of the disease. These findings highlight the profound and rapidly progressive oligodendrocyte damage in the twitcher mice and emphasize the redundancy of the chemokine system in the progression of disease. It appears that other therapeutic interventions would be ineffective if the primary enzyme deficiency is not corrected.

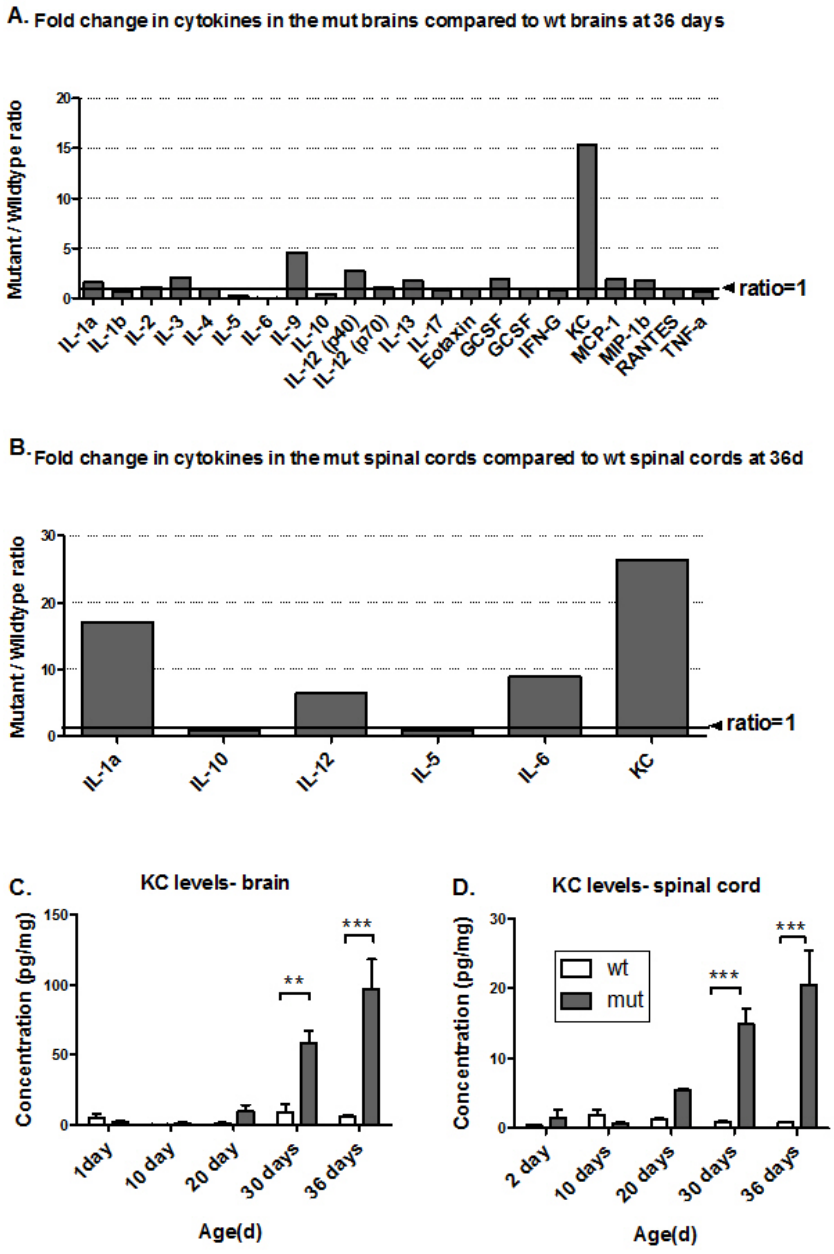

Figure 4.1: Cytokines and chemokines in the CNS of the twitcher mice.The fold-elevation of various cytokines/chemokines assayed in the brain (A) and the spinal cord (B) are shown. Among all the assayed molecules, the chemokine KC showed greatest fold change in the brain (>15-fold) and in the spinal cord (>25-fold) of the twitcher mice. The levels of KC in the brains and the spinal cords of the twitcher mice showed a progressive increase with time (C and D). The bars represent the mean and the error bars represent SEM. (**$p<0.01$, ***$p<0.001$)

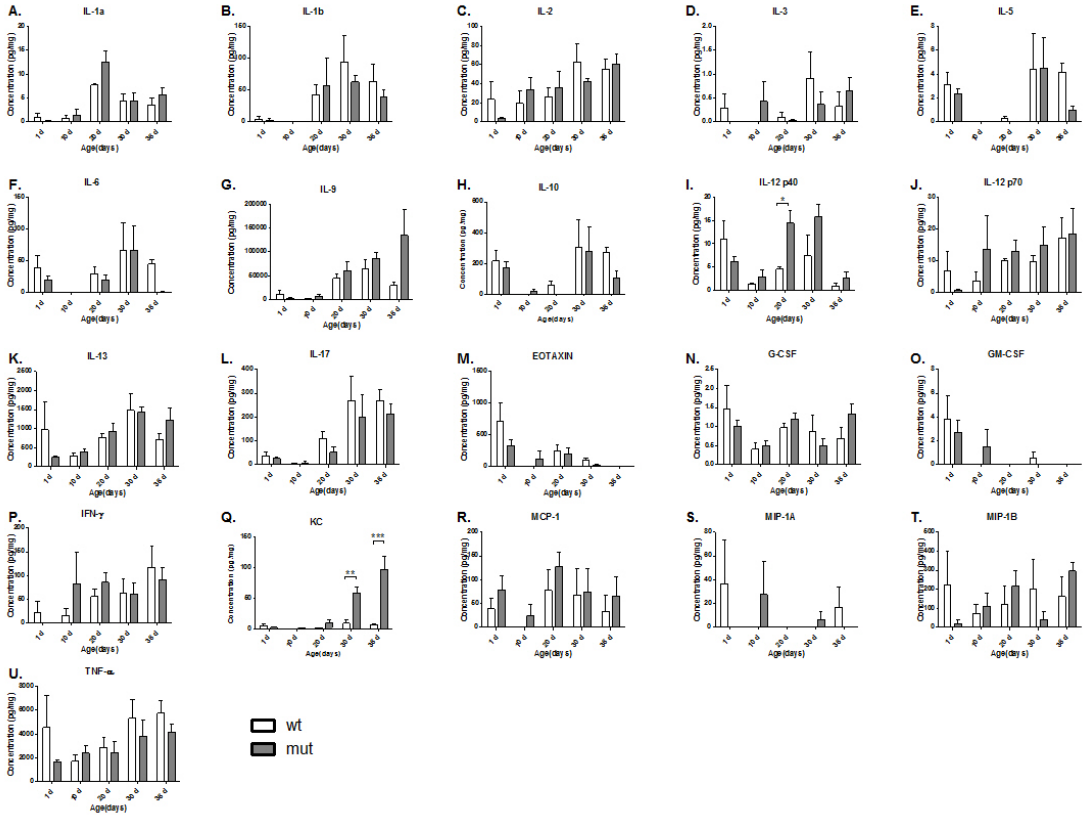

Figure 4.2: Cytokine profile in the brains of twitcher mice.The data obtained using 23-plex assay were normalized to the protein concentration of the individual samples and plotted as shown below. Each individual cytokine was measured at five time points. Two-way ANOVA were performed on each cytokine. The vertical bars represent the means and the error bars represent SEM (*$p<0.05$, **$p<0.01$, ***$p<0.001$).

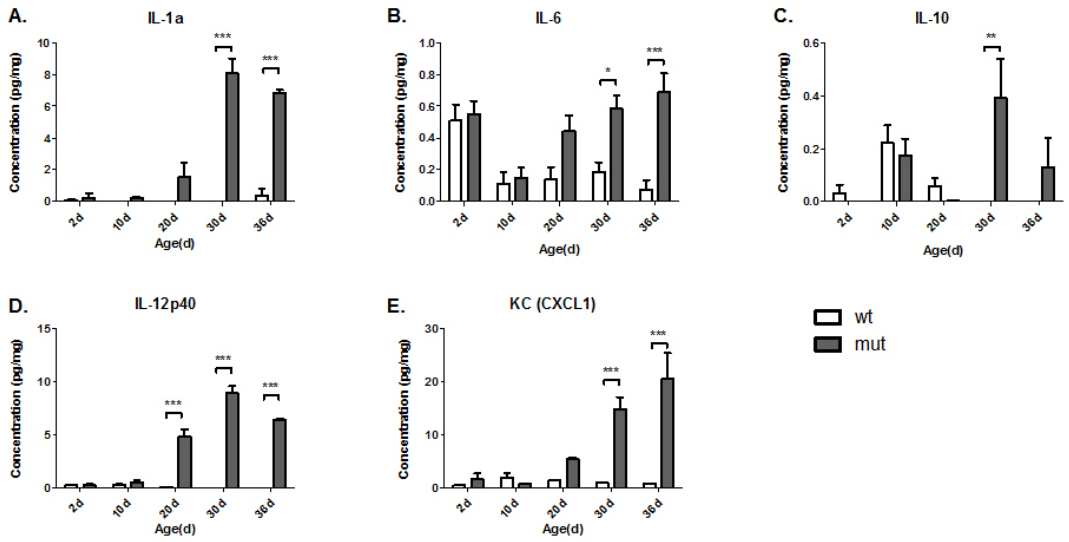

Figure 4.3: Cytokine profile in the spinal cords of the twitcher mice.The data obtained using assay similar to above were normalized to the protein concentration of the individual spinal cord samples. Only the cytokines that showed major alterations in the brains were assayed in the spinal cord. The cytokines were measured at five time points. Two-way ANOVAs were performed on individual cytokines. The bars represent the means and the error bars represent SEM (*$p<0.05$, **$p<0.01$, ***$p<0.001$).

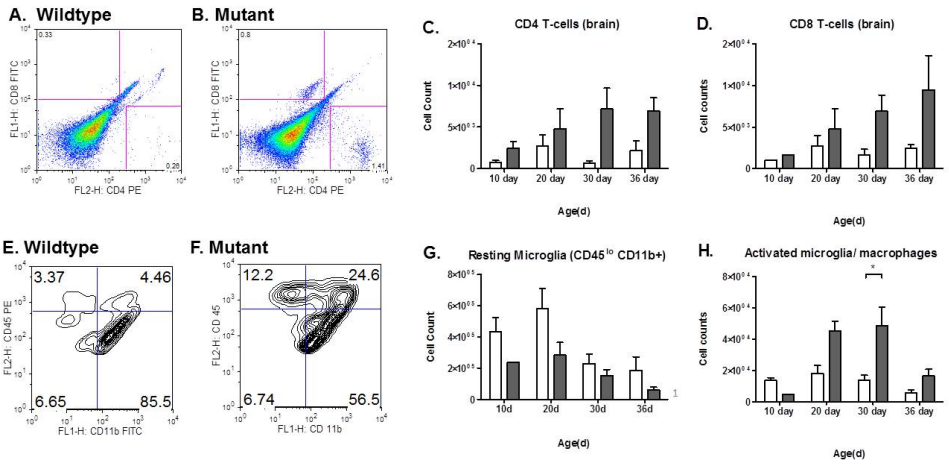

Figure 4.4: Characterization of the cellular inflammation in the twitcher CNS. Representative bivariate flow cytometry plots of CD4 and CD8 T-cells isolated from the wildtype (A) and twitcher (B) brains at day 36. These changes are summarized for different time points in C and D, which show a trend towards an increase in CD4 and CD8 T-cells. In panel E and F, representative bivariate contour plots derived from CD45+ gated cells isolated from the CNS are shown. In the wildtype (E), there are a large proportion of resting microglia ($CD45^{lo}$ CD11b+) and the presence of a small percentage of activated microglia ($CD45^{hi}$CD11b+). In the twitcher mice (F), there is an increase in the percentage of activated microglia with time. These changes are quantified in G and H. There is a significant increase in the number of activated microglia in the twitcher mice brains at day 30. (Error bars represent SEM, *$p<0.05$).

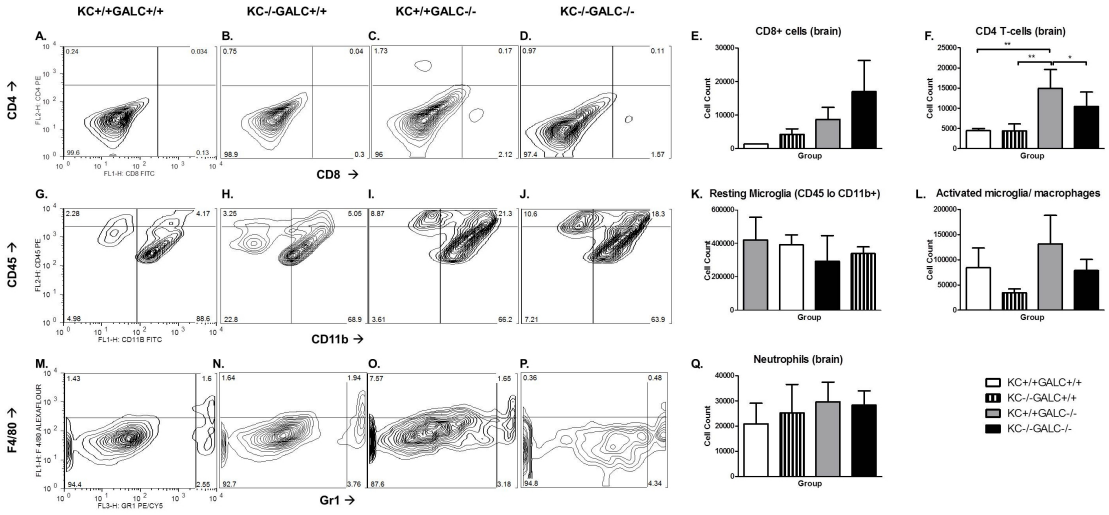

Figure 4.5: Cellular inflammation in KC-/- mice brains. Flow cytometric characterization of inflammation in the KC-/-GALC-/- mice. Panels A-D show the representative bivariate contour plots with CD8 and CD4 T-cells at day 36 in various groups of mice. The cell numbers are quantified in E and F. There is a significant increase in the CD4 T-cells in the brains of the KC-/-GALC-/- and KC+/+GALC-/- mice compared to the KC+/+GALC+/+ mice (E). There is a trend toward increase in the CD8 T-cells in the KC-/-GALC-/- and KC+/+GALC-/- mice compared to the KC+/+GALC+/+ mice (F). Panels G-J show the representative bivariate contour plots showing resting and activated microglia isolated from the brain at 36 days of age. Panel K and L shows the quantitation of the resting and activated microglia. There is no apparent difference between the KC+/+GALC-/- mice and KC-/-GALC-/- mice. Panels M-P show the representative bivariate contour plots of neutrophils (Gr1^{hi}F4/80-) isolated from the brain. These cells are quantitated in panel Q. There is no significant alteration in the neutrophil numbers isolated from the CNS in all the groups tested. The bars represent the mean and the error bars represent the standard error and *p$<$0.05.

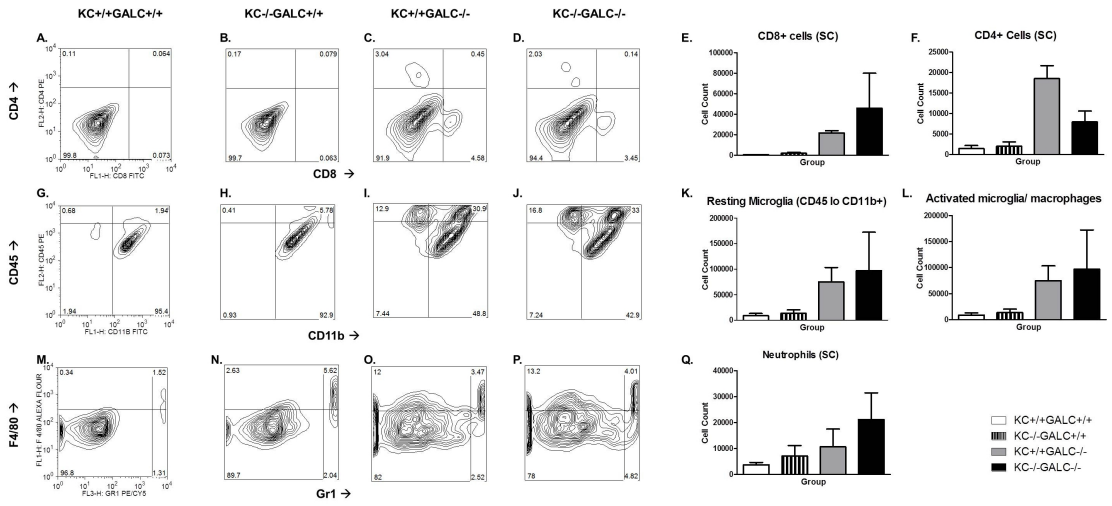

Figure 4.6: Cellular inflammation in KC-/- mice spinal cords. Flow cytometric characterization of inflammation in the KC-/-GALC-/- mice. Panels A-D show the representative bivariate contour plots with CD8 and CD4 T-cells at day 36 in various groups of mice. The cell numbers are quantified in E and F. There is a trend towards an increase in the CD4 T-cells in the spinal cords of the KC-/-GALC-/- and KC+/+GALC-/- mice compared to the KC+/+GALC+/+ mice (E). There is a trend toward increase in the CD8 T-cells in the KC-/-GALC-/- and KC+/+GALC-/- mice compared to the KC+/+GALC+/+ mice (F). Panels G-J show the representative bivariate contour plots showing resting and activated microglia isolated from the spinal cords at 36 days of age. Panel K and L shows the quantitation of the resting and activated microglia. There is no significant difference between the cell counts of KC-/-GALC-/- and KC+/+GALC-/- mice. Panels M-P show the representative bivariate contour plots of neutrophils isolated from the spinal cords. Neutrophils are Gr1^{hi}F4/80-. These cells are quantitated in Q. There is no significant alteration in the neutrophil numbers isolated from the CNS in all the groups tested. The bars represent the mean and the error bars represent the standard error.

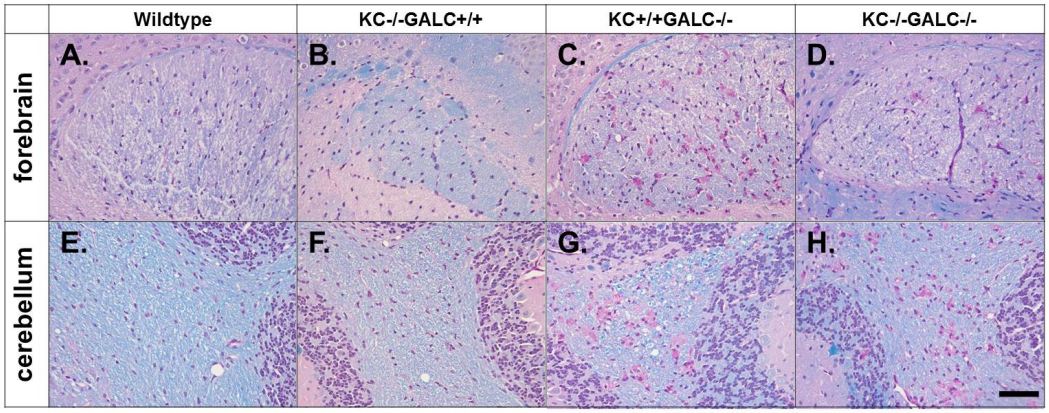

Figure 4.7: LFB-PAS staining of twitcher mice lacking KC. Histology of the brains and spinal cords showing LFB staining (blue) and PAS staining (pink) in the corpus callosum (A-D) and cerebellum (E-H) in the various groups of mice lacking KC and GALC. There is no difference in the KC+/+GALC+/+ and KC-/-GALC+/+ mice in all the tissues examined. The KC-/-GALC-/- tissues show histology which is essentially similar to the KC+/+GALC-/- (twitcher) with similar myelin staining and distribution of globoid cells. Scale bars are approximately 50 μ m.

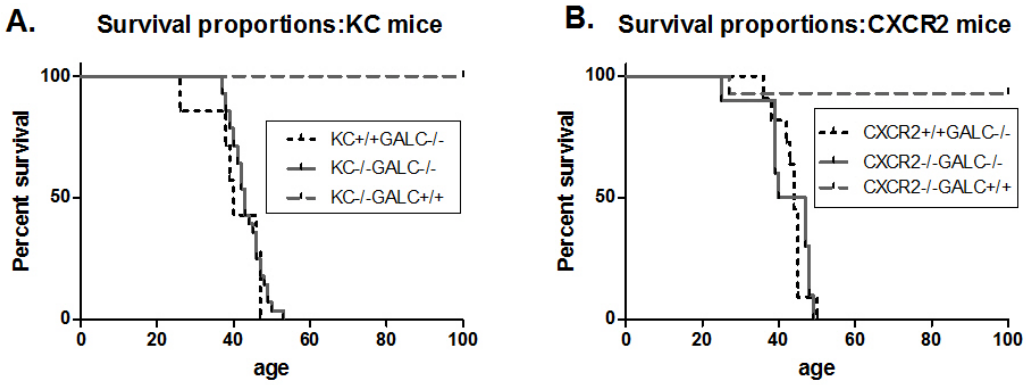

Figure 4.8: Survival of KC-/-GALC-/- and CXCR2-/-GALC-/- mice. Kaplan-Meier curves showing survival proportions of KC-/-GALC-/- mice (A) and CXCR2-/-GALC-/- mice (B). There is no significant difference in survival between KC-/-GALC-/- and KC+/+GALC-/- mice or between CXCR2-/-GALC-/- and CXCR2+/+GALC-/- mice (log-rank test).

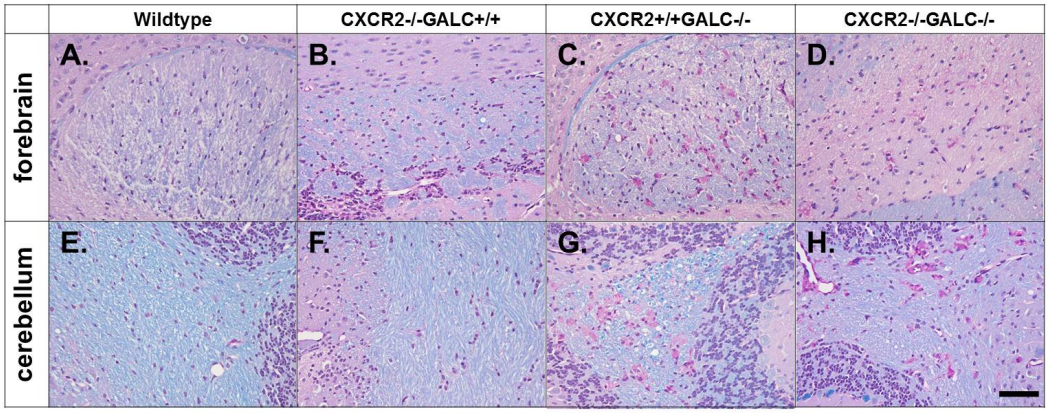

Figure 4.9: LFB-PAS staining of CXCR2-/-GALC-/- mice. Histology of CXCR2-/-GALC-/- mice compared to CXCR2+/+GALC-/- (twitcher) mice. There is no difference in the histology of these two groups in the forebrain (A-D) and cerebellum (E-H) in either with LFB (blue staining) or PAS staining (pink). Scale bar in H is approximately 50 μm.

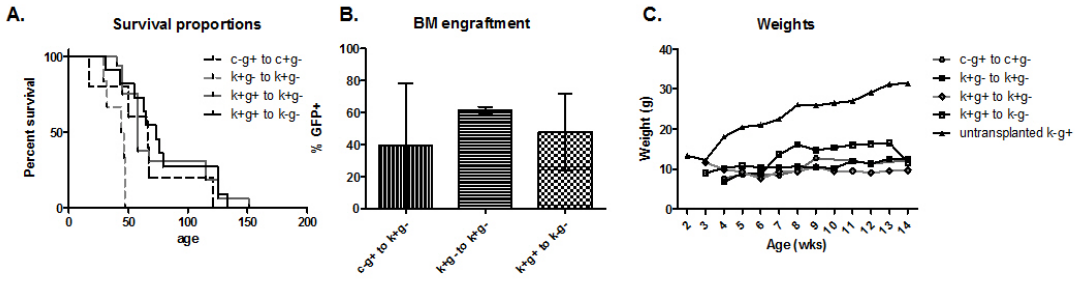

Figure 4.10: Effect of CXCR2 and KC bone marrow chimeras on the progression of GLD. The survival of the various chimeras lacking KC or CXCR2 only in the CNS or only in the periphery is shown in A. Transplanting wildtype bone-marrow in to the twitcher mice (k+g+ to k+g-; solid gray line) is therapeutic and extends the survival to a median of approximately 80 days. When GALC-/- bone marrow is transplanted to GALC-/- mice (k+g- to k+g- ; dashed gray line), the median lifespan is 45 days as compared to the untransplanted KC+/+GALC-/- mice which is 40 days (data not shown). The survival after BMT was similar in various chimeras lacking KC only in the CNS (k+g+ to k-g-) or CXCR2 in the periphery (c-g+ to c+g-). Bone marrow engraftment determined at 36 days of age (26d post transplant), shows that the engraftment of various groups is between 40 and 60% (B). There was no significant difference between the various groups. The weights (C) of various bone marrow chimeras are not significantly different from each other, but are significantly decreased compared to the wild-type chimera controls.

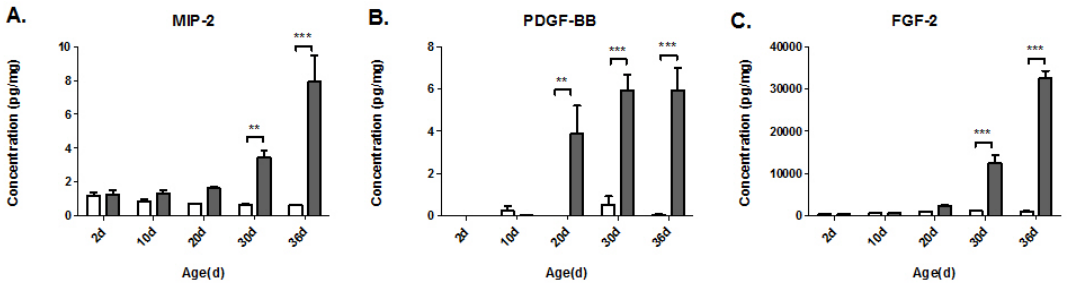

Figure 4.11: Alteration of cytokines and growth factors that could possibly compensate for the lack of KC or CXCR2. MIP-2, PDGF-BB and FGF-2 levels in the spinal cords of twitcher mice. MIP-2 (CXCL2) levels are progressively elevated in the spinal cords of the twitcher mice (A). Similar progressive increase is seen in FGF-2 and PDGF-BB. Vertical bars represent the mean and the error bars represent SEM (*$p<0.05$, **$p<0.01$, ***$p<0.001$).

Chapter 5

Summary, Conclusions and Future Directions

5.1 Combination therapy experiment

5.1.1 Summary and Conclusions

In our current study, described in chapter 2, additional targeting of the spinal cord and the cerebellum results in an improvement in lifespan compared to the limited targeting of only the forebrain and thalamus (Lin et al., 2007). In the previous study performed in our lab (Lin et al., 2007), the median lifespan of the twitcher mice was extended from 38 days in the untreated twitcher mice to about 55 days with AAV2/5 alone or to about 105 days using AAV+BMT. In our current study, the cerebellum and spinal cord were also targeted, since it appeared that the pa-thology in these regions was not corrected in the previous study. This led to an improvement in the lifespan to a median of 72 days using AAV2/5 alone and a median of 123 days using both AAV2/5 and BMT. This also led to associated improvements in biochemical and histological pa-rameters. However, in the mice that received AAV2/5 alone, inflammation markers (CD4 T-cells, CD8 T-cells and activated microglia) were increased. Interestingly, addition of BMT to AAV2/5 appeared to result in an overall decrease in inflammation

even though BMT alone provides no GALC activity and no reduction in psychosine. It is possible that the addition of BMT to AAV results in a direct decrease in inflammation resulting from immunomodulation.

5.1.2 Future directions

Although the CNS was extensively targeted and the brain showed a greater than 5-fold increase in overall enzyme activity, the median lifespan was only about 72 days in the animals that received AAV2/5. This may imply that 1) all of the cells in the CNS were not uniformly tar-geted, 2) the peripheral nerves and organs are important targets for therapy, or 3) the secondary processes in the disease were inadequately targeted. Based on the findings of the study, several future experiments can be envisioned that could improve therapeutic efficacy and address the mechanism of synergy and are discussed in detail below.

Strategies targeting oligodendrocytes

Oligodendrocytes are prominently affected in the disease. Targeting oligodendrocytes should be the primary focus of therapy. Some of the gene therapy vectors like AAV and adeno-virus mostly target the neurons and show poor targeting of oligodendrocytes (Howard et al., 2008). Using viral vectors that show higher affinity towards oligodendrocytes (e.g. AAV8 and AAV serotype rh43) (Lawlor et al., 2009) could prove to be an improvement over existing viral vectors. Another method for improved targeting of oligodendrocytes is to use phage panning (Chen et al., 2009). In phage panning, a phage library is created with various peptides on the phage capsid and the phages that are bound to the spe-

cific cell types (e.g. endothelial cells or oli-godendrocytes) are isolated after the phages are delivered *in vivo*. One of the important therapeutic principles in the treatment of lysosomal storage diseases is cross-correction, which is discussed in detail in chapter 1. However, with GALC, it appears that the cross-correction in the oligodendrocytes is poor, which could be a limiting factor in therapy. *In vitro* transwell experiments have shown that the enzyme cross-correction obtained in oligodendrocytes is significantly lower than that of fibroblasts (Luddi et al., 2001). This suggests that the enzyme uptake machinery (mannose-6-phosphate receptor) of oligodendrocytes is not as functional as that of the other cells in the periphery. Several approaches can be utilized to enhance the cross-correction and diffusivity of GALC in the CNS: a. Upregulation of the mannose-6-phosphate receptors: Strategies to increase mannose-6-phosphate receptor expression could potentially serve as adjunctive therapies for gene therapy or enzyme replacement therapy. In fibroblasts, mannose 6-phosphate, insulin like growth factors I and II, and epidermal growth factor have been shown to cause acute upregulation of mannose-6-phosphate receptors. Interestingly, radiation damage in the intestine upregulates the mannose-6-phosphate expression in the epithelial cells (Wang et al., 1999) and such a phenomenon in oligodendrocytes could potentially explain the synergy seen in our study. So far, no studies have examined this phenomenon in detail in oligodendrocytes. Since mannose-6-phosphate receptors are downregulated at a relatively fast rate (Kornfeld, 1992), methods for chronic upregulation of mannose-6-phosphate receptors could be an interesting avenue for future research. b. tat modification of GALC: Tat is a protein from the Human Immunodeficiency Virus. The protein

transduction domain contains an 11- amino acid sequence that allows the entry of proteins into cells by penetrating the cell membrane (Frankel and Pabo, 1988). The 11-amino acid sequence also enhances cytoplasmic entry of proteins when they are fused with it (Schwarze et al., 2000). Tat modification of another lysosomal enzyme β-glucuronidase has been shown to increase enzyme distribution in the CNS (Xia et al., 2001). Preliminary studies in our lab using such an approach have shown that the enzyme activity is preserved in the GALC-tat fusion protein. It would be interesting to test whether the uptake and cross-correction and proper targeting to the lysosome are higher in the fusion protein and whether the overall therapeutic effi-ciency is increased.

Strategies targeting bone marrow

After myeloablative BMT, an increase in GFP+ donor cells in the CNS is seen (Wu et al., 2000). Since transplantation of enzyme-deficient donor cells has minimal impact on the disease, it is likely that the enzyme-expressing donor cells provide therapeutic benefit at least partially by supplying the enzyme to the CNS. In our current protocol, the sensitivity of mice to high levels of radiation prevents further increasing the radiation dose for conditioning on postnatal day 3-4. In this scenario, several alternate approaches to increase the total enzyme in the bone marrow could be considered, especially in combination with CNS-directed gene therapy. a. Hematopoietic-directed gene therapy with lentiviruses (Naldini, 2011). b. Increasing bone marrow engraftment: Using busulphan *in utero* in addition to postnatal conditioning appears to result in an increased level of engraftment which might translate into greater enzyme activity (Yeager et al., 1991). Another approach to experimentally increase the

engraftment would be by using W41 mice. These mice have point mutations in the c-kit re-ceptor and as a result have a competitive disadvantage with wild-type bone marrow cells in terms of proliferation (Miller et al., 1996). Using these mice, a very high level of engraftment can be obtained using very low levels of radiation (Hall et al., 2007). Administering c-kit antagonists (Kelly et al., 2002) in combination with a mild conditioning regimen could be a potential combination to achieve high-level engraftment in humans. c. Increasing cell entry into the CNS: Disrupting the integrity of the blood-brain barrier using vascular endothelial growth factor (VEGF) in conjunction with BMT expressing a high level of GALC could also lead to improved enzyme delivery into the CNS (Young et al., 2004). When leukocytes enter the brain parenchyma, most of the cells are localized to the perivascular space due to the interaction of membrane CXCL12 (present on the basal side of the endothelial cells) with the chemokine receptor CXCR4 (McCandless et al., 2006). Disrupting interactions between immune cells and chemokine receptors using CXCR4 antagonist AMD 3100, in a murine model of experimental allergic encephalomyelitis, results in greater spread of immune cells in the CNS parenchyma and worsening of pathology (McCandless et al., 2006). This approach could be potentially adapted for enhanced entry of enzyme-expressing cells into the CNS. d. Expressing modified GALC with increased CNS bioavailability: Metaperiodate fol-lowed by Borohydride reduction of another lysosomal enzyme β-glucuronidase leads to a removal of mannose-6-phosphate residues and an increase in the circulating half-life and CNS bioavailability of the enzyme (Grubb et al., 2008). It is possible that the CNS uptake is mediated by a non-receptor mechanism. A similar approach

could be attempted in Krabbe's disease. The mannose-6-phosphate residues are attached to the N-linked and O-linked oligosaccharides to aspargine or serine side chains of the protein (Kornfeld, 1992). Recombinant proteins which lack sites for attachment of N-linked and O-linked oligosaccharides but preserved or enhanced enzyme activity could be synthesized using combinatorial approaches. These genes could then be used in viral vectors to transduce bone marrow cells or for direct systemic gene therapy.

Strategies targeting peripheral nerves and autonomic nerves

Although GALC is highly expressed in the CNS, its function is important in the peripheral nervous system as well. Twitcher mice have inflamed peripheral nerves with edema and infiltra-tion of globoid cells and a decrease in peripheral nerve conduction (Hoogerbrugge et al., 1988b). Hindlimb paralysis is also a prominent feature of late stage disease in twitcher mice. In humans, the cranial nerves seem to be more prominently affected with the presence of swallowing difficulties and visual defects (Suzuki et al., 2000). Recently, twitcher mice have also been shown to have autonomic neuropathy which leads to a progressive thymic and splenic atrophy (Galbiati et al., 2007a). Although a significant amount of enzyme activity is present in the normal liver, kidney and bone marrow, the exact function of the enzyme in these peripheral organs is not known. Like in other lysosomal storage diseases, it could be speculated that the CNS pathology is the ”rate-limiting” step in the disease and hence the peripheral manifestations of enzyme deficiency are less obvious. However, once the CNS is corrected to a certain extent, the peripheral manifestations of the disease may then need correction. The presence of numerous peripheral nerves and

autonomic nerves presents a challenge for targeting them individually. BMT (myeloablative) is associated with improved peripheral nerve function and histology (Hoogerbrugge et al., 1988a). This indicates that a systemic approach is more pragmatic. This approach could be complemented by specific targeting of important nerves, such as the sciatic nerve. Recent studies have shown very effective retrograde transport of AAV6 when injected into the gastrocnemius muscle and efficient transduction of the peripheral nerve (Towne et al., 2010). High level of transduction was also obtained by direct targeting of the sciatic nerve with AAV8 (Homs et al., 2011). Another approach for correcting the disease in the peripheral and autonomic nervous system is targeting a peripheral organ as a 'reservoir' for the enzyme. This approach is similar to other disease like hemophilia B (Vandenberghe et al., 2006), mucopolysaccharidosis VII (Daly et al., 1999a, 1999b) etc. Several viral vectors such as AAV2, lentivirus, and adenovirus (Sands and Davidson, 2006) have been used for efficient targeting of the liver.

Understanding the mechanism of synergy

The mechanism of dramatic synergy observed in the previous study (Lin et al., 2007) was addressed in the current study. It is not entirely surprising that CD4 and CD8 T-cell numbers are increased in the CNS of the mice receiving AAV2/5, as it represents the naturally occuring antiviral response. Although AAV2/5 is a relatively inert virus, inflammatory reactions with increases in CD8 and CD4 T-cells have been known to occur in the liver (Vandenberghe et al., 2006; Mays et al., 2009). The evidence from our study, discussed in chapter 2, is strongly suggestive of the direct immunomodulatory role of the BMT. Independent confir-

mation of the increase in T-cells using histology or Q-PCR should be sought. In order to address the mechanism of synergy in greater detail, the studies could begin by narrowing the role of the innate versus the adaptive immune system. The role of the adaptive immune system could be studied by testing the presence of synergy in the mice that lack T-cells and B-cells (for e.g. rag mice, SCID mice) (Mombaerts et al., 1992; Shinkai et al., 1992). These studies could be further narrow the various subtypes of cells involved using twitcher mice lacking CD4, CD8 mouse etc. (Simard et al., 1997; Krieger et al., 1997; Hofling et al., 2003). The role of the innate immune system in synergy could be addressed by using twitcher mice lacking microglia (e.g., PU.1 knockout mouse) (Beers et al., 2006). Other important mechanisms that might be playing a role in BMT-mediated immunosuppression include deletion of alloreactive T-cells and the induction of tolerance to viral antigens after transplantation by T-regulatory cells (Walsh et al., 2004). One experiment to address the role of T-regulatory cells would be to use donor bone marrow that is selectively depleted of T-regulatory cells (CD4+CD25+ and CD8+CD25+ cells). Another possible explanation for the observed synergy is the peripheral correction of the disease brought about by BMT. A recent study (Galbiati et al., 2007a) has demonstrated the presence of atrophy in the various autonomic neurons innervating the thymus and the spleen. BMT could improve the autonomic dysfunction seen in the disease and bring about synergy. The thymus and spleen have to be examined in detail to see if the synergy correlates with the improvement in pathology in these organs. Synergy could also result from the increased accessibility of the enzyme from the donor cells that enter the CNS to sites that are inaccessible to injec-

tions. The pathology in the brain-stem is profound and poor correction of the brainstem could lead to a rapid compromise of the various vital centers that are present in this part of the CNS. The rapidly progressive nature of the disease might limit the optimal cross-correction and diffusivity of the enzyme. BMT could possibly increase the enzyme levels to the sites inaccessible to gene therapy. This could be tested by immunohistochemical localization of GALC in animals receiving combination therapy

The role of regional differences in the progression of disease and therapy

In the current study, the enzyme assays, psychosine measurements, flow cytometry and cytokine quantitation were performed using the whole brain. Although differences are present in the whole brain between various groups, it is possible that some of the differences are not obvi-ous because the whole brain was analyzed. For example, it appears that the psychosine levels are similar in the AAV-mut and AAV+BMT-mut group. It is possible that the differences in psy-chosine levels may correlate better with the efficacy of treatment, when only white matter rich regions (like corpus callosum) are analyzed. Then, the differences between animals receiving AAV2/5 and AAV+BMT-mut animals might be more obvious. Similarly, some of the cytokines such as TNF-α and IFN-γ may show regional differences which are less obvious when whole brain is analyzed. Future studies should explore these differences and their alteration with various therapies.

Timing of therapy

In humans, most of the myelination takes place after birth (Brody et al., 1987; Kinney et al., 1988), so it is reasonable to assume that delivering enzyme after birth would be an optimal time to begin therapy, at least with the current methods of enzyme delivery. Although there are no obvious clinical or biochemical markers of disease in affected newborns, it is possible that the disease is present even at birth. In human subjects, umbilical cord transplantation prior to the on-set of symptoms (age range: 12 to 44 days) results in a significant clinical improvement in the newborns compared to subjects transplanted with cord blood after the onset of symptoms (age range: 142 to 352 days) (Escolar et al., 2005). BMT has been attempted *in utero* in 3 human subjects, however, none of the subjects survived post-procedure (Bambach et al., 1997). Increased safety of *in utero* BMT would probably allow testing this approach. Another approach is to increase cell or enzyme transfer from the mother to the fetus. Maternal-fetal chimerism of hematopoietic-derived cells is known to occur physiologically at low levels (1-2

5.2 Characterization of tremor

5.2.1 Summary and conclusions

Although the addition of BMT to AAV2/5 resulted in an improvement in the various be-havioral parameters and lifespan, it worsened the tremor. This alteration in the tremor was sur-prising and was investigated in detail in chapter 3. The detailed characterization of tremor was performed using a modified force-plate actometer. Twitcher mice have a broader band tremor with the presence of higher

frequency components of movements compared to the wildtype an-imals. In order to test if the actometer was sensitive to known tremors, wildtype mice were treated with a tremorogenic agent harmaline and the current modification of the force-plate actometer appeared sensitive. Interestingly, harmaline could not induce tremor in the twitcher mice which indicates that the tremorogenic locus of harmaline (olive and cerebellum) is affected in the twitch-er mice. After therapy, the AAV group showed a power spectrum similar to that of the wildtype, but the addition of BMT negates the 'therapeutic benefit'. So, the effect of conditioning and BMT on the movement phenotype was further investigated. Interestingly, wildtype animals receiving BMT have an altered power spectrum compared to that of the untreated wildtype, and the twitcher mice treated with BMT have altered power spectrum compared to that of the untreated twitcher mice. Also, the wildtype animals treated with harmaline show a blunted tremor response. Since it is known that the neonatal conditioning and BMT lead to cerebellar dysplasia (Sands et al., 1993), it is possible that the function of the cerebellum is affected. Taking all the findings together, the tremor in the twitcher mice has a prominent cerebellar component and the physiological properties of olive and the cerebellum are altered in the twitcher mice and in wildtype mice treated with BMT.

5.2.2 Future Directions

Two important findings from the characterization of the tremor phenotype need further understanding: the origin of tremor and the exact effect of BMT on the movement phenotype. The origin of the tremor could be addressed based on the two types of tremors that are known to exist: a low frequency (8-10 Hz)

tremor that is known to arise after disruption of the basal ganglia pathways and a higher frequency tremor (12-14 Hz) tremor that is known to arise after disruption of cerebellar function. Our studies have revealed that the tremor in the twitcher mice is predominantly of higher frequencies and also the response to the drug acting on the olivo-cerebellar circuit (harmaline) is blunted. Although greater power is present in the power spectra of twitcher mice at higher frequencies, greater power is also present at lower frequencies. This implies that basal ganglia could also be involved in generating the complex tremor phenotype. This could be tested by using physostigmine (a cholinergic agent) (Wang and Fowler, 2001) which produces a low frequency tremor. If the lower frequency tremor is not inducible in the twitcher mice, then it is possible that basal ganglia are similarly affected. Since the CNS pathology in the twitcher mice is extensive, it would be difficult to localize the exact origin of tremor. However, identifying the predominant sites of the origin of tremor would be useful in terms of targeting and monitoring various therapies.

Intention tremor versus resting tremor

Our preliminary analyses have revealed that the differences in power spectra in the twitcher mice and wildtype are greater during active movements than during rest. This appears similar to the intention tremor that is seen in humans with cerebellar lesions. This could possibly imply that the cerebellum is the predominant origin of the tremor. Further exploration with a more precise definition of the resting state of the animal would help in understanding this possibility in a definite way.

Alternative therapies that do not worsen tremor after treatment

One of the surprising findings of the study was that the power spectra in the mice receiv-ing both AAV and BMT was similar to that of the untreated twitcher mice, whereas the mice re-ceiving only AAV had power spectra similar to that of the wildtype mice. Interestingly, wildtype mice receiving BMT also had alterations in the power spectra. This clearly highlights the damag-ing effects of BMT and the associated radiation conditioning prior to the procedure. Neonatal cerebellum has numerous proliferating granule cells (Galbiati et al., 2007b; Noguchi et al., 2008) and as such is vulnerable to genotoxic insults. Similar motor defects are also seen in children who received BMT for Krabbe's disease on extended follow up (Escolar et al., 2005), although the exact causal link is uncertain. The exact therapeutic mechanism of BMT probably involves multiple mechanisms. Nevertheless, alternative therapies that are less toxic to rapidly proliferat-ing cells in the CNS (such as anti-inflammatory drugs, agents that promote cell entry into the CNS e.g. VEGF) are highly desirable. Understanding the exact molecular pathways altered by BMT in the CNS could lead to therapies that spare the untoward effects on rapidly proliferating cells in the CNS.

5.3 The role of KC and CXCR2 in the pathogenesis of Krabbe's disease

5.3.1 Summary and conclusions

Since inflammation was a prominent feature in the CNS of the twitcher mice, the role of the various cellular and humoral mediators of inflammation was sur-

veyed, as detailed in chapter 4. There was a trend towards a progressive increase in the CD4 and CD8 T-cells in the brains of the twitcher mice with time. There was a significant increase in the activated microglial numbers in the brains of the twitcher mice. Several chemokines and cytokines were surveyed and the cyto-kine KC was highly elevated in both the brains and the spinal cords of the twitcher mice. KC was known to be involved both in inflammation and oligodendrocyte proliferation, both prominent features of the disease. Interestingly, detailed characterization of the KC-/-GALC-/- mice and CXCR2-/-GALC-/- mice revealed no difference in the cellular inflammation seen in the CNS of twitcher mice. Selective deficiency of KC in the CNS or selective deficiency of CXCR2 in the bone marrow did not alter the course of the disease. Twitcher mice have been shown to have increased proliferation in the spinal cord (Taniike and Suzuki, 1995). The role of KC and CXCR2 in oligodendrocyte proliferation seen in the disease is currently under investigation. Although very high levels of KC were seen in the disease, the lack of phenotype in the absence of KC or CXCR2 implies redundancies in the chemokines and the growth factors. Also, the lack of KC or CXCR2 failed to show an effect in the twitcher mice, probably implying that the primary disease is profound and that targeting secondary processes like elevated KC would not have any benefit in treating the disease without first targeting the primary enzyme deficiency.

5.3.2 Future Directions

Exploring the role of KC and CXCR2 in oligodendrocyte prolifera-tion

It is possible that the primary role of KC is to control the oligodendrocyte proliferation and to localize the oligodendrocyte precursors to areas of myelin dam-

age. This possibility could be further explored using immunostaining for NG2 (oligodendrocyte precursor marker) and BrdU (marker of cell proliferation). Preliminary evidence suggests that the number of NG2 +BrdU+ cells in the spinal cord of the twitcher mice is increased. The effect of the lack of KC or CXCR2 in the twitcher mice on the proliferation of NG2+BrdU+ cells is currently under investigation. It would be interesting to know if other ligands of CXCR2 and other growth factors are further elevated in these mice, compensating for the lack of KC or CXCR2.

Exploring the role of other chemokines and growth factors in disease progression

Since redundancies exist in the chemokine KC and its receptor CXCR2 for inflammation and oligodendrocyte proliferation, deletion of other molecules that might be responsible for the compensatory effect (FGF-2, PDGF-BB, CXCL2) could be attempted. Unfortunately, deletion of multiple molecules would make the effects less easy to interpret. Previous experiments in which a single cytokine like IL-6 or TNF-α was deleted (Pedchenko et al., 2000; Biswas et al., 2001) also had minimal effect on altering the course of the disease. Similarly, minimal alteration in the course of the disease was seen when MHC-Ia was de-leted in the twitcher mice (Matsushima et al., 1994). This highlights the numerous redun-dancies that exist in the system. One approach to overcome the redundancies would be to use models that result in a known phenotype in a particular cell type that is known to be involved in the disease. These models are usually a result of the lack of a transcription factor like PU.1 (which plays an important role in the development of myeloid lineage/ microglia; Beers et

al., 2001) or the lack of microRNAs that suppress several factors responsible for cell differentiation (e.g. mir-219 is responsible for oligodendrocyte differentiation and myelination and suppresses expression of several transcription factors and PDGF-β) (Dugas et al., 2010). As mentioned above, the progression of the disease, the inflammation and oligodendrocyte proliferation could be studied in twitcher mice that lack microglia (PU.1 knockout mice; Beers et al., 2001) and twitcher mice that have delayed oligodendrocyte maturation (mir-219 knockout mice; Dugas et al., 2010).

Effect of correcting primary disease in KC and CXCR2 mice

It is possible that the effect of lack of KC and CXCR2 on inflammation or oligodendrocyte prolif-eration is not apparent with the current model, because of the rapidly progressive pathology. It is possible, however, that the effect of the lack of KC and CXCR2 would be more apparent if the progression of the disease is slowed. Two models could be utilized where the progression of the disease is slowed: a. adult onset Krabbe's disease model (Luzi et al., 2001) in which a pathology similar to the twitcher mouse is seen but the course of the disease is protracted b. twitcher mice lacking KC or CXCR2 treated with AAV2/5 expressing GALC to delay the pro-gression of the disease.

References

Arnett HA, Mason J, Marino M, Suzuki K, Matsushima GK, Ting JP (2001) TNF alpha promotes proliferation of oligodendrocyte progenitors and remyelination. Nat. Neurosci 4:1116-1122 Available at: [Accessed December 14, 2010].

Bambach BJ, Moser HW, Blakemore K, Corson VL, Griffin CA, Noga SJ, Perlman EJ, Zuckerman R, Wenger DA, Jones RJ (1997) Engraftment following in utero bone marrow transplantation for globoid cell leukodystrophy. Bone Marrow Transplant 19:399-402 Available at: [Accessed June 14, 2011].

Bansal R (2002) Fibroblast growth factors and their receptors in oligodendrocyte development: implications for demyelination and remyelination. Dev. Neurosci 24:35-46 Available at: [Accessed April 25, 2011].

Beers DR, Henkel JS, Xiao Q, Zhao W, Wang J, Yen AA, Siklos L, McKercher SR, Appel SH (2006) Wild-type microglia extend survival in PU.1 knockout mice with familial amyotrophic lateral sclerosis. Proc. Natl. Acad. Sci. U.S.A 103:16021-16026 Available at: [Accessed June 14, 2011].

Biswas S, LeVine SM (2002) Substrate-reduction therapy enhances the benefits of bone marrow transplantation in young mice with globoid cell leukodystrophy. Pediatr Res 51:40-7

Biswas S, Pinson DM, Bronshteyn IG, LeVine SM (2001) IL-6 deficiency allows for enhanced therapeutic value after bone marrow transplantation across a minor histocompatibility barrier in the twitcher (globoid cell leukodystrophy) mouse. J Neurosci Res 65:298-307

Boisvert WA, Rose DM, Johnson KA, Fuentes ME, Lira SA, Curtiss LK, Terkeltaub RA (2006) Up-Regulated Expression of the CXCR2 Ligand KC/GRO-alpha in Atherosclerotic Lesions Plays a Central Role in Macrophage Accumulation and Lesion Progression. Am J Pathol 168:1385-1395 Available at: [Accessed January 1, 2008].

Boisvert WA, Santiago R, Curtiss LK, Terkeltaub RA (1998) A Leukocyte Homologue of the IL-8 Receptor CXCR-2 Mediates the Accumulation of Macrophages in Atherosclerotic Lesions of LDL Receptor-deficient Mice. J. Clin. Invest. 101:353-363 Available at: [Accessed January 1, 2008].

Brody BA, Kinney HC, Kloman AS, Gilles FH (1987) Sequence of central nervous system myelination in human infancy. I. An autopsy study of myelination. J. Neuropathol. Exp. Neurol 46:283-301 Available at: [Accessed June 10, 2011].

Bruscia EM, Ziegler EC, Price JE, Weiner S, Egan ME, Krause DS (2006) Engraftment of donor-derived epithelial cells in multiple organs following bone marrow transplantation into newborn mice. Stem Cells 24:2299-2308 Available at: [Accessed April 1, 2011].

Campanella M, Sciorati C, Tarozzo G, Beltramo M (2002) Flow cytometric analysis of inflammatory cells in ischemic rat brain. Stroke 33:586-592 Available at: [Accessed November 11, 2009].

Cardona AE, Huang D, Sasse ME, Ransohoff RM (2006) Isolation of murine microglial cells for RNA analysis or flow cytometry. Nat Protoc 1:1947-1951 Available at: [Accessed July 19, 2010].

Carlson T, Kroenke M, Rao P, Lane TE, Segal B (2008) The Th17-ELR+ CXC chemokine pathway is essential for the development of central nervous system autoimmune disease. J. Exp. Med. 205:811-823 Available at: [Accessed January 13, 2009].

Chen YH, Chang M, Davidson BL (2009) Molecular signatures of disease brain endothelia provide new sites for CNS-directed enzyme therapy. Nat. Med 15:1215-1218 Available at: [Accessed June 12, 2011].

Consiglio A, Martino S, Dolcetta D, Cusella G, Conese M, Marchesini S, Benaglia G, Wrabetz L, Orlacchio A, Dglon N, Aebischer P, Severini GM, Bordignon C (2007) Metabolic correction in oligodendrocytes derived from metachromatic leukodystrophy mouse model by using encapsulated recombinant myoblasts. J. Neurol. Sci 255:7-16 Available at: [Accessed April 23, 2011].

Daly TM, Okuyama T, Vogler C, Haskins ME, Muzyczka N, Sands MS (1999)(a) Neonatal Intramuscular Injection with Recombinant Adeno-Associated Virus Results in Prolonged beta-Glucuronidase Expression in Situ and Correction of Liver Pathology in Mucopolysaccharidosis Type VII Mice. hum gene ther 10:85-94 Available at: [Accessed January 8, 2010].

Daly TM, Vogler C, Levy B, Haskins ME, Sands MS (1999)(b) Neonatal gene transfer leads to widespread correction of pathology in a murine model of lysosomal storage disease. Proceedings of the National Academy of Sciences of the United States of America 96:2296-2300 Available at: [Accessed January 8, 2010].

De Gasperi R, Friedrich VL, Perez GM, Senturk E, Wen PH, Kelley K, Elder GA, Gama Sosa MA (2004) Transgenic rescue of Krabbe disease in the twitcher mouse. Gene Ther 11:1188-94

Doherty PC (1985) T cells and viral infections. Br. Med. Bull 41:7-14 Available at: [Accessed December 4, 2010].

Dolcetta D, Perani L, Givogri MI, Galbiati F, Orlacchio A, Martino S, Roncarolo MG, Bongarzone E (2004) Analysis of galactocerebrosidase activity in the mouse brain by a new histological staining method. J Neurosci Res 77:462-4

Duchen LW, Eicher EM, Jacobs JM, Scaravilli F, Teixeira F (1980) Hereditary leucodystrophy in the mouse: the new mutant twitcher. Brain 103:695-710

Duffner PK et al. (2009) Newborn screening for Krabbe disease: the New York State model. Pediatr. Neurol 40:245-252; discussion 253-255 Available at: [Accessed October 29, 2010].

Dugas JC, Cuellar TL, Scholze A, Ason B, Ibrahim A, Emery B, Zamanian JL, Foo LC, McManus MT, Barres BA (2010) Dicer1 and miR-219 Are Required for Normal Oligodendrocyte Differentiation and Myelination. Neuron 65:597-611 Available at: [Accessed June 13, 2011].

Elliger SS, Elliger CA, Aguilar CP, Raju NR, Watson GL (1999) Elimination of lysosomal storage in brains of MPS VII mice treated by intrathecal administration of an adeno-associated virus vector. Gene Ther 6:1175-1178 Available at: [Accessed July 17, 2010].

Escolar ML, Poe MD, Provenzale JM, Richards KC, Allison J, Wood S, Wenger DA, Pietryga D, Wall D, Champagne M, Morse R, Krivit W, Kurtzberg J (2005) Transplantation of umbilical-cord blood in babies with infantile Krabbes disease. N. Engl. J. Med 352:2069-2081 Available at: [Accessed October 29, 2010].

Filipovic R, Jakovcevski I, Zecevic N (2003) GRO-alpha and CXCR2 in the human fetal brain and multiple sclerosis lesions. Dev. Neurosci 25:279-290 Available at: [Accessed July 19, 2010].

Fowler SC, Birkestrand BR, Chen R, Moss SJ, Vorontsova E, Wang G, Zarcone TJ (2001) A force-plate actometer for quantitating rodent behaviors: illustrative data on locomotion, rotation, spatial patterning, stereotypies, and tremor. Journal of Neuroscience Methods 107:107-124 Available at: [Accessed November 11, 2009].

Frankel AD, Pabo CO (1988) Cellular uptake of the tat protein from human immunodeficiency virus. Cell 55:1189-1193 Available at: [Accessed June 13, 2011].

Fratantoni JC, Hall CW, Neufeld EF (1968) Hurler and Hunter syndromes: mutual correction of the defect in cultured fibroblasts. Science 162:570-572 Available at: [Accessed April 22, 2011].

Frisella WA, OConnor LH, Vogler CA, Roberts M, Walkley S, Levy B, Daly TM, Sands MS (2001) Intracranial Injection of Recombinant Adeno-associated Virus Improves Cognitive Function in a Murine Model of Mucopolysaccharidosis Type VII. Mol Ther 3:351-358 Available at: [Accessed April 23, 2011].

Fry EJ, Ho C, David S (2007) A role for Nogo receptor in macrophage clearance from injured peripheral nerve. Neuron 53:649-662 Available at: [Accessed April 25, 2011].

Galbiati F, Basso V, Cantuti L, Givogri MI, Lopez-Rosas A, Perez N, Vasu C, Cao H, van Breemen R, Mondino A, Bongarzone ER (2007)(a) Autonomic denervation of lymphoid organs leads to epigenetic immune atrophy in a mouse model of Krabbe disease. J. Neurosci 27:13730-13738 Available at: [Accessed June 13, 2010].

Galbiati F, Clementi G, Superchi D, Givogri MI, Bongarzone ER (2007)(b) Effects of irradiation on the postnatal development of the brain in a genetic mouse

model of globoid cell leukodystrophy. Neurochem Res 32:377-88

Galbiati F, Givogri MI, Cantuti L, Rosas AL, Cao H, van Breemen R, Bongarzone ER (2009) Combined hematopoietic and lentiviral gene-transfer therapies in newborn Twitcher mice reveal contemporaneous neurodegeneration and demyelination in Krabbe disease. J. Neurosci. Res 87:1748-1759 Available at: [Accessed April 1, 2011].

Gee K, Guzzo C, Che Mat NF, Ma W, Kumar A (2009) The IL-12 family of cytokines in infection, inflammation and autoimmune disorders. Inflamm Allergy Drug Targets 8:40-52 Available at: [Accessed December 3, 2010].

Gentner B, Visigalli I, Hiramatsu H, Lechman E, Ungari S, Giustacchini A, Schira G, Amendola M, Quattrini A, Martino S, Orlacchio A, Dick JE, Biffi A, Naldini L (2010) Identification of hematopoietic stem cell-specific miRNAs enables gene therapy of globoid cell leukodystrophy. Sci Transl Med 2:58ra84 Available at: [Accessed April 1, 2011].

Grubb JH, Vogler C, Levy B, Galvin N, Tan Y, Sly WS (2008) Chemically modified beta-glucuronidase crosses blood-brain barrier and clears neuronal storage in murine mucopolysaccharidosis VII. Proc. Natl. Acad. Sci. U.S.A 105:2616-2621 Available at: [Accessed May 23, 2011].

Hall SL, Lau K-HW, Chen S-T, Felt JC, Gridley DS, Yee J-K, Baylink DJ (2007) An improved mouse Sca-1+ cell-based bone marrow transplantation model for use in gene- and cell-based therapeutic studies. Acta Haematol 117:24-33 Available at: [Accessed June 10, 2011].

Hannun YA, Bell RM (1989) Regulation of protein kinase C by sphingosine and lysosphingolipids. Clin. Chim. Acta 185:333-345 Available at: [Accessed April 23, 2011].

Hawkins-Salsbury JA, Reddy AS, Sands MS (2011) Combination therapies for lysosomal storage disease: is the whole greater than the sum of its parts? Hum Mol Genet Available at: http://www.ncbi.nlm.nih.gov/pubmed/21421999 [Accessed April 18, 2011].

Hess DC, Abe T, Hill WD, Studdard AM, Carothers J, Masuya M, Fleming PA, Drake CJ, Ogawa M (2004) Hematopoietic origin of microglial and perivascular cells in brain. Exp. Neurol 186:134-144 Available at: [Accessed April 23, 2011].

Hill DF, Bullock PN, Chiappelli F, Rome LH (1985) Binding and internalization of lysosomal enzymes by primary cultures of rat glia. J. Neurosci. Res 14:35-47 Available at: [Accessed April 25, 2011].

Hofling AA, Kim JH, Fantz CR, Sands MS, Song S-K (2009) Diffusion tensor imaging detects axonal injury and demyelination in the spinal cord and cranial nerves of a murine model of globoid cell leukodystrophy. NMR Biomed 22:1100-1106 Available at: [Accessed April 13, 2011].

Hofling AA, Vogler C, Creer MH, Sands MS (2003) Engraftment of human CD34+ cells leads to widespread distribution of donor-derived cells and correction of tissue pathology in a novel murine xenotransplantation model of lysosomal storage disease. Blood 101:2054-2063 Available at: [Accessed June 14,

2011].

Homs J, Ariza L, Pages G, Udina E, Navarro X, Chillon M, Bosch A (2011) Schwann cell targeting via intrasciatic injection of AAV8 as gene therapy strategy for peripheral nerve regeneration. Gene Ther.

Hoogerbrugge PM, Poorthuis BJ, Romme AE, van de Kamp JJ, Wagemaker G, van Bekkum DW (1988)(a) Effect of bone marrow transplantation on enzyme levels and clinical course in the neurologically affected twitcher mouse. J Clin Invest 81:1790-4

Hoogerbrugge PM, Suzuki K, Suzuki K, Poorthuis BJ, Kobayashi T, Wagemaker G, van Bekkum DW (1988) Donor-derived cells in the central nervous system of twitcher mice after bone marrow transplantation. Science 239:1035-8

Horuk R, Martin AW, Wang Z, Schweitzer L, Gerassimides A, Guo H, Lu Z, Hesselgesser J, Perez HD, Kim J, Parker J, Hadley TJ, Peiper SC (1997) Expression of chemokine receptors by subsets of neurons in the central nervous system. J. Immunol 158:2882-2890 Available at: [Accessed April 25, 2011].

Howard DB, Powers K, Wang Y, Harvey BK (2008) Tropism and toxicity of adeno-associated viral vector serotypes 1, 2, 5, 6, 7, 8, and 9 in rat neurons and glia in vitro. Virology 372:24-34 Available at: [Accessed June 10, 2011].

Huh GS, Boulanger LM, Du H, Riquelme PA, Brotz TM, Shatz CJ (2000) Functional requirement for class I MHC in CNS development and plasticity. Science 290:2155-2159 Available at: [Accessed April 16, 2011].

Hulse RE, Kunkler PE, Fedynyshyn JP, Kraig RP (2004) Optimization of multiplexed bead-based cytokine immunoassays for rat serum and brain tissue. J Neurosci Methods 136:87-98

Ichioka T, Kishimoto Y, Brennan S, Santos GW, Yeager AM (1987) Hematopoietic cell transplantation in murine globoid cell leukodystrophy (the twitcher mouse): effects on levels of galactosylceramidase, psychosine, and galactocerebrosides. Proc Natl Acad Sci U S A 84:4259-63

Igisu H, Suzuki K (1984) Progressive accumulation of toxic metabolite in a genetic leukodystrophy. Science 224:753-755 Available at: [Accessed April 23, 2011].

Igisu H, Takahashi H, Suzuki K, Suzuki K (1983) Abnormal accumulation of galactosylceramide in the kidney of twitcher mouse. Biochem Biophys Res Commun 110:940-4

Jacobsohn DA, Duerst R, Tse W, Kletzel M (2004) Reduced intensity haemopoietic stem-cell transplantation for treatment of non-malignant diseases in children. Lancet 364:156-162 Available at: [Accessed July 19, 2010].

Jacobson GA, Rokni D, Yarom Y (2008) A model of the olivo-cerebellar system as a temporal pattern generator. Trends Neurosci 31:617-625 Available at: [Accessed January 4, 2011].

Jatana M, Giri S, Singh AK (2002) Apoptotic positive cells in Krabbe brain and induction of apoptosis in rat C6 glial cells by psychosine. Neurosci. Lett

330:183-187 Available at: [Accessed April 23, 2011].

Jiang X, Yang K, Han X (2009) Direct quantitation of psychosine from alkaline-treated lipid extracts with a semi-synthetic internal standard. Journal of Lipid Research 50:162 -172 Available at: [Accessed October 26, 2010].

Kagitani-Shimono K, Mohri I, Fujitani Y, Suzuki K, Ozono K, Urade Y, Taniike M (2005) Anti-inflammatory therapy by ibudilast, a phosphodiesterase inhibitor, in demyelination of twitcher, a genetic demyelination model. J Neuroinflammation 2:10

Kelly LM, Yu J-C, Boulton CL, Apatira M, Li J, Sullivan CM, Williams I, Amaral SM, Curley DP, Duclos N, Neuberg D, Scarborough RM, Pandey A, Hollenbach S, Abe K, Lokker NA, Gilliland DG, Giese NA (2002) CT53518, a novel selective FLT3 antagonist for the treatment of acute myelogenous leukemia (AML). Cancer Cell 1:421-432 Available at: [Accessed May 22, 2011].

Khan M, Haq E, Giri S, Singh I, Singh AK (2005) Peroxisomal participation in psychosine-mediated toxicity: implications for Krabbes disease. J Neurosci Res 80:845-54

Kinney HC, Brody BA, Kloman AS, Gilles FH (1988) Sequence of central nervous system myelination in human infancy. II. Patterns of myelination in autopsied infants. J. Neuropathol. Exp. Neurol 47:217-234 Available at: [Accessed June 10, 2011].

Koay CG, Chang L-C, Carew JD, Pierpaoli C, Basser PJ (2006) A unifying theoretical and algorithmic framework for least squares methods of estimation in diffusion tensor imaging. J. Magn. Reson 182:115-125 Available at: [Accessed November 3, 2010].

Kondo Y, Adams JM, Vanier MT, Duncan ID (2011) Macrophages counteract demyelination in a mouse model of globoid cell leukodystrophy. J. Neurosci 31:3610-3624 Available at: [Accessed March 14, 2011].

Kornfeld S (1992) Structure and function of the mannose 6-phosphate/insulinlike growth factor II receptors. Annu. Rev. Biochem 61:307-330 Available at: [Accessed April 23, 2011].

Krabbe K (1916) A NEW FAMILIAL, INFANTILE FORM OF DIFFUSE BRAIN-SCLEROSIS. Available at: http://brain.oxfordjournals.org/cgi/content/citation/39/1-2/74 [Accessed July 11, 2010].

Krieger NR, Ito H, Garrison Fathman C (1997) Rat Pancreatic Islet and Skin Xenograft Survival in CD4 and CD8 Knockout Mice. Journal of Autoimmunity 10:309-315 Available at: [Accessed June 14, 2011].

Krivit W, Shapiro EG, Peters C, Wagner JE, Cornu G, Kurtzberg J, Wenger DA, Kolodny EH, Vanier MT, Loes DJ, Dusenbery K, Lockman LA (1998) Hematopoietic stem-cell transplantation in globoid-cell leukodystrophy. N. Engl. J. Med 338:1119-1126 Available at: [Accessed December 30, 2009].

Lawlor PA, Bland RJ, Mouravlev A, Young D, During MJ (2009) Efficient Gene Delivery and Selective Transduction of Glial Cells in the Mammalian Brain by

AAV Serotypes Isolated From Nonhuman Primates. Mol Ther 17:1692-1702 Available at: [Accessed May 22, 2011].

Leonard EJ, Yoshimura T (1990) Human monocyte chemoattractant protein-1 (MCP-1). Immunol. Today 11:97-101 Available at: [Accessed December 4, 2010].

LeVine SM, Brown DC (1997) IL-6 and TNFalpha expression in brains of twitcher, quaking and normal mice. J Neuroimmunol 73:47-56

Lin D, Donsante A, Macauley S, Levy B, Vogler C, Sands MS (2007) Central nervous system-directed AAV2/5-mediated gene therapy synergizes with bone marrow transplantation in the murine model of globoid-cell leukodystrophy. Mol. Ther 15:44-52 Available at: [Accessed November 9, 2009].

Lin D, Fantz CR, Levy B, Rafi MA, Vogler C, Wenger DA, Sands MS (2005) AAV2/5 vector expressing galactocerebrosidase ameliorates CNS disease in the murine model of globoid-cell leukodystrophy more efficiently than AAV2. Mol. Ther 12:422-430 Available at: [Accessed January 8, 2010].

Liu L, Belkadi A, Darnall L, Hu T, Drescher C, Cotleur AC, Padovani-Claudio D, He T, Choi K, Lane TE, Miller RH, Ransohoff RM (2010) CXCR2-positive neutrophils are essential for cuprizone-induced demyelination: relevance to multiple sclerosis. Nat Neurosci.

Luddi A, Volterrani M, Strazza M, Smorlesi A, Rafi MA, Datto J, Wenger DA, Costantino-Ceccarini E (2001) Retrovirus-mediated gene transfer and galactocerebrosidase uptake into twitcher glial cells results in appropriate localization and phenotype correction. Neurobiol Dis 8:600-10

Luzi P, Abraham RM, Rafi MA, Curtis M, Hooper DC, Wenger DA (2009) Effects of treatments on inflammatory and apoptotic markers in the CNS of mice with globoid cell leukodystrophy. Brain Res 1300:146-158 Available at: [Accessed August 25, 2010].

Luzi P, Rafi MA, Zaka M, Curtis M, Vanier MT, Wenger DA (2001) Generation of a mouse with low galactocerebrosidase activity by gene targeting: a new model of globoid cell leukodystrophy (Krabbe disease). Mol Genet Metab 73:211-23

Luzi P, Rafi MA, Zaka M, Rao HZ, Curtis M, Vanier MT, Wenger DA (2005) Biochemical and pathological evaluation of long-lived mice with globoid cell leukodystrophy after bone marrow transplantation. Mol. Genet. Metab 86:150-159 Available at: [Accessed April 23, 2011].

Mandel RJ, Burger C (2004) Clinical trials in neurological disorders using AAV vectors: promises and challenges. Curr. Opin. Mol. Ther 6:482-490 Available at: [Accessed October 17, 2010].

Matsushima GK, Taniike M, Glimcher LH, Grusby MJ, Frelinger JA, Suzuki K, Ting JP (1994) Absence of MHC class II molecules reduces CNS demyelination, microglial/macrophage infiltration, and twitching in murine globoid cell leukodystrophy. Cell 78:645-56

Mays LE, Vandenberghe LH, Xiao R, Bell P, Nam H-J, Agbandje-McKenna M,

Wilson JM (2009) Adeno-associated virus capsid structure drives CD4-dependent CD8+ T cell response to vector encoded proteins. J. Immunol 182:6051-6060 Available at: [Accessed May 22, 2011].

McCandless EE, Wang Q, Woerner BM, Harper JM, Klein RS (2006) CXCL12 limits inflammation by localizing mononuclear infiltrates to the perivascular space during experimental autoimmune encephalomyelitis. J. Immunol 177:8053-8064 Available at: [Accessed July 19, 2010].

McMahon A, Fowler SC, Perney TM, Akemann W, Knpfel T, Joho RH (2004) Allele-dependent changes of olivocerebellar circuit properties in the absence of the voltage-gated potassium channels Kv3.1 and Kv3.3. European Journal of Neuroscience 19:3317-3327 Available at: [Accessed December 9, 2009].

Meikle PJ, Hopwood JJ, Clague AE, Carey WF (1999) Prevalence of lysosomal storage disorders. JAMA 281:249-254 Available at: [Accessed April 18, 2011].

Meng X-L, Shen J-S, Watabe K, Ohashi T, Eto Y (2005) GALC transduction leads to morphological improvement of the twitcher oligodendrocytes in vivo. Mol Genet Metab 84:332-43

Miller CL, Rebel VI, Lemieux ME, Helgason CD, Lansdorp PM, Eaves CJ (1996) Studies of W mutant mice provide evidence for alternate mechanisms capable of activating hematopoietic stem cells. Exp. Hematol. 24:185-194

Miller SD, McMahon EJ, Schreiner B, Bailey SL (2007) Antigen presentation in the CNS by myeloid dendritic cells drives progression of relapsing experimental autoimmune encephalomyelitis. Ann. N. Y. Acad. Sci 1103:179-191 Available at: [Accessed April 25, 2011].

Miwa H (2007) Rodent models of tremor. Cerebellum 6:66-72 Available at: [Accessed January 4, 2011].

Mombaerts P, Iacomini J, Johnson RS, Herrup K, Tonegawa S, Papaioannou VE (1992) RAG-1-deficient mice have no mature B and T lymphocytes. Cell 68:869-877 Available at: [Accessed June 13, 2011].

Naldini L (2011) Ex vivo gene transfer and correction for cell-based therapies. Nat Rev Genet Available at: http://www.ncbi.nlm.nih.gov/pubmed/21445084 [Accessed April 1, 2011].

Noguchi KK, Walls KC, Wozniak DF, Olney JW, Roth KA, Farber NB (2008) Acute neonatal glucocorticoid exposure produces selective and rapid cerebellar neural progenitor cell apoptotic death. Cell Death Differ 15:1582-1592 Available at: [Accessed December 23, 2010].

Okabe M, Ikawa M, Kominami K, Nakanishi T, Nishimune Y (1997) Green mice as a source of ubiquitous green cells. FEBS Lett 407:313-319 Available at: [Accessed July 18, 2010].

Patel JR, McCandless EE, Dorsey D, Klein RS (2010) CXCR4 promotes differentiation of oligodendrocyte progenitors and remyelination. Proceedings of the National Academy of Sciences 107:11062 -11067 Available at: [Accessed July 28, 2010].

Pedchenko TV, Bronshteyn IG, LeVine SM (2000) TNF-receptor 1 deficiency fails to alter the clinical and pathological course in mice with globoid cell leukodystrophy (twitcher mice) but affords protection following LPS challenge. J Neuroimmunol 110:186-94

Pedchenko TV, LeVine SM (1999) IL-6 deficiency causes enhanced pathology in Twitcher (globoid cell leukodystrophy) mice. Exp Neurol 158:459-68

Pellegatta S, Tunici P, Poliani PL, Dolcetta D, Cajola L, Colombelli C, Ciusani E, Di Donato S, Finocchiaro G (2006) The therapeutic potential of neural stem/progenitor cells in murine globoid cell leukodystrophy is conditioned by macrophage/microglia activation. Neurobiol Dis 21:314-23

Rafi MA, Zhi Rao H, Passini MA, Curtis M, Vanier MT, Zaka M, Luzi P, Wolfe JH, Wenger DA (2005) AAV-mediated expression of galactocerebrosidase in brain results in attenuated symptoms and extended life span in murine models of globoid cell leukodystrophy. Mol. Ther 11:734-744 Available at: [Accessed July 17, 2010].

Robinson S, Franic LA (2001) Chemokine GRO1 and the spatial and temporal regulation of oligodendrocyte precursor proliferation. Dev. Neurosci 23:338-345 Available at: [Accessed April 25, 2011].

Robinson S, Tani M, Strieter RM, Ransohoff RM, Miller RH (1998) The chemokine growth-regulated oncogene-alpha promotes spinal cord oligodendrocyte precursor proliferation. J. Neurosci 18:10457-10463 Available at: [Accessed July 19, 2010].

Sakai N, Inui K, Tatsumi N, Fukushima H, Nishigaki T, Taniike M, Nishimoto J, Tsukamoto H, Yanagihara I, Ozono K, Okada S (1996) Molecular cloning and expression of cDNA for murine galactocerebrosidase and mutation analysis of the twitcher mouse, a model of Krabbes disease. J Neurochem 66:1118-24

Sands MS, Barker JE (1999) Percutaneous intravenous injection in neonatal mice. Lab. Anim. Sci 49:328-330 Available at: [Accessed July 19, 2010].

Sands MS, Barker JE, Vogler C, Levy B, Gwynn B, Galvin N, Sly WS, Birkenmeier E (1993) Treatment of murine mucopolysaccharidosis type VII by syngeneic bone marrow transplantation in neonates. Lab. Invest 68:676-686 Available at: [Accessed November 5, 2010].

Sands MS, Davidson BL (2006) Gene therapy for lysosomal storage diseases. Mol. Ther 13:839-849 Available at: [Accessed July 17, 2010].

Schwarze SR, Hruska KA, Dowdy SF (2000) Protein transduction: unrestricted delivery into all cells? Trends Cell Biol 10:290-295 Available at: [Accessed June 13, 2011].

Sedgwick JD, Schwender S, Imrich H, Drries R, Butcher GW, ter Meulen V (1991) Isolation and direct characterization of resident microglial cells from the normal and inflamed central nervous system. Proc. Natl. Acad. Sci. U.S.A 88:7438-7442 Available at: [Accessed July 19, 2010].

Shapiro EG, Lockman LA, Balthazor M, Krivit W (1995) Neuropsychological

outcomes of several storage diseases with and without bone marrow transplantation. Journal of Inherited Metabolic Disease 18:413-429 Available at: [Accessed December 30, 2009].

Shenoy S, Grossman WJ, DiPersio J, Yu LC, Wilson D, Barnes YJ, Mohanakumar T, Rao A, Hayashi RJ (2005) A novel reduced-intensity stem cell transplant regimen for nonmalignant disorders. Bone Marrow Transplant 35:345-352 Available at: [Accessed July 19, 2010].

Shinkai Y, Rathbun G, Lam KP, Oltz EM, Stewart V, Mendelsohn M, Charron J, Datta M, Young F, Stall AM (1992) RAG-2-deficient mice lack mature lymphocytes owing to inability to initiate V(D)J rearrangement. Cell 68:855-867 Available at: [Accessed June 13, 2011].

Simard C, Klein SJ, Mak T, Jolicoeur P (1997) Studies of the susceptibility of nude, CD4 knockout, and SCID mutant mice to the disease induced by the murine AIDS defective virus. J Virol 71:3013-3022

Stejskal EO, Tanner JE (1965) Spin Diffusion Measurements: Spin Echoes in the Presence of a Time-Dependent Field Gradient. J. Chem. Phys. 42:288 Available at: [Accessed November 3, 2010].

Stevens A, Nelson JL (2002) Maternal and Fetal Microchimerism: Implications for Human Diseases. NeoReviews 3:11e-19 Available at: [Accessed June 10, 2011].

Stevens B, Allen NJ, Vazquez LE, Howell GR, Christopherson KS, Nouri N, Micheva KD, Mehalow AK, Huberman AD, Stafford B, Sher A, Litke AM, Lambris JD, Smith SJ, John SWM, Barres BA (2007) The classical complement cascade mediates CNS synapse elimination. Cell 131:1164-1178 Available at: [Accessed March 14, 2011].

Suzuki K (1998) Twenty five years of the psychosine hypothesis: a personal perspective of its history and present status. Neurochem Res 23:251-9

Suzuki K, Hoogerbrugge PM, Poorthuis BJ, Bekkum DW, Suzuki K (1988) The twitcher mouse. Central nervous system pathology after bone marrow transplantation. Lab Invest 58:302-9

Suzuki K, Suzuki Y, Suzuki K, Wenger DA (2000) Galactosylceramide Lipidosis: Globoid Cell Leukodystrophy (Krabbe Disease) In Metabolic and Molecular Bases of Inherited Diseases McGraw-Hill Professional.

Tani M, Fuentes ME, Peterson JW, Trapp BD, Durham SK, Loy JK, Bravo R, Ransohoff RM, Lira SA (1996) Neutrophil infiltration, glial reaction, and neurological disease in transgenic mice expressing the chemokine N51/KC in oligodendrocytes. J. Clin. Invest 98:529-539 Available at: [Accessed March 13, 2011].

Taniike M, Suzuki K (1995) Proliferative capacity of oligodendrocytes in the demyelinating twitcher spinal cord. J. Neurosci. Res 40:325-332 Available at: [Accessed July 28, 2010].

Towne C, Schneider BL, Kieran D, Redmond DE Jr, Aebischer P (2010) Efficient

transduction of non-human primate motor neurons after intramuscular delivery of recombinant AAV serotype 6. Gene Ther 17:141-146 Available at: [Accessed June 10, 2011].

Tsai H-H, Frost E, To V, Robinson S, Ffrench-Constant C, Geertman R, Ransohoff RM, Miller RH (2002) The chemokine receptor CXCR2 controls positioning of oligodendrocyte precursors in developing spinal cord by arresting their migration. Cell 110:373-383 Available at: [Accessed July 19, 2010].

Ullrich K, Mersmann G, Weber E, Von Figura K (1978) Evidence for lysosomal enzyme recognition by human fibroblasts via a phosphorylated carbohydrate moiety. Biochem. J 170:643-650 Available at: [Accessed April 23, 2011].

Vandenberghe LH, Wang L, Somanathan S, Zhi Y, Figueredo J, Calcedo R, Sanmiguel J, Desai RA, Chen CS, Johnston J, Grant RL, Gao G, Wilson JM (2006) Heparin binding directs activation of T cells against adeno-associated virus serotype 2 capsid. Nat. Med 12:967-971 Available at: [Accessed July 19, 2010].

Vite CH, McGowan JC, Niogi SN, Passini MA, Drobatz KJ, Haskins ME, Wolfe JH (2005) Effective gene therapy for an inherited CNS disease in a large animal model. Ann. Neurol 57:355-364 Available at: [Accessed April 22, 2011].

Vitner EB, Platt FM, Futerman AH (2010) Common and uncommon pathogenic cascades in lysosomal storage diseases. J. Biol. Chem 285:20423-20427 Available at: [Accessed December 29, 2010].

Walsh PT, Taylor DK, Turka LA (2004) Tregs and transplantation tolerance. J Clin Invest 114:1398-1403

Wang G, Fowler S (2001) Concurrent quantification of tremor and depression of locomotor activity induced in rats by harmaline and physostigmine. Psychopharmacology 158:273-280 Available at: [Accessed January 1, 2010].

Wang J, Richter KK, Sung CC, Hauer-Jensen M (1999) Upregulation and spatial shift in the localization of the mannose 6-phosphate/insulin-like growth factor II receptor during radiation enteropathy development in the rat. Radiother Oncol 50:205-213 Available at: [Accessed May 22, 2011].

Weinberg KI (2005) Early use of drastic therapy. N. Engl. J. Med 352:2124-2126 Available at: [Accessed July 17, 2010].

Wenger D (1991) Screening for lysosomal disorders In Techniques in Diagnostics Human Biochemical Genetics New York: Wiley-Liss, p. 587-617.

White AB, Givogri MI, Lopez-Rosas A, Cao H, van Breemen R, Thinakaran G, Bongarzone ER (2009) Psychosine accumulates in membrane microdomains in the brain of krabbe patients, disrupting the raft architecture. J. Neurosci 29:6068-6077 Available at: [Accessed June 13, 2010].

Wu Q, Miller RH, Ransohoff RM, Robinson S, Bu J, Nishiyama A (2000)(a) Elevated levels of the chemokine GRO-1 correlate with elevated oligodendrocyte progenitor proliferation in the jimpy mutant. J. Neurosci 20:2609-2617 Available at: [Accessed July 19, 2010].

Wu YP, McMahon E, Kraine MR, Tisch R, Meyers A, Frelinger J, Matsushima GK, Suzuki K (2000) Distribution and characterization of GFP(+) donor hematogenous cells in Twitcher mice after bone marrow transplantation. Am J Pathol 156:1849-54

Xia H, Mao Q, Davidson BL (2001) The HIV Tat protein transduction domain improves the biodistribution of beta-glucuronidase expressed from recombinant viral vectors. Nat. Biotechnol 19:640-644 Available at: [Accessed May 22, 2011].

Yeager AM, Brennan S, Tiffany C, Moser HW, Santos GW (1984) Prolonged survival and remyelination after hematopoietic cell transplantation in the twitcher mouse. Science 225:1052-4

Yeager AM, Shinohara M, Shinn C (1991) Hematopoietic cell transplantation after administration of high-dose busulfan in murine globoid cell leukodystrophy (the twitcher mouse). Pediatr Res 29:302-5

Young PP, Fantz CR, Sands MS (2004) VEGF disrupts the neonatal blood-brain barrier and increases life span after non-ablative BMT in a murine model of congenital neurodegeneration caused by a lysosomal enzyme deficiency. Exp. Neurol 188:104-114 Available at: [Accessed November 9, 2010].

Young PP, Fantz CR, Sands MS (2004) VEGF disrupts the neonatal blood-brain barrier and increases life span after non-ablative BMT in a murine model of congenital neurodegeneration caused by a lysosomal enzyme deficiency. Exp. Neurol 188:104-114 Available at: [Accessed November 9, 2010].

Zolotukhin S, Byrne BJ, Mason E, Zolotukhin I, Potter M, Chesnut K, Summerford C, Samulski RJ, Muzyczka N (1999) Recombinant adeno-associated virus purification using novel methods improves infectious titer and yield. Gene Ther 6:973-985 Available at: [Accessed July 18, 2010].

Zou YR, Kottmann AH, Kuroda M, Taniuchi I, Littman DR (1998) Function of the chemokine receptor CXCR4 in haematopoiesis and in cerebellar development. Nature 393:595-599 Available at: [Accessed March 14, 2011].

Curriculum Vitae

[letterpaper]article

Adarsh Surya Reddy

660 S.Euclid Avenue
Campus Box 8007
St. Louis, Missouri 63110

Phone: (314) 362-5496; (314) 518-3890
Email: adarsh.reddy@wustl.edu
Email 2: adarsh.reddy@gmail.com

Education

M.B., B.S. (equivalent of MD), St. John's Medical College, Bangalore, India, 2004

Neuroscience Ph.D. program, Washington University in St. Louis, 2004 onwards

Publications

Journal Articles

1. Reddy AS et al., Bone Marrow Transplantation augments the effect of brain and spinal cord-directed AAV2/5 gene therapy by altering inflammation in the murine model of Globoid-cell Leukodystrophy., *Journal of Neuroscience* (in press).

2. Reddy AS et al., Bone Marrow Transplantation worsens the altered olivocerebellar dynamics in murine model of Globoid cell leukodystrophy,*Behavioral Brain Research* (submitted) .

3. Hawkins-Salsbury JA, **Reddy AS**, Sands MS. Combination therapies for lysosomal storage disease: is the whole greater than the sum of its parts? *Hum Mol Genet.* 2011 Apr 5. [Epub ahead of print] PubMed PMID: 21421999.

4. Reddy AS et al., Neurodegeneration Progresses Independently of CXCL1 and CXCR2 in Globoid-Cell Leukodystrophy (in preparation) .

Conference Presentations

1. Reddy AS,“Forebrain, cerebellar and spinal cord directed AAV2/5 gene therapy augments therapeutic effect of bone marrow transplantation in murine model of globoid cell leukodystrophy.” (Nanosymposium: Demyelinating diorders-cellular mechanisms. The Society for Neuroscience annual meeting, San Diego, CA, November 14, 2010).

2. Reddy AS, “Bone Marrow Transplantation worsens the altered olivocerebellar dynamics in murine model of Globoid cell leukodystrophy” (Nanosymposium: Demyelinating diorders-cellular mechanisms. The Society for Neuroscience annual meeting, San Diego, CA, November 14, 2010).

3. Reddy AS, “Combination Gene Therapy and Bone Marrow Transplantation for Krabbe’s disease” (Towards Clinical Progress in the Mucopolysaccharidoses meeting; Washington D.C. March 7-8, 2007)

4. Macauley SL, **Reddy AS**, Pekny M, Sands MS., “The role of astrocyte activation in Infantile Neuronal Ceroid Lipofuschinosis”. 12th international congress of Neuronal Ceroid Lipofuschinosis, Hamburg, June3-6, 2009. (Presenter: Macauley SL)

Poster Presentations

1. The role of the chemokine KC in the pathogenesis of Globoid cell leukodystrophy. International Society for Neuroimmunology meeting; Fortworth, Texas, 2008

2. The role of chemokine receptor CXCR2 in the pathogenesis of Globoid-Cell Leukodystrophy. Poster 2009-S-4395-SfN. SFN Annual Meeting, Chi - cago, 2009.

Last updated: June 21, 2011